Improving the Durability of the Inverted T-Beam Bridge System[1]

FINAL REPORT
November 2018

Submitted by:

Carin Roberts-Wollmann
Professor

Vijaykanth Pulumati
Graduate Research Assistant

Via Department of Civil and Environmental Engineering
Virginia Tech
200 Patton Hall
Blacksburg, VA 24061

Project Manager
Bernie Kassner, Ph.D., P.E.
Research Scientist
Virginia Transportation Research Council

In cooperation with

Rutgers, The State University of New Jersey
And
Virginia Transportation Research Council
And
U.S. Department of Transportation
Federal Highway Administration

[1]*This report has been published as a thesis for the degree of Master of Science in Civil Engineering, Virginia Polytechnic Institute and State University ("Investigation of Concrete Mixtures to Reduce Differential Shrinkage Cracking in Inverted T-Beam System").*

Disclaimer Statement

The contents of this report reflect the views of the authors, who are responsible for the facts and the accuracy of the information presented herein. This document is disseminated under the sponsorship of the Department of Transportation, University Transportation Centers Program, in the interest of information exchange. The U.S. Government assumes no liability for the contents or use thereof.

The Center for Advanced Infrastructure and Transportation (CAIT) is a National UTC Consortium led by Rutgers, The State University. Members of the consortium are the University of Delaware, Utah State University, Columbia University, New Jersey Institute of Technology, Princeton University, University of Texas at El Paso, Virginia Polytechnic Institute, and University of South Florida. The Center is funded by the U.S. Department of Transportation.

1. Report No.	2. Government Accession No.	3. Recipient's Catalog No.
CAIT-UTC-NC28		

4. Title and Subtitle	5. Report Date
Improving the Durability of the Inverted T-Beam Bridge System	November 2018
	6. Performing Organization Code CAIT/Virginia Tech

TECHNICAL REPORT STANDARD	8. Performing Organization Report No.
7. Author(s) Carin Roberts-Wollmann and Vijaykanth Pulumati	CAIT-UTC-NC28

9. Performing Organization Name and Address	10. Work Unit No.
Via Department of Civil and Environmental Engineering Virginia Tech 200 Patton Hall Blacksburg, VA 24061	11. Contract or Grant No. DTRT13-G-UTC28

12. Sponsoring Agency Name and Address	13. Type of Report and Period Covered
Center for Advanced Infrastructure and Transportation Rutgers, The State University of New Jersey 100 Brett Road Piscataway, NJ 08854	Final Report 2/10/2016 to 5/9/2017
	14. Sponsoring Agency Code

15. Supplementary Notes
U.S. Department of Transportation/Research and Innovative Technology Administration
1200 New Jersey Avenue, SE
Washington, DC 20590-0001

16. Abstract

The inverted T-beam system provides an accelerated bridge construction alternative. The system consists of adjacent precast inverted T-beams finished with a cast-in-place concrete topping. The system offers enhanced performance against reflective cracking and reduces the likelihood of cracking due to time dependent effects. Differential shrinkage is believed to be one of the causes of deck cracking in inverted T-beam systems. The objective of this study was to develop mix designs that exhibit lower shrinkage and higher creep compared to typical deck mixtures, recommend a prescriptive mix design and a performance criterion to VDOT that can be used in the inverted T-beam system to combat effects of differential shrinkage.

Ten different mix designs using different strategies to reduce shrinkage were tested for their compressive strength, splitting tensile strength, modulus of elasticity and unrestrained shrinkage. The four best performing mixes were selected for further study of their time dependent properties. The test data was compared against the data from various prediction models to determine the model that closely predicts the measured data. It was observed that ACI 209.2R-08 model best predicted the time dependent properties for the four mixes tested in this project. Tensile stresses in the composite cross-section of deck and girder, created due to difference in shrinkage and creep were quantified using an age adjusted effective modulus method.

In this analysis, it was observed that mixes with normal weight coarse aggregate developed smaller stresses compared to those of mixes with lightweight coarse aggregate. Mixes with fly ash as supplementary cementitious material (SCM) developed smaller stresses at the bottom of deck when compared to mixes with slag as the SCM.

17. Key Words	18. Distribution Statement
Differential Shrinkage, Creep, Concrete Bridge deck, Reflective cracking	

19. Security Classification (of this report)	20. Security Classification (of this page)	21. No. of Pages	22. Price
Unclassified	Unclassified	95	

Acknowledgments

Funding for this project was provided by the Virginia Transportation Research Council (VTRC) and the National University Transportation Center Consortium led by CAIT at Rutgers University. The researchers would like to thank Dennis Huffmann, Brett Farmer and Dr. David Mokarem for their support in the laboratory. The guidance and technical assistance provided by the engineers at VTRC and VDOT, including Dr. Bernie Kassner and Andy Zickler are also gratefully acknowledged. The opinions expressed in this report are those of the authors and not necessarily those of the sponsors.

TABLE OF CONTENTS

List of Tables

List of Figures

1. INTRODUCTION

To accelerate the process of bridge construction, the Federal Highway Administration (FHWA) and the American Association of State Highway and Transportation Officials (AASHTO) funded a scanning tour in April 2004 through Japan and several countries in Europe to identify innovative bridge systems that help accelerate the construction process using prefabricated elements. One of the systems identified was the Poutre-Dalle system in France (Figure 1-1).

Figure 1-1: Poutre-Dalle system (Bell, 2006)

Inspired by the Poutre-Dalle systems observed in France, the state of Minnesota was the first state in the United States to implement this concept. Engineers in Minnesota developed a similar system, which featured the same precast inverted T-beam shape and the extended transverse bars. This system was targeted for implementation in the state of Minnesota for bridges with spans ranging from 20 ft to 65 ft (Hagen, 2005). The inverted T-beam system developed in Minnesota was implemented on twelve bridges between 2005 and 2011 (Dimaculangan, 2010). During this time the original concept underwent a number of modifications to improve performance in different design generations. To determine the effect of these design modifications on performance, a series of field inspections was done (Dimaculangan, 2010) and Figure 1-2 shows that the longitudinal and transverse surface cracking is extensive.

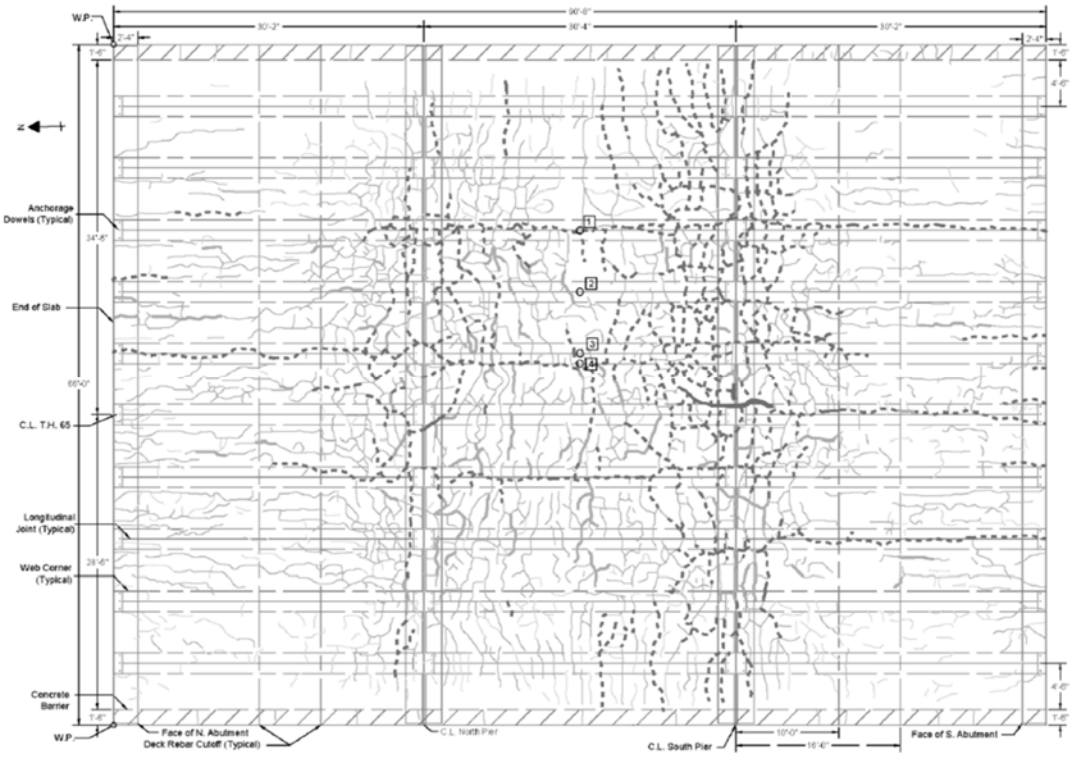

Figure 1-2: Crack map for Bridge No. 33008, Inspection No. 3, June 16 and August 10, 2011 with core specimen locations indicated (Halverson, 2012)

Although the inverted T-beam system showed promise with respect to addressing reflective cracking concerns, the fabrication challenges presented by the extended transverse bars and the surface cracking observed in Minnesota's bridges prompted the need for additional research.

Being aware of reflective cracking problems present in short-to-medium-span bridges built with adjacent voided slabs and adjacent box beam systems, the Virginia Department of Transportation (VDOT) expressed interest in implementing the precast inverted T-beam system for the first time in Virginia. The application was a bridge replacement project near Richmond, Virginia, on US 360. The most pressing issue of interest to VDOT was that related to reflective cracking. The objective was to build on Minnesota's experience and investigate modifications to the inverted T-beam system that would lead to more durable, crack resistant bridges. Differential shrinkage is believed to be one of the causes of deck cracking in this system.

The design of bridges is typically done considering the effects of dead, live, seismic and wind loads. The effects of the time dependent properties like shrinkage and creep are not considered as significant. Load cases including these time dependent deformations may reveal tensile stresses which may exceed the tensile strength of concrete and cause cracking. The inverted T-beam is cast off site and has undergone most of its shrinkage and creep deformations long before being put into use on site. After placement, the deck concrete will try to shrink but is restrained by the girder. This restraint stress may exceed the tensile strength of the concrete and cause cracking.

1.1 Objective

The objective of this research was to investigate the effect of time dependent properties of concrete deck topping on the magnitude of tensile stresses generated in the composite cross-section of the inverted T-beam system in the transverse direction and develop recommendations for mix designs to minimize these stresses. Controlling the magnitude of these tensile stresses is important to avoid excessive cracking.

This was approached by varying the mineral and chemical admixtures used in the topping concrete and also comparing mixtures with lightweight aggregate to those with traditional normal weight aggregate. Different mixes were tested for their material and time-dependent properties. The time-dependent data was then compared with the available shrinkage and creep prediction models to evaluate the best model for prediction of these properties in future. The impact of shrinkage and creep of the deck topping on the composite section was analyzed using an age adjusted effective modulus method. All this data is used to recommend a prescriptive mix design and a performance criterion to VDOT that can be used in the inverted T-beam system.

1.2 Scope

This research includes the evaluation of several mixes to determine the effectiveness of saturated lightweight coarse and fine aggregates (SLWA) along with supplementary cementitious materials (SCM) and chemical admixtures in reducing shrinkage and increasing creep in the topping concrete. Cracking has been found to increase as compressive strength increases, which corresponds to increasing cement content (Schmitt, 1999), and so the mixes with normal weight aggregate had a cement content capped at 600 lb/yd^3, and the mixes with SLWA had cement content restricted to 650 lb/yd^3 as practiced by VDOT to reduce cracking. Mixtures with both types of aggregates had a water to cement ratio of 0.45, and air content was maintained at 6.5% ± 1.5%. Cracking decreases as air contents increases, particularly for air contents greater than 6% (Schmitt, 1999). All the specimens used in this project underwent 7-day moist curing. The project included two phases:

1. Phase I, whose objective was to evaluate the best performing combinations of SLWA and SCM.
    1. There were ten different design mixes in Phase I
    2. These mixes were tested for compressive strength, splitting tensile strength, modulus of elasticity and unrestrained shrinkage.
    3. The best performing mixes were further investigated in Phase II

2. Phase II, whose objective was to further study the best performing mixes from Phase I for their time dependent properties.
    1. Four best performing mixes were selected from Phase I.
    2. They were tested for compressive strength, splitting tensile strength, modulus of elasticity, unrestrained shrinkage, compressive and tensile creep.
    3. The data obtained from Phase II was then compared to available prediction models such as, ACI 209 – 08, AASHTO – 2014, CEB MC 90-99 models.

4. The effect of shrinkage and creep of concrete on the composite structure was evaluated using an age adjusted effective modulus (AAEM) method.

2 LITERATURE REVIEW

2.1 Shrinkage

During its service life concrete experiences volume changes while in a plastic or hardened state. These volumetric changes are relatively small compared to the entire volume of concrete. Volume change can be either in the form of swelling (expansion) or shrinkage (contraction). Volume change in plastic and early age concrete is commonly due to shrinkage. When shrinkage of concrete is restrained, shrinkage cracks can occur. Concrete shrinkage is restrained by supporting subbase/base materials or from reinforcing steel and other structural elements. A combination of shrinkage of concrete materials and restraint is the mechanism that produces cracking. This restraint of shrinkage causes cracks to form as restrained shrinkage stresses exceed the strength of the concrete. This shrinkage occurs as a result of chemical shrinkage, autogenous shrinkage, settlement, and plastic shrinkage (Kosmatka, 2002).

2.1.1 Plastic Shrinkage

Plastic shrinkage is a combination of chemical shrinkage, autogenous shrinkage, and rapid evaporation while the concrete is still in a plastic state. Plastic shrinkage is often the cause of surface cracking that can occur during final finishing operations. Plastic shrinkage is addressed in specifications with curing methods to reduce rapid evaporation (Kosmatka, 2002). Plastic shrinkage was not considered in this study because rapid evaporation was prevented by using moist curing for 7 days.

2.1.2 Chemical Shrinkage

Chemical shrinkage is a reduction in absolute volume of solids and liquids in cement paste that result from cementitious materials reacting with water. Portland cement and water occupy more volume in their individual state than when they are chemically combined. Consequently, as concrete sets and gains strength during hydration its volume shrinks. (Kosmatka, 2002)

2.1.3 Autogenous Shrinkage

Autogenous shrinkage occurs as water in the pores of the cementitious paste is consumed by hydration. This shrinkage is much less than the absolute volume changes of chemical shrinkage (Kosmatka, 2002). It is more prominent in concrete with high cementitious contents and low water contents. Autogenous shrinkage is most prominent in concrete having a water to cement ratio less than 0.42. This additional consumption of water by hydration results in reduced volume and shrinkage in the cementitious paste (Mindess, 1996).

2.1.4 Drying Shrinkage

Drying shrinkage is caused by external evaporation of moisture from concrete. Drying shrinkage is the dominant mode in concrete slabs (or structures with slab-like volume/surface ratio) with plentiful water (water/cement ratio greater than 0.41). This process can continue for a number of years, depending on the shape and volume/surface ratio of the concrete structure. However, within the first 11 months, tests have shown that approximately 90 percent of shrinkage had taken place, although this number is dependent on many other factors (Kosmatka, 2002).

2.2 Differential Shrinkage

The term differential shrinkage represents the difference between shrinkage characteristics of the in-situ concrete and the total strain characteristics of the precast concrete due to shrinkage and creep (Banerjee, 1971) . A cast-in-place bridge deck topping on a precast girder is an example of structure in which differential shrinkage will occur. As the precast component has been aged, it will have already undergone some amount of shrinkage. The cast-in-place deck topping will shrink considerably, but will be restrained by the precast section. The resulting differential shrinkage causes stresses in the composite section which are mainly tensile in the deck (Silfwerbrand, 1997).

The resulting tensile stresses from differential shrinkage, in combination with stresses from other loadings, can cause cracking in the bridge deck. This allows for the ingress of harmful materials such as moisture and deicing salts, causing further deterioration due to corrosion of reinforcement. This deterioration, if not addressed, can lead to serious issues with the long-term serviceability of the structure, including concrete spalling, delamination, and eventual requirement of total deck rehabilitation or replacement.

This effect can be minimized by reducing shrinkage and increasing creep. Reducing shrinkage will reduce the magnitude of the tensile stress built up in the cross section and increasing creep will help dissipate the tensile stresses produced.

2.3 Creep

Creep is a volume change or deformation caused by sustained stress or load. When concrete is loaded, the deformation caused by the load can be divided into two parts: a deformation that occurs immediately (elastic strain) as per Hooke's law and a time-dependent deformation that begins immediately but continues at a decreasing rate for as long as the concrete is loaded. This latter deformation is called creep (Kosmatka, 2002).

Creep of concrete is composed of two components: basic creep, or deformation under constant load without moisture loss or gain, and drying creep. Drying creep is the time-dependent deformation of a drying specimen under constant load minus the sum of the drying shrinkage and basic creep (Mokarem, 2003).

Creep in concrete is often seen as an unwanted effect, however, in the case of differential shrinkage it can be beneficial. Concrete will creep in tension due to the tensile stresses caused by differential shrinkage. This creep effect serves to relax these stresses and reduce the likelihood of the concrete cracking due to the aforementioned stresses (Kosmatka, 2002).

2.4 Methods to Reduce Shrinkage and Increase Creep

In this project, the objective is to investigate mix designs for improved behavior in its time dependent properties that can be used to help recommend a prescriptive mix design and a performance-based criterion to VDOT. This was approached by use of saturated lightweight coarse and fine aggregates (SLWA), use of supplementary cementitious materials (SCM) and use of shrinkage reducing admixtures (SRA) in the mix designs as a part of the investigation.

2.4.1 Saturated Lightweight Aggregates, SLWA

Concrete with lightweight aggregate has a lower modulus of elasticity and more water in the pores of aggregates for continued internal curing when compared to normal weight concrete (NWC). These properties tend to reduce cracking in the concrete and are highly desirable in bridge decks. Having a lower modulus of elasticity, concrete can be considered more flexible than one with a greater modulus. Therefore, less rigidity of the concrete can provide better performance, reducing early-age cracking that is caused by autogenous shrinkage, moisture loss, and restrained shrinkage. Further, NWC weighs about 150 lb/ft^3 as compared to structural lightweight concrete (LWC) that weighs about 115 to 120 lb/ft^3. This is significant since using LWC decreases the dead load compared to NWC by about 20% (Ozyildirim, 2005). Lightweight aggregate replacement beyond 20% by volume of the total aggregate may significantly reduce strength (Ye Jiajun, 2006).

Henkensiefken et al. (2009) found that the concrete including SLWA exhibited reduction in autogenous and drying shrinkage when compared to a reference concrete which did not contain SLWA. They concluded in their study that the addition of SLWA resulted in a reduction in the total shrinkage during the first 28 days. This may be due to the initial reduction in self-desiccation and the additional water that can complete hydration and temporarily replace the water that is lost to the environment. The time to cracking is prolonged for mixtures with SLWA (Henkensiefken, 2009). This is likely due to the reduced shrinkage; in addition, although not specifically examined in their study, reduced elastic modulus, increased relaxation, and increased fracture toughness of the mixtures with SLWA could also contribute to this increase in time to cracking.

2.4.2 Supplementary Cementitious Material, SCM

A supplementary cementitious material, when used in combination with portland cement, contributes to the properties of the hardened concrete through hydraulic or pozzolanic activity or both. As such, SCMs include both pozzolans and hydraulic materials. A pozzolan is defined as a siliceous or siliceous and aluminous material that in itself possesses little or no cementitious value, but that will, in finely divided form and in the presence of moisture, chemically react with calcium hydroxide at ordinary temperatures to form compounds having cementitious properties.

Pozzolans that are commonly used in concrete include fly ash, silica fume, Nano silica and a variety of natural pozzolans such as calcined clay and shale, and volcanic ash. SCMs that are hydraulic in behavior include ground granulated blast furnace slag and fly ashes with high calcium contents (Thomas, 2007).

In his study, Yang (2012) concluded that the use of nano silica powder in concrete as a SCM will increase the mechanical strength but will also increase shrinkage in concrete. The 28 day drying shrinkage ratios, compared with ordinary concrete, were 75.5%, 127.1% ,163.0% when the mixed contents of nano silica powder were 0.5%, 0.75%, 1.0% respectively. The result indicates the addition of nano silica powder increased the drying shrinkage of concrete significantly (Yang, 2012).

In their study, Akkaya et al. (2007) have shown that concrete with portland cement as the only binder exhibited the highest autogenous shrinkage, whereas concrete with binary binders exhibited lower autogenous shrinkage. The autogenous shrinkage of concrete with 10% fly ash replacement was closer to the portland cement concrete, and the autogenous shrinkage of the concrete with 20% fly ash replacement was less than that of concrete with only portland cement (Akkaya, 2007). It is suggested that unless indicated otherwise, a minimum amount of 15% fly ash is needed to achieve the desired properties (Thomas, 2007).

In their report, Hooton et al. (2009) stated that the drying shrinkage of concrete containing slag is approximately 3% higher than a similar concrete not containing slag. When corrected to a constant paste content, this increase reduces to about 1.5%. This is independent of slag content and water-cement ratio of the concrete mixture over the typical range in concrete (Hooton, 2009). Such a small difference is not significant. While some references state that the relative increase in drying shrinkage of concrete containing slag decreases with drying time, no evidence of this could be established. Part of the small increase in drying shrinkage is due to the reduced aggregate content of the concretes containing slag.

It is clear from the review, the use of SCM helps in reducing shrinkage of concrete. It was decided to move forward with fly ash and ground granulated blast furnace slag (GGBS), simply called as slag, as the SCMs in this project. Use of SLWA will eventually result a decrease in strength, unit weight and modulus of elasticity resulting in increased creep of concrete. Use of SCM will help decrease the permeability of concrete (232.1R-12, 2012) which is useful in reducing cracking. Reducing permeability restricts the flow of chemicals, used for various reasons, to penetrate into concrete that cause corrosion. It also restricts the flow of water to the top surface reducing evaporation, which helps in reducing cracking.

2.4.3 Shrinkage Reducing Admixture

Another widely used method to reduce shrinkage in concrete is the use of chemical admixtures. Use of shrinkage-reducing admixtures is practiced as one of the most effective ways of reducing shrinkage cracking. The reduction in capillary tension by organic agents of shrinkage- reducing admixtures decreases the concrete volume changes due to internal self-desiccation or air drying of concrete. Ribeiro et al. (2003) reported the effectiveness of SRAs on different concrete mixtures using two SRA products at different dosage rates. All the mixtures

had 25% of cement replaced with fly ash. Their study showed a maximum reduction in drying shrinkage of about 30% with the use of SRA (Ribeiro, 2003).

2.5 Prediction Models

Creep and shrinkage are highly variable properties of concrete and depend on many factors. To calculate the creep coefficients and the shrinkage strains of the concrete mixes under consideration, which are a part of Inverted T-beam system, the AASHTO LRFD bridge Specifications were used. The AASHTO LRFD Bridge Design Specifications (2014) recommend three models to calculate creep and shrinkage. These include the AASHTO LRFD model (AASHTO, 2014), ACI 209.2R-08 (ACI-209, 2008) model and CEB-MC-90-99 (ACI-209, 2008) model. Comparing the data obtained from these models to the experimental data is essential to find the model that best predicts the actual behavior of concrete.

According to ACI 209, the following simplifying assumptions are adopted in the development of prediction models.

- Shrinkage and creep are independent of each other.
- It is assumed that shrinkage and creep strains in a specimen occur uniformly through the specimen.
- Creep is separated into basic and drying creep.
- The stresses induced during curing phase are negligible.
- Creep of concrete is approximately proportional to stress applied.

A detailed procedure of each of the three models is described in the methods section.

2.6 Time Dependent Analysis – Age Adjusted Effective Modulus Method

Concrete behaves in a much more complex way when the effects of creep and shrinkage are combined with external loads. The effect of creep and shrinkage must be considered in the analysis of concrete structures. This has been approached, previously, in many ways. Some of procedures are discussed below.

Effective modulus (EM) method involves, a reduction of the modulus of elasticity in order to account for creep in concrete (McMillan, 1916). The effective modulus is given by

$$E_{eff} = \frac{E(t_o)}{1 + \phi(t, t_o)} \qquad \text{Equation 2-1}$$

Where E_{eff} is the effective modulus, $E(t_o)$ is the elastic modulus, $\phi(t, t_o)$ is the creep coefficient. The EM method is simple and independent of stress history but is not accurate for variable stresses.

Another method for predicting time-dependent effects in concrete was inspired by the results of experiments performed by Glanville. Glanville concluded that the rate at which

concrete creeps is unrelated to the concrete's age when it is loaded; in other words, all creep curves are parallel (Dilger, 2005). While creep curves for fairly young concrete may be approximately parallel, this assumption is definitely inaccurate for older concrete.

Another widely used method is the age-adjusted effective modulus (AAEM) method. The AAEM method is simply an improved version of the EM method. The AAEM method supplement the EM method by including a quantity called the aging coefficient, μ, which was first presented by Trost in 1967, and further refined by Bazant (Bazant, 1972). The age-adjusted effective modulus is given by:

$$E^*_{eff} = \frac{E(t_o)}{1 + \mu * \phi(t, t_o)} \qquad \text{Equation 2-2}$$

Where E_{eff} is the effective modulus, $E(t_o)$ is the elastic modulus, $\phi(t, t_o)$ is the creep coefficient, μ is the ageing coefficient. The addition of the ageing coefficient helps linearize the creep and shrinkage equations (Wollmann, 2003). The aging coefficient can be taken as between 0.7 to 0.9 for concrete loaded between 10-100 days. In this project, concrete is assumed to be loaded at 56 days and a value of 0.85 is assumed as the ageing coefficient. By using a single, constant aging coefficient, time dependent effect calculations can be simplified and reduced to the solution of a set of linear equations. The AAEM is discussed further in the methods section.

3 METHODS

This chapter describes the procedures used in the laboratory, the materials used to perform the evaluation of the mix designs as well as the test programs. Two phases of experimentation were conducted in this project. Phase I evaluated ten design mixes with different amounts of lightweight/ normal weight aggregates along with SCM and chemical admixtures. Phase I included mixes with lightweight coarse aggregate and mixes with normal weight aggregate. Phase I included two control mixes, one normal weight coarse-aggregate mix and one lightweight coarse-aggregate mix. Out of the ten mixes, the four best performing mixes were further studied for their long terms properties in Phase II.

3.1 Design Mix

A total of ten mixes were designed for Phase I: five normal weight aggregate mixtures and five lightweight aggregate mixtures. Table 3-1 describes the nomenclature used for each mixture. The total cementitious content and replacement levels for supplementary cementitious materials were chosen based on VDOT practice and previous research. Slag cement and fly ash were used to replace Portland cement on a 30% and 20% by weight ratio respectively. The water-cement ratio used was 0.45. The air content was targeted at 6.5% ± 1.5%. The targeted slump was 6 in. ± 1.5 in. The targeted compressive strength was 4000 psi. All the batches had chemical admixtures in quantities as shown in

Table **3-2**.

Normal weight coarse-aggregate mixtures are shown in Table 3-3. VDOT Class A4—General Bridge Deck Concrete using Portland cement only (Mokarem, 2008) was used as base

mix with 600 lb/yd^3 as a limit to total cementitious content. All other quantities were adjusted as per ACI 211.1.

Table 3-1: Design Mixes Abbreviation

Design Mix	Explanation
LWCA+SLAG	Lightweight coarse aggregate with 30% slag
LWCA+SLAG+SLWF	Lightweight coarse aggregate with 30% slag and saturated lightweight fines
LWCA+FA	Lightweight(LW) coarse aggregate with 20% fly ash
LWCA+SLAG+SRA	Lightweight coarse aggregate with 30% slag and shrinkage reducing admixture
Control mix LWCA	Lightweight coarse aggregate with OPC
NWCA+SLAG	Normal weight coarse aggregate with 30% slag
NWCA+SLAG+SLWF	Normal weight(NW) coarse aggregate with 30% slag and saturated lightweight fines
NWCA+FA	Normal weight coarse aggregate with 20% fly ash
NWCA+SLAG+SRA	Normal weight coarse aggregate with 30% slag and shrinkage reducing admixture
Control mix NWCA	Normal weight coarse aggregate with OPC

Table 3-2: Quantities of Admixtures Used

Admixture	Quantities
High range water reducer	10
Air entraining admixture	0.75
Shrinkage reducing admixture	15

*All quantities are in # Oz/100 wt. of cementitious materials

Table 3-3: Normal Weight Aggregate Mixtures

Ingredients	NWCA+ SLAG	NWCA+ SLAG+ SLWF	NWCA+ FA	NWCA+ SLAG + SRA	Control mix NWCA
Portland cement	420	420	480	420	600
Slag cement	180	180	0	180	0
Fly ash	0	0	120	0	0
NW coarse aggregate	1703	1700	1637	1703	1644
NW fine aggregate	1282	1028	1328	1283	1353
LW fine aggregate	0	142	0	0	0
Water	270	270	270	270	270
Total	3855	3740	3835	3856	3867
Unit weight	143	138	142	143	143

*All weights are in lb./yd3

Table 3-4 shows the lightweight aggregate design mixes. Total cementitious content in lightweight aggregate mixes was limited to 650 lb/yd^3. The amount of fine aggregate replacement with saturated lightweight fine aggregate was limited to 12% based on previous studies.

Table 3-4: Lightweight Aggregate Mixtures

Ingredients	LWCA+ SLAG	LWCA+ SLAG+ SLWF	LWCA+ FA	LWCA+ SLAG + SRA	Control mix LWCA
Portland cement	455	455	520	455	650
Slag cement	195	195	0	195	0
Fly ash	0	0	130	0	0
LW coarse aggregate	841	900	816	841	875
NW fine aggregate	1378	1100	1400	1377	1333
LW fine aggregate	0	150	0	0	0
Water	295	295	295	295	295
Total	3164	3095	3161	3163	3153
Unit weight	117	115	117	117	117

*All weights are in lb./yd3

3.2 Materials and Mixing

The materials used in this study included natural sand, lightweight expanded slate, slag, fly ash, Type I /II cement, water reducing admixture, shrinkage reducing admixture and air entraining agent. Cement used was a Type I/II ordinary Portland cement with a specific gravity of 3.15 as given by the manufacturer. Mineral admixtures used in this project were fly ash and slag cement which were used as partial replacement for ordinary Portland cement. Fly ash was obtained from Boral America conforming to ASTM C 618 has a specific gravity of 2.4. Slag cement- ground granulated blast furnace slag was obtained from Lafarge conforming to ASTM C 989 with a specific gravity of 2.9. Lightweight aggregates were obtained from Stalite, North Carolina. The specific gravity of lightweight coarse aggregate was 1.52 and that of lightweight fine aggregate was 1.75 as given by the manufacturer (Stalite). Shrinkage reducing admixture used was obtained from SIKA corporation conforming to ASTM C 494 standard. High range water reducing admixture and air entraining admixture were obtained from Conrock. All the chemical admixtures were used in quantities as described by the manufacturer.

All batches were mixed by hand using a 2.5 ft^3 capacity pan mixer. The batch size for all of the batches was 1.5 ft^3. The lightweight course aggregates were allowed to soak in water for a minimum of 24 hours and batched in the SSD condition. Moisture content and absorption of all the aggregates was determined and required corrections were made in the amount of water added into the mixer. The mixing procedure was the same for each batch to minimize variation due to batching. The procedure was as follows:

- The interior surfaces of the mixer were dampened.
- The desired coarse aggregate, fine aggregate and fifty percent of the mixing water was added to the pan mixer and allowed to mix for 2 minutes.
- The cement and SCM (as required) was added slowly and allowed to mix for 2 minutes.
- The super plasticizer was added with 10% of the mixing water and allowed to mix for 1 minute.
- The air entraining agent was added with the remaining mix water for 1 minute.
- The plastic concrete was mixed for 3 minutes after addition of any shrinkage reducing admixture (as needed).
- The concrete was then ready for the slump, unit weight and air test.

3.3 Material Testing

This section describes the methods used in testing of concrete specimens. After casting the concrete, the specimens were covered with a plastic tarp to prevent loss of water and then demolded after 24 hours. The demolded specimens were moist cured for seven days using wet burlap.

3.3.1 Testing Specimens

For every batch of concrete that was cast in Phase I, 16 – 4 x 8in. cylinders and three 11.25 x 3 x 3in. prisms were cast in accordance to ASTM C192/C192M section 7. Testing for compressive strength, tensile strength and modulus of elasticity was done at 7, 14, 28, 56 days. Data from unrestrained shrinkage bars was collected on 1,7,14,28 days and every month thereafter. In Phase II, along with the tests and specimen above, four 6 x 12in. cylinders and two dog bone specimens described below in tensile creep section, were also cast for compressive creep test and tensile creep tests respectively.

3.3.2 Fresh Concrete Properties

Slump, air content and unit weight were the fresh properties tested for each batch of concrete cast. Slump was tested according to ASTM C143 – standard test method for slump of hydraulic-cement concrete. Air content and unit weight were tested according to ASTM C231 – standard test method for air content of freshly mixed concrete by the pressure method.

3.3.3 Compressive Strength

Compressive strength testing was done in accordance with ASTM C39 – Standard Test Method for Compressive Strength of Cylindrical Concrete Specimens. Every mix was tested for compressive strength using 4 x 8in. cylinders at 7, 14, 28, 56 days and the data obtained was an average of two cylinders for every reading.

3.3.4 Splitting Tensile Strength

Splitting tensile strength testing was done in accordance with ASTM C496 – Standard Test Method for splitting tensile Strength of Cylindrical Concrete Specimens. Every mix was tested for splitting tensile strength using 4 x 8in. cylinders at 7, 14, 28, 56 days and the data obtained was an average of two cylinders for every reading.

3.3.5 Modulus of Elasticity

Test to determine the modulus of elasticity of the concrete specimen was done in accordance with ASTM C469 – Standard Test Method for Static Modulus of Elasticity and Poisson's Ratio of Concrete in Compression. Modulus of elasticity of every mix was determined using 4 x 8in. cylinders at 7, 14, 28, 56 days and the data obtained was an average of two cylinders for every reading.

3.3.6 Unrestrained Shrinkage Test

The unrestrained shrinkage test was performed in accordance with ASTM C157 – Standard Test Method for Length Change of Hardened Hydraulic-cement Mortar and Concrete. Specimens used to test unrestrained shrinkage were 11.25 x 3 x 3in. prism specimens. These specimens were stored in an environmental chamber which has a humidity of 35%. The unrestrained shrinkage data was collected just after demolding, which is used as the base to determine the length change of the specimens. This data is recorded for 7, 14, 28 and 56 days after casting.

3.3.7 Compressive Creep Test

Compressive creep test was performed for each concrete mix in Phase II in accordance with ASTM C512 – standard test method for creep of concrete in compression. Four 6 x 12 in. concrete cylinders were cast for each mix. Specimens were demolded twenty-four hours after placement and placed under moist cure for seven days. Two sets of DEMEC mechanical strain gauge locating discs were installed on each cylinder to determine length change over time. Data from compressive strength testing was collected and used to calculate the appropriate compressive load for creep testing (40% of compressive strength).

Three cylinders were stacked under a hydraulic load cell in a controlled environmental chamber. An initial reading was taken to determine a reference. Cylinders were then loaded to the calculated compressive load and monitored for length change over time. Readings were taken every 24 hours for 7 days, then weekly for 30 days, then monthly thereafter. The fourth cylinder was placed adjacent to the creep test and monitored for length change, referred to as on-shelf shrinkage. Total strain is equal to the summation of elastic strain, shrinkage strain and creep strain. Elastic strain is the strain measured immediately after the creep specimens are loaded. Shrinkage strain is the strain due to the shrinkage of the creep specimens during the creep tests and is measured from unloaded cylinders. Creep strain is the increase in strain in the creep

specimens over time as a result of the applied load. Creep strain divided by initial elastic strain gives the value of the creep coefficient.

3.3.8 Tensile Creep Test

Tensile creep testing was performed for each concrete mix in Phase II. It was desired to use a load application method which did not rely on hydraulics to avoid loss of load over time. A tensile creep frame was developed by Nelson (2013) to apply mechanical tensile loads to concrete specimens utilizing a beam with unequal length cantilevers supported by a fulcrum (Nelson, 2013).

Concrete specimens are 24 in. tall dog bone specimens, see Figure 3-1 to Figure 3-3. Reinforcement was inserted into the top and bottom flanges of each specimen to allow load to be transferred to the web of the specimen without fracturing them. Corners were chamfered to avoid stress concentrations at the corners. Specimens were instrumented with two sets of DEMEC points on opposite sides. The specimen was inserted into the grips and held stationary while weights were added at the opposite end of the frame in order to reach the desired loading values.

One specimen was loaded on the tensile creep frame, while one specimen was measured to determine shrinkage values. Shrinkage values were subtracted from creep to determine total tensile creep strain.

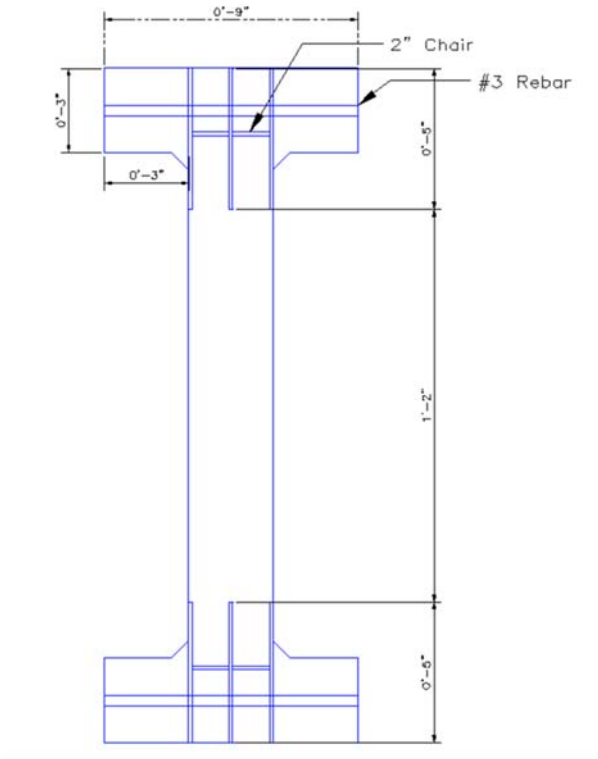

Figure 3-1: Tensile Creep Specimen, Schematic.

Figure 3-2: Tensile Creep Specimen

Figure 3-3: Tensile Creep Specimen Loaded

Figure 3-4: Grips for Tensile Creep Test

3.4 Prediction Models.

AASHTO LRFD Bridge Specifications (2014) allow the use of three models, the AASHTO (2014), ACI 209.2R-08 and CEB MC 90-99 models, to predict the time dependent properties of concrete that is part of a bridge system. These models are briefly explained below:

3.4.1 ACI 209.2R – 08 Model

The ACI 209.2R model is recommended by the ACI 209 committee. It was developed by Branson and Christianson (1971). This model is applicable to all normal weight and lightweight concrete with Type I and Type III cement. The ACI model accounts for humidity and volume to surface ratio but not the compressive strength of the concrete under consideration. With a known mix design, the ACI model also includes factors for slump, aggregate proportions, air content and cement content.

3.4.1.1 ACI 209.2R Shrinkage Model

The shrinkage strain by ACI 209.2R model is given by,

$$\varepsilon_{sh}(t, t_c) = \frac{(t - t_c)^{\alpha}}{f + (t - t_c)^{\alpha}} * \varepsilon_{shu} \qquad \text{Equation 3-1}$$

Where, $\varepsilon_{sh}(t, t_c)$ is the shrinkage strain at age of t(days) measured from start of drying at t_c (days), f (days) and α are constants for a given shape and member size that define the time ratio part, ε_{shu} is the ultimate shrinkage and $(t - t_c)$ represents the time from the end of the initial curing. The value of f is recommended as 35 and 55 days for 7 days of moist curing and 1 to 3 days of steam curing respectively. The average value of α is recommended to be taken as 1.0. The shape and size affect can be considered on the time ratio by replacing α= 1, and f as given by the equation below. Here V/S is the volume surface ratio.

$$f = 26 * e^{0.36*\frac{V}{S}}$$ Equation 3-2

For standard conditions and a relative humidity of 40% the value of ultimate shrinkage strain ε_{shu} is taken as 780 x 10^{-6} (in./in.). For non-standard conditions ε_{shu} is given by:

$$\varepsilon_{\text{shu}} = 780 * 10^{-6} * \gamma_{sh,tc} * \gamma_{sh,vs} * \gamma_{sh,s} * \gamma_{sh,RH} * \gamma_{sh,\psi} * \gamma_{sh,c} * \gamma_{sh,\alpha}$$ Equation 3-3

Where, $\gamma_{\text{sh},tc}$ is the curing factor, $\gamma_{\text{sh},vs}$ is the volume- to-surface area ratio factor, $\gamma_{\text{sh},s}$ is the slump factor, $\gamma_{sh,RH}$ is the ambient relative humidity factor, $\gamma_{\text{sh},\psi}$ is the fine aggregate factor, $\gamma_{\text{sh},c}$ is the cement content factor and $\gamma_{\text{sh},\alpha}$ is the air content factor.

$$\gamma_{sh,tc} = 1.202 - 0.2337 * \log(t_c)$$ Equation 3-4

$$\gamma_{sh,vs} = 1.2 * e^{-0.12*\frac{V}{S}}$$ Equation 3-5

Where V/S is the volume surface ratio.

$$\gamma_{sh,s} = 0.89 + 0.041 * s$$ Equation 3-6

Where, s is the slump of fresh concrete in in.

$$\gamma_{sh,RH} = 1.4 - 1.02 * h$$ Equation 3-7

for $0.4 \leq h \leq 0.8$

$$\gamma_{sh,RH} = 3 - 3.0 * h$$ Equation 3-8

for $0.8 \leq h \leq 1$

Where relative humidity, h, is in decimals. For h < 40%, values higher than 1 should be used for shrinkage $\gamma_{sh,RH}$.

$$\gamma_{sh,\psi} = 0.3 + 0.041 * \psi$$ Equation 3-9

for $\psi \leq 50\%$

$$\gamma_{sh,\psi} = 0.9 + 0.002 * \psi$$ Equation 3-10

for $\psi > 50\%$

Where, ψ is the ratio of fine aggregate to total aggregate by weight expressed as percentage.

$$\gamma_{sh,c} = 0.75 + 0.00036 * c \qquad \text{Equation 3-11}$$

Where, c is cement content in lb/yd$^{3.}$

$$\gamma_{sh,\alpha} = 0.75 + 0.008 * \alpha \geq 1 \qquad \text{Equation 3-12}$$

Where, α is the air content percent.

3.4.1.2 ACI 209.2R Creep Model

The creep coefficient by ACI 209R-92 is given by:

$$\varphi(t, t_o) = \frac{(t - t_o)^{\psi}}{d + (t - t_o)^{\psi}} * \varphi_u \qquad \text{Equation 3-13}$$

Where, $\varphi\ (t, to)$ is the creep coefficient at concrete age t due to a load applied at the age t_o,$(t - t_o)$ is the time since the application of the load and φ_u is the ultimate creep coefficient. The value of d and ψ are recommended to be taken as 10 and 0.6 under standard conditions. The value of φ_u is taken as 2.35 under standard conditions. For non-standard conditions φ_u is given by:

$$\varphi_u = \gamma_{c,t_o} * \gamma_{c,vs} * \gamma_{c,RH} * \gamma_{c,s} * \gamma_{c,\psi} * \gamma_{c,c\alpha} * 2.35 \qquad \text{Equation 3-14}$$

Where, $\gamma_{c,\ to}$ is the age of loading factor, $\gamma_{c,\ RH}$ is the ambient relative humidity factor, $\gamma_{c,\ vs}$ is the volume-to-surface area ratio factor, $\gamma_{c,s}$ is the slump factor, $\gamma_{c,\psi}$ is the fine aggregate factor and $\gamma_{c,c\alpha}$ is the air content factor.

$$\gamma_{c,t_o} = 1.25 * t_o^{-0.118} \qquad \text{Equation 3-15}$$

for moist curing

$$\gamma_{c,t_o} = 1.13 * t_o^{-0.094} \qquad \text{Equation 3-16}$$

for steam curing

$$\gamma_{c,RH} = 1.27 - 0.67 * h \; for \; h \geq 0.4 \qquad \text{Equation 3-17}$$

Where h is the relative humidity in decimals. $\gamma_{c,\ RH}$ is equal to 1 if humidity is less than 40%

$$\gamma_{c,s} = 0.82 + 0.067 * s \qquad \text{Equation 3-18}$$

Where s is the slump value in in.

$$\gamma_{c,vs} = \frac{2}{3} * (1 + 1.13 * e^{-0.54*\frac{V}{S}}) \quad \text{Equation 3-19}$$

Where V is the volume of the specimen in in^3 and S is the surface area in in^2.

$$\gamma_{c,\psi} = 0.88 + 0.0024 * \psi \quad \text{Equation 3-20}$$

Where ψ is the ratio of fine aggregate to total aggregate by weight expressed as a percentage.

$$\gamma_{c,c\alpha} = 0.46 + 0.09 * \alpha \geq 1 \quad \text{Equation 3-21}$$

Where α is the air content in percent.

3.4.2 AASHTO LRFD Model

The AASHTO model accounts for effects of relative humidity, volume/surface ratio, and compressive strength at time of loading. The time development factor varies with the compressive strength at time of loading. A detailed description of calculating shrinkage and creep is given in section 5.4.2.3 of AASHTO LRFD Bridge Design Specifications, 2014.

3.4.2.1 AASHTO Creep Model

The creep coefficient is calculated as shown below:

$$\psi(t, t_i) = 1.9 * k_s * k_{hc} * k_f * k_{td} * t_i^{-0.118} \quad \text{Equation 3-22}$$

Where k_s is the volume-to-surface area ratio factor, k_{hc} is the relative humidity factor, kf is the factor to account the concrete strength and ktd is the time development factor.

$$k_s = 1.45 - 0.13 * \frac{V}{S} \geq 1 \quad \text{Equation 3-23}$$

$$k_{hc} = 1.56 - 0.008 * h \quad \text{Equation 3-24}$$

$$k_f = \frac{5}{1 + f`_{ci}} \quad \text{Equation 3-25}$$

$$k_{td} = \frac{t}{61 - 4 * f`_{ci} + t} \quad \text{Equation 3-26}$$

Where, V is the volume of the member in in^3, S is the surface area of the member in in^2, h is the ambient relative humidity in %, $'_{ci}$ is the compressive strength of the member at the time of load application. If the value is unknown, then f'_{ci} can be taken as approximately as $0.8f'_c$. t is the age of concrete between time of loading for creep calculations, or end of curing for shrinkage

calculations, and time being considered for analysis of creep or shrinkage effects, t_i is age of concrete at time of load application (day).

3.4.2.2 AASHTO Shrinkage Model

The shrinkage strain at a time t is given by:

$$\varepsilon_{sh} = k_s * k_{hs} * k_f * k_{td} * 0.48 * 10^{-3} \qquad \text{Equation 3-27}$$

Where, the factors k_s, k_f and k_{td} are the same as those defined above. k_{hs} is the relative humidity factor and is given by,

$$k_{hs} = 2 - 0.014 * h \qquad \text{Equation 3-28}$$

3.4.3 CEB MC 90-99 Model

The CEB MC90-99 model also accounts for relative humidity and strength, cement type, age at loading, and duration of loading.

3.4.3.1 CEB MC 90-99 Creep Model

Within the range of service stresses (not greater than the mean compressive strength at the time of loading t_o), 28-day creep coefficient is calculated as follows:

$$\varphi_{28}(t, t_o) = \varphi_o * \beta_c(t - t_o) \qquad \text{Equation 3-29}$$

Where, φ_o is the notional creep coefficient, $\beta_c\,(t - t_{o)}$ is the coefficient that describes the development of creep over time, t is the age of concrete at the moment considered (days) and t_o is the age of concrete at loading (days).The notional creep coefficient is given by:

$$\varphi_o = \varphi_{Rh}(h) * \beta(f_{cm28}) * \beta(t_o) \qquad \text{Equation 3-30}$$

With,

$$\varphi_{RH}(h) = \left\{ 1 + \frac{1 - \frac{h}{h_o}}{\sqrt[3]{0.1 * \frac{\left(\frac{V}{S}\right)}{\left(\frac{V_o}{S_o}\right)}}} * \alpha_1 \right\} * \alpha_2 \qquad \text{Equation 3-31}$$

$$\beta(f_{cm28}) = \frac{5.3}{\sqrt{\frac{f_{cm28}}{f_{cmo}}}}$$ Equation 3-32

$$\beta(t_o) = \frac{1}{0.1 + \left(\frac{t_o}{t_1}\right)^{0.2}}$$ Equation 3-33

$$\alpha_1 = \left(\frac{3.5 * f_{cmo}}{f_{cm28}}\right)^{0.7}$$ Equation 3-34

$$\alpha_2 = \left(\frac{3.5 * f_{cmo}}{f_{cm28}}\right)^{0.2}$$ Equation 3-35

Where, f_{cm28} is the 28-day mean compressive strength in psi, f_{cmo} is 1450 psi, h is the relative humidity in decimals, h_o is 1, V/S is the volume-surface ratio in in., (V_o/S_o) is 2 in. and t_1 is 1 day. And

$$\beta_c(t - t_o) = \left[\frac{\frac{t - t_o}{t_1}}{\beta_H + \frac{t - t_o}{t_1}}\right]^{0.3}$$ Equation 3-36

$$\beta_H = 150 * \left[1 + \left(1.2 * \frac{h}{h_o}\right)^{18}\right] * \frac{\left(\frac{V}{S}\right)}{\left(\frac{V_o}{S_o}\right)} + 250 * \alpha_3 \leq 1500$$ Equation 3-37

$$* \alpha_3$$

$$\alpha_3 = \left(\frac{3.5 * f_{cmo}}{f_{cm28}}\right)^{0.5}$$ Equation 3-38

3.4.3.2 CEB MC 90-99 Shrinkage Model

The total shrinkage of concrete is expressed as,

$$\varepsilon_{sh}(t, t_c) = \varepsilon_{cas}(t) + \varepsilon_{cds}(t, t_c)$$ Equation 3-39

Where, $\varepsilon_{cas}(t)$ is the autogenous shrinkage and $\varepsilon_{cds}(t, t_c)$ is the drying shrinkage at concrete age t (days) after beginning of drying at t_c (days).

The autogenous shrinkage component is given by,

$$\varepsilon_{cas}(t) = \varepsilon_{caso}(f_{cm28}) * \beta_{as}(t) \qquad \text{Equation 3-40}$$

Where, (f_{cm28}) is the notional autogenous shrinkage coefficient and $\beta_{as}(t)$ is the function describing the time development of autogenous shrinkage.

$$\varepsilon_{caso}(f_{cm28}) = -\alpha_{as} * \left\{ \frac{\left(\frac{f_{cm28}}{f_{cmo}}\right)}{6 + \left(\frac{f_{cm28}}{f_{cmo}}\right)} \right\}^{2.5} * 10^{-6} \qquad \text{Equation 3-41}$$

$$\beta_{as}(t) = 1 - \exp\left(-0.2 * \left(\frac{t}{t_1}\right)^{0.5}\right) \qquad \text{Equation 3-42}$$

α_{as} is the coefficient that depends on the type of cement. For normal or rapid hardening cement the value of α_{as} is taken as 700.

The drying shrinkage component is given by,

$$\varepsilon_{cds}(t, t_c) = \varepsilon_{cdso}(f_{cm28}) * \beta_{RH}(h) * \beta_{ds}(t - t_c) \qquad \text{Equation 3-43}$$

Where, (f_{cm28}) is the notional drying shrinkage coefficient, $\beta_{RH}(t)$ is the relative humidity coefficient and $\beta_{ds}(t - t_c)$ is a function describing the time development of drying shrinkage.

$$\varepsilon_{cdso}(f_{cm28}) = \left[(220 + 110 * \alpha_{ds1}) * \exp(-\alpha_{ds2} * \frac{f_{cm28}}{f_{cmo}})\right] * 10^{-6} \qquad \text{Equation 3-44}$$

$$\beta_{RH}(h) = -1.55\left[1 - \left(\frac{h}{h_o}\right)^3\right] \; for \; 0.4 \leq h \leq 0.99 * \beta_{s1} \qquad \text{Equation 3-45}$$

$$\beta_{ds}(t-t_c)=\left[\frac{\left(\frac{t-t_c}{t_1}\right)}{350*\left[\frac{\left(\frac{V}{S}\right)}{\left(\frac{V_o}{S_o}\right)}\right]^2+\left(\frac{t-t_c}{t_1}\right)}\right]^{0.5} \quad \text{Equation 3-46}$$

$$\beta_{s1}=\left(\frac{3.5*f_{cmo}}{f_{cm28}}\right)^{0.1} \leq 1 \quad \text{Equation 3-47}$$

The values of α_{ds1} and α_{ds2} are to be taken as 4 and 0.12, respectively, for normal or rapid hardening concrete.

3.5 Age Adjusted Effective Modulus Method

AAEM method was used to investigate the effects of variations in shrinkage and creep coefficients of the deck topping mixture. The system which was investigated consists of a cast in place deck of 7 in. thick and an 18-in. thick girder. The reinforcement details shown in the section are from the design plans of the bridge on Route 360 near Mechanicsville. The procedure used in this analysis is briefly explained below.

As the deck and the girder are cast at different times, there will be e a difference in their shrinkage and creep characteristics and their behavior after the deck and girder begin to act compositely. This difference in shrinkage and creep will create forces in the deck and girder which, when totaled, equates to zero. These forces increase in magnitude with increase in difference in age of deck and girder. When the topping is placed on top of the girder, it will try to shrink but is restrained by the girder which has undergone most of its deformations before the concrete deck is placed. This restraint provided by the girder on the deck creates tensile forces in the deck. These forces can sometimes be greater than the tensile strength of the concrete and cause cracking in the deck. These internal forces act as a constant stress applied to the deck and result in creep of concrete. This shrinkage induced creep is quantified using AAEM method. The quantification of these stresses and strains can be done using equilibrium principles, material constitutive relationship and compatibility relations. Figure 3-5 shows the forces and moments acting on the composite section due to differential shrinkage and creep.

For instance, the change in strains of the deck and girder are determined by calculating the change in elastic and creep strains due to changes in forces in that particular section and shrinkage strains as given in Equation 3-48 and Equation 3-49. The change in strain in any steel layer can be determined by calculating the elastic strain due to the change in axial force in that corresponding layer (Equation 3-50). Similarly, the change in curvature can be determined by calculating elastic and creep curvatures due to the change in moment as shown in Equation 3-51

and Equation 3-52. Moreover, because there are no additional external forces and moments acting, the sum of the change in axial forces and moments due to the change in shrinkage and creep has to be zero as shown in Equation 3-53 and Equation 3-54. The principle of compatibility as shown in Equation 3-55 and Equation 3-56, can be used here by assuming perfect bond between the reinforcement, deck and girder concrete.

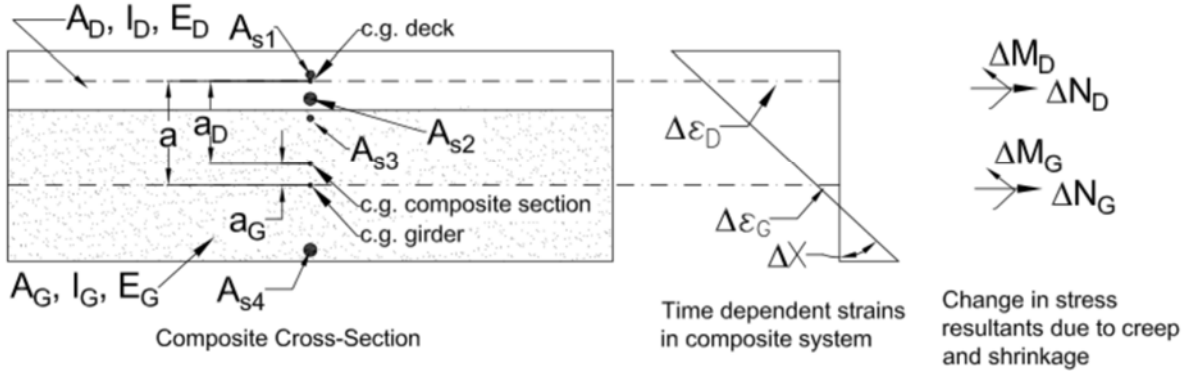

Figure 3-5: Forces in the Cross Section Due to Differential Shrinkage and Creep. *(Menkulasi F. , 2014)*

$$\Delta\varepsilon_d = \frac{\Delta \mathrm{N_d}}{E_d * A_d}(1 + \mu * \varphi_d) + \varepsilon_{shd} \qquad \text{Equation 3-48}$$

$$\Delta\varepsilon_g = \frac{\Delta \mathrm{N_g}}{E_g * A_g}\left(1 + \mu * \varphi_g\right) + \varepsilon_{shg} \qquad \text{Equation 3-49}$$

$$\Delta\varepsilon_s = \frac{\Delta \mathrm{N_s}}{E_s * A_s} \qquad \text{Equation 3-50}$$

$$\Delta X_d = \frac{\Delta \mathrm{M_d}}{E_d * I_d}(1 + \mu * \varphi_d) \qquad \text{Equation 3-51}$$

$$\Delta X_g = \frac{\Delta \mathrm{M_g}}{E_g * I_g}(1 + \mu * \varphi_g) \qquad \text{Equation 3-52}$$

$$\Delta N_d + \Delta N_g + \sum_{i=1}^{n} \Delta N_{s-i} = 0 \qquad \text{Equation 3-53}$$

$$\Delta M_d + \Delta M_g + \sum_{i=1}^{n} (\Delta N_{s-i} * a_{s-i}) \quad \text{Equation 3-54}$$

$$\Delta \varepsilon_d = \Delta \varepsilon_g - \Delta X * y_{cg} \quad \text{Equation 3-55}$$

$$\Delta \varepsilon_s = \Delta \varepsilon_g \pm \Delta X * y_{cg} \quad \text{Equation 3-56}$$

Using the cross-sectional parameters, a set of equations can be formed and solved for the unknowns using any mathematical tool. Once the unknowns are evaluated, the stress in any layer of the composite section can be found using Equation 3-57 to Equation 3-59.

$$\Delta \sigma_d = \frac{\Delta N_d}{A_d} \pm \frac{\Delta M_d}{I_d} * y \quad \text{Equation 3-57}$$

$$\Delta \sigma_g = \frac{\Delta N_g}{A_g} \pm \frac{\Delta M_g}{I_g} * y \quad \text{Equation 3-58}$$

$$\Delta \sigma_s = \frac{\Delta N_s}{A_s} \quad \text{Equation 3-59}$$

Where:

A_d = area of cast-in-place deck

A_g = area of precast girder

A_S = area of steel layer considered

a_{s-i} = distance between centroids of the steel layer considered and the point of interest

E_d = modulus of elasticity of the cast-in-place deck

E_g = modulus of elasticity of the precast girder

E_s = modulus of elasticity of mild steel

I_d = moment of inertia of the cast-in-place deck

I_g = moment of inertia of the precast girder

y_{cg} = distance between centroids of layers considered

ε_{shd} = Shrinkage strain of the deck

ε_{shd} = Shrinkage strain of the girder

$\Delta\varepsilon_d$ = Change in strain in the deck due to shrinkage and creep

$\Delta\varepsilon_g$ = Change in strain in the girder due to shrinkage and creep

$\Delta\varepsilon_s$ = Change in strain in the any steel layer due to shrinkage and creep

ΔX_d = Change in curvature of the deck due to shrinkage and creep
ΔX_g = Change in curvature of the girder due to shrinkage and creep
ΔN_d = Change is axial force in deck due to shrinkage and creep
ΔN_g = Change is axial force in girder due to shrinkage and creep
ΔN_s = Change is axial force in any steel layer due to shrinkage and creep
ΔM_d = Change is moment in deck due to shrinkage and creep
ΔM_g = Change is moment in girder due to shrinkage and creep
$\Sigma \Delta N_{s-i}$ = Sum of change in axial forces in all the steel layers
μ = ageing coefficient
φ_d = Creep coefficient of the deck
φ_g = Creep coefficient of the girder
$\Delta \sigma_d$ = Change in stress in the deck due to shrinkage and creep.
$\Delta \sigma_g$ = Change in stress in the girder due to shrinkage and creep.
$\Delta \sigma_s$ = Change in stress in the steel layer due to shrinkage and creep.

As described above, the AAEM method was used to quantify stresses and strains and analyze the effect of reducing shrinkage and increasing creep in the transverse direction of the deck at 20 years. The ageing coefficient used in this project was 0.85. The shrinkage and creep data for the deck was obtained by using ACI 209 prediction model, which was observed to be the best model compared to the data measured. The time dependent properties of the girder were predicted using AASHTO model, which is widely accepted for high strength concrete, such as the 6000psi concrete used for girder.

The section considered (Figure 3-5) has a girder of 18 in. thick and a deck of 7 in. thick. Any of the models used to analyze stresses at the cross section of deck and girder do not consider the condition of saturation of the girder before placing the deck. A saturated girder surface implies water has to travel to the top of deck to evaporate i.e. 7 in. in the section considered, whereas, a partially saturated girder surface before placement allows the movement of water into the girder, this flow of water from deck to girder reduces the distance travelled by water in the deck. Therefore, a sensitivity analysis was performed to investigate the stresses in the deck for different volume to surface ratios of deck and girder. The V/S ratio used for deck are 2, 3.5, 7 in. The V/S ratio for the girder were 4, 9, 18 in. The thin values are based on the assumption that moisture can be lost in both directions, while the thick value assumes that the interface was well saturated, so moisture is only lost in one direction, to the atmosphere.

The slump of concrete mixes measured in Phase II was after the addition of water reducing admixtures. To better understand the effect of water content, which is directly related to the slump, a sensitivity analysis was performed using the V/S ratio for deck and girder as 3.5, 9 in. respectively, and by varying the slump of the concrete used in deck. The slump values used were 3, 4.5, 6, 7.5. These slump values are before addition of any plasticizers.

This data is used in the above Equation 3-48 to Equation 3-56 to form a set of 11 equations and solve for 11 unknowns (ΔN_d, ΔN_g, ΔN_{s1}, ΔN_{s2}, ΔN_{s3}, ΔN_{s4}, ΔM_d, ΔM_g, $\Delta \varepsilon_d$, $\Delta \varepsilon_g$, ΔX). The stress in any layer of the composite section can be calculated using Equation 3-57 to Equation 3-59.

4 RESULTS

Ten different mix designs were investigated for their mechanical properties such as compressive strength, modulus of elasticity, splitting tensile strength and unrestrained shrinkage in Phase I. The four best performing mix designs were further tested for creep and shrinkage in Phase II. This data from creep and shrinkage was then compared to the data obtained from prediction models available i.e. ACI 209, AASHTO, CEB model. A parametric study was performed using AAEM method to investigate the magnitude of stresses in the deck and girder due to change in shrinkage and creep of the deck. This study was performed for all four design mixes from Phase II. This chapter presents the results of material testing in Phase I and Phase II, a comparison between measured and calculated shrinkage and creep of concrete mixes in Phase II and the effects of shrinkage and creep on the section considered. These results are further discussed in Chapter 5.

4.1 Results – Phase I

4.1.1 Fresh Concrete Properties

Table 4-1, Table 4-2 present the fresh concrete properties for mixes with NWCA and LWCA respectively in Phase I.

Table 4-1: Fresh Concrete Properties for NWCA Mixtures.

Property/ Batch	***NWCA+ SLAG***	***NWCA+ SLAG+ SLWF***	***NWCA+ FA***	***NWCA+ SLAG + SRA***	***Control mix NWCA***
Slump (in.)	7	5.5	5	5	6
Air content-%	6	7	6.5	6.5	5.5
Unit weight (lb./yd^3)	145	137	145	144	141

Table 4-2: Fresh Concrete Properties for LWCA Mixtures.

Property/ Batch	***LWCA+ SLAG***	***LWCA+ SLAG+ SLWF***	***LWCA+ FA***	***LWCA+ SLAG + SRA***	***Control mix LWCA***
Slump (in.)	5	7.5	6	8	7.5
Air content-%	7.5	6	7.5	6.5	7
Unit weight (lb./yd^3)	117	112	117	116	118

4.1.2 Compressive Strength

Table 4-3, Table 4-4, Figure 4-1 and Figure 4-2 show the compressive strength of NWCA and LWCA mixtures respectively.

Table 4-3: Compressive Strength – NWCA Mixtures

Age (days)	Compressive strength of NWCA mixtures				
	NWCA+ SLAG	***NWCA+ SLAG+ SLWF***	***NWCA+ FA***	***NWCA+ SLAG + SRA***	***Control mix NWCA***
7	3680	4000	4050	3740	5650
14	5190	4320	4370	4970	5780
28	5890	5390	5120	5660	6610
56	6430	5840	5580	6010	7010

*All values are in psi, rounded to nearest 10.

Table 4-4: Compressive Strength – LWCA Mixtures

Age (days)	Compressive strength of LWCA mixtures				
	LWCA+ SLAG	***LWCA+ SLAG+ SLWF***	***LWCA+ FA***	***LWCA+ SLAG + SRA***	***Control mix LWCA***
7	2810	4080	3230	3180	3490
14	3640	5150	4010	4940	4260
28	4280	5880	4320	5070	4730
56	4770	6530	5450	5520	5480

*All values are in psi, rounded to nearest 10.

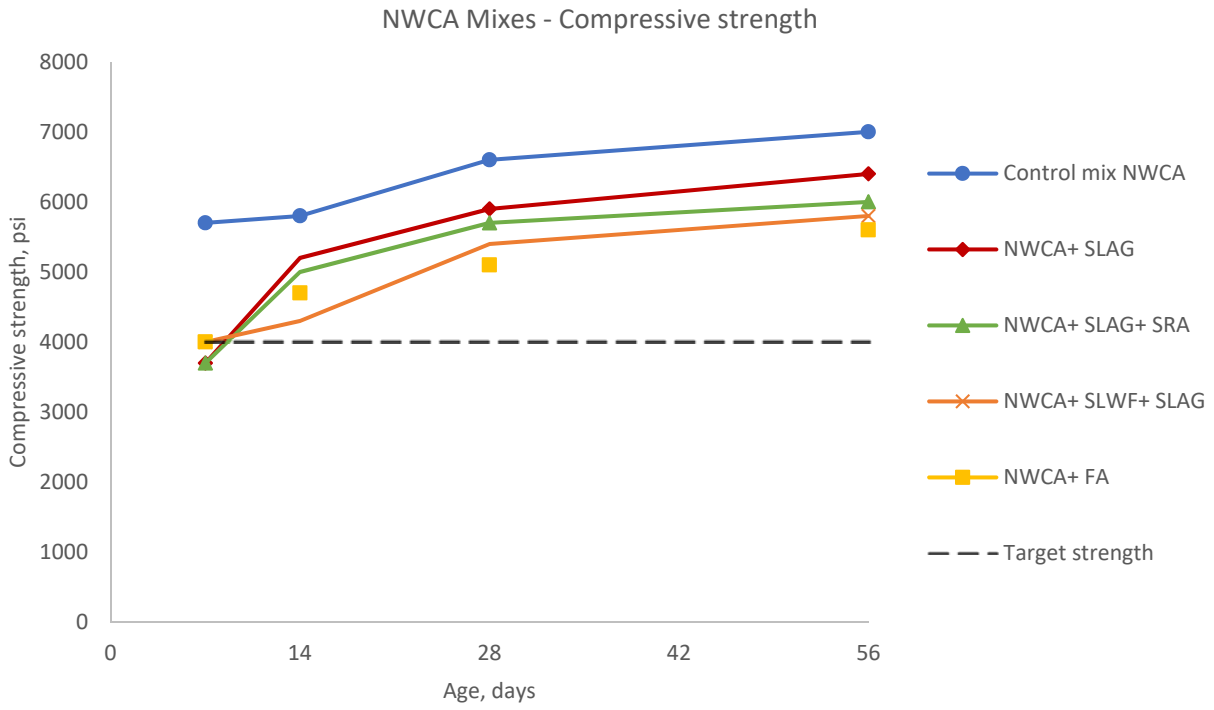

Figure 4-1: Compressive Strength, NWCA Mixes

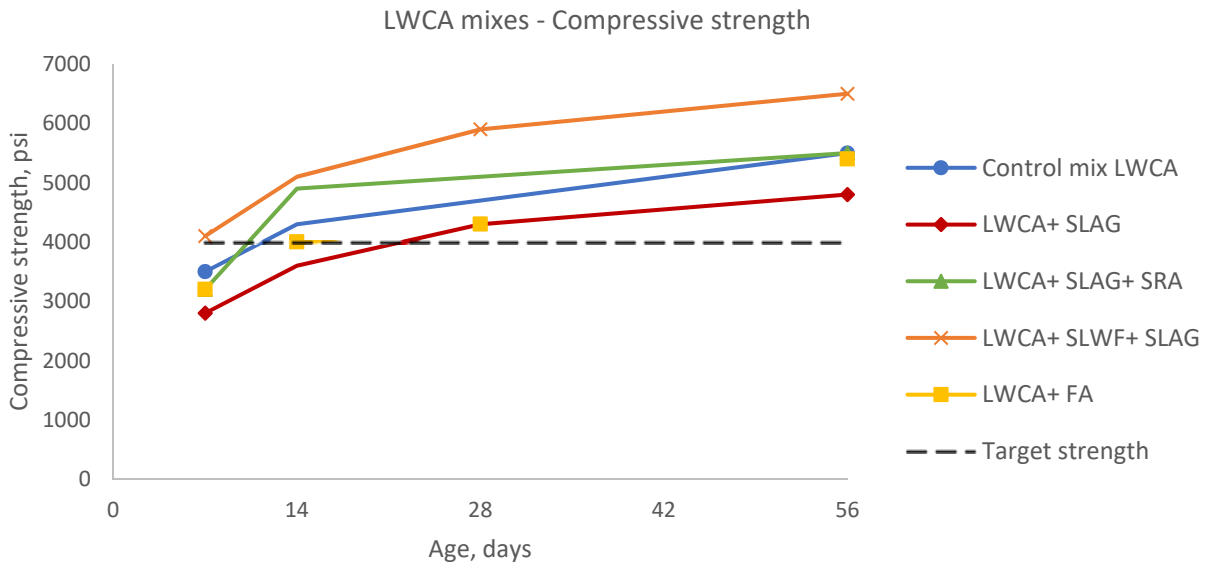

Figure 4-2 Compressive Strength, LWCA Mixes

4.1.3 Splitting Tensile Strength

Table *4-5* and **Table *4-6*** show the splitting tensile strength of mixes in Phase I.

Table 4-5: Splitting Tensile Strength – NWCA mixtures

Age (days)	Splitting tensile strength of NWCA mixtures				
	NWCA+ SLAG	***NWCA+ SLAG+ SLWF***	***NWCA+ FA***	***NWCA+ SLAG + SRA***	***Control mix NWCA***
7	351	310	389	361	427
14	428	356	437	410	627
28	475	421	475	446	665
56	513	478	513	490	694

*All values are in psi.

Table 4-6: Splitting Tensile Strength – LWCA mixtures

Age (days)	Splitting tensile strength of LWCA mixtures				
	LWCA+ SLAG	***LWCA+ SLAG+ SLWF***	***LWCA+ FA***	***LWCA+ SLAG + SRA***	***Control mix LWCA***
7	313	323	327	303	380
14	378	380	380	385	437
28	418	437	435	454	465
56	446	484	489	498	475

*All values are in psi.

4.1.4 Modulus of elasticity

Table *4-7* and **Table *4-8*** show the Modulus of elasticity of mixes in Phase I.

Table 4-7: Modulus of Elasticity – NWCA mixtures

Age (days)	Modulus of elasticity of NWCA mixtures				
	NWCA+ SLAG	***NWCA+ SLAG+ SLWF***	***NWCA+ FA***	***NWCA+ SLAG + SRA***	***Control mix NWCA***
7	3710	3540	4400	3470	3520
14	4270	3620	4450	3910	4360
28	4780	3890	4320	4930	4760
56	5520	4440	4430	5190	5140

*All values are in ksi, rounded to nearest 10.

Table 4-8: Modulus of Elasticity – LWCA mixtures

Age (days)	Modulus of elasticity of NWCA mixtures				
	LWCA+ SLAG	***LWCA+ SLAG+ SLWF***	***LWCA+ FA***	***LWCA+ SLAG + SRA***	***Control mix LWCA***
7	2100	2880	3170	2780	2940
14	2460	2930	3620	3010	2990
28	3420	3310	4250	3530	3490
56	3870	3840	5260	4450	3810

*All values are in ksi, rounded to nearest 10.

4.1.5 Unrestrained Shrinkage

Table 4-9, Table 4-10, Figure 4-3 and Figure 4-4 show the unrestrained shrinkage of the NWCA and LWCA mixes respectively, in Phase I.

Table 4-9: Unrestrained Shrinkage of NWCA Mixtures

Age (days)	Unrestrained Shrinkage of NWCA mixtures				
	NWCA+ SLAG	***NWCA+ SLAG+ SLWF***	***NWCA+ FA***	***NWCA+ SLAG + SRA***	***Control mix NWCA***
7	221	296	141	181	108
14	374	437	284	281	340
28	458	515	433	457	455
56	587	568	494	501	570

*All values are in -1 x micro strain.

Table 4-10: Unrestrained Shrinkage of LWCA Mixtures

Age (days)	Unrestrained Shrinkage of LWCA mixtures				
	LWCA+ SLAG	***LWCA+ SLAG+ SLWF***	***LWCA+ FA***	***LWCA+ SLAG + SRA***	***Control mix LWCA***
7	136	303	50	105	143
14	375	542	275	225	292
28	470	718	387	332	442
56	561	750	462	469	547

*All values are in -1 x micro strain.

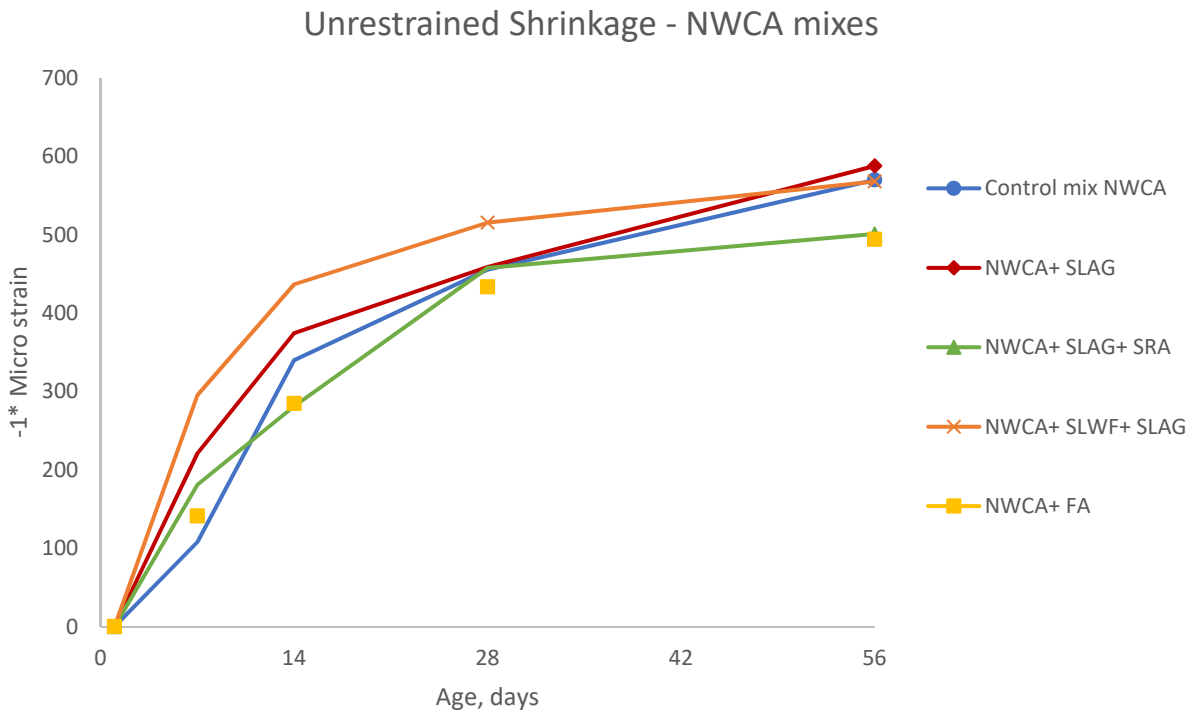

Figure 4-3: Unrestrained Shrinkage of NWCA Mixtures

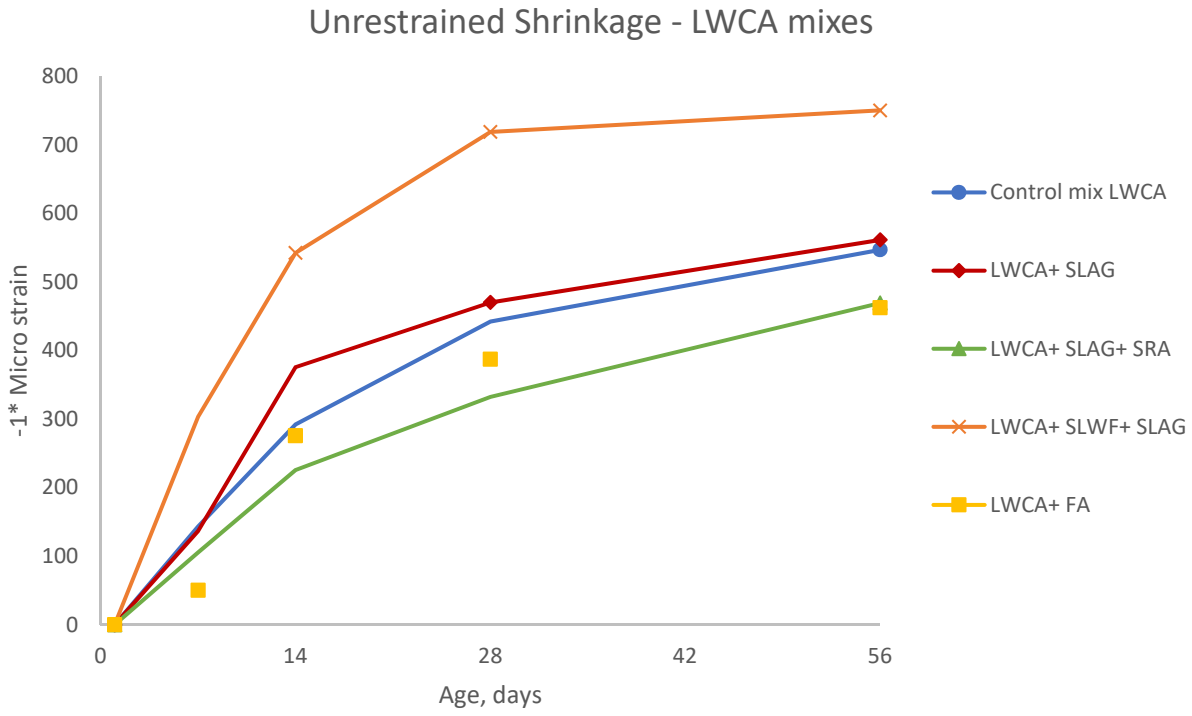

Figure 4-4: Unrestrained Shrinkage of LWCA Mixtures

4.2 Results – Phase II

From the results obtained in Phase I, the four best performing mix designs were selected based on their compressive strength and unrestrained shrinkage performance. The four mixtures selected were:

- LWCA+SLAG+SRA
- NWCA+SLAG+SRA
- LWCA+FA
- NWCA+FA

These four mixes were tested for compressive strength, splitting tensile strength, modulus of elasticity, unrestrained shrinkage and creep (compressive and tensile). The data from shrinkage and creep for the mixes in Phase II was used in a parametric study to investigate the stresses at the bottom of deck due to shrinkage and creep of concrete. This section presents these results and they are further discussed in Chapter 5.2

4.2.1 Fresh Concrete Properties

Table *4-11* shows the fresh concrete properties observed for the mixes in Phase II.

Table 4-11: Fresh Concrete Properties, Phase II

Property/ Batch	LWCA+ SLAG+ SRA	NWCA+ SLAG+ SRA	LWCA+ FA	NWCA+ FA
Slump (in.)	6.5	6.5	7.5	5.5
Air content-%	7	5.5	7.5	7
Unit weight lb/yd^3	116	143	117	142

4.2.2 Compressive Strength

Table *4-12* shows the compressive strength data for mixes in Phase II.

Table 4-12: Compressive Strength of Mixes in Phase II

Age, days	Compressive strength – Phase II			
	LWCA+ SLAG+ SRA	NWCA+ SLAG+ SRA	LWCA+ FA	NWCA+ FA
7	3510	4890	3840	4370
14	3590	5580	4070	4630
28	5540	6830	4690	5310
56	6670	6880	5730	5560

*All values are in psi, rounded to nearest 10.

4.2.3 Splitting Tensile Strength

Table *4-13* shows the splitting tensile strength of mixes used in Phase II.

Table 4-13: Splitting Tensile Strength of Mixes in Phase II

Age, days	Splitting tensile strength – Phase II			
	LWCA+ SLAG+ SRA	**NWCA+ SLAG+ SRA**	**LWCA+ FA**	**NWCA+ FA**
7	314	370	380	318
14	380	399	404	399
28	418	446	427	484
56	466	475	461	513

*All values are in psi.

4.2.4 Modulus of Elasticity

Table 4-14 shows the modulus of elasticity of mixes in Phase II.

Table 4-14: Modulus of Elasticity of Mixes in Phase II

Age, days	Modulus of Elasticity – Phase II			
	LWCA+ SLAG+ SRA	**NWCA+ SLAG+ SRA**	**LWCA+ FA**	**NWCA+ FA**
7	2180	3760	-	3570
14	2530	5020	2810	4880
28	3190	-	3080	5540
56	3510	5290	3440	5820

*All values are in ksi, rounded to nearest 10.

4.2.5 Unrestrained Shrinkage

Figure *4-5* shows the unrestrained shrinkage of the specimens in Phase II.

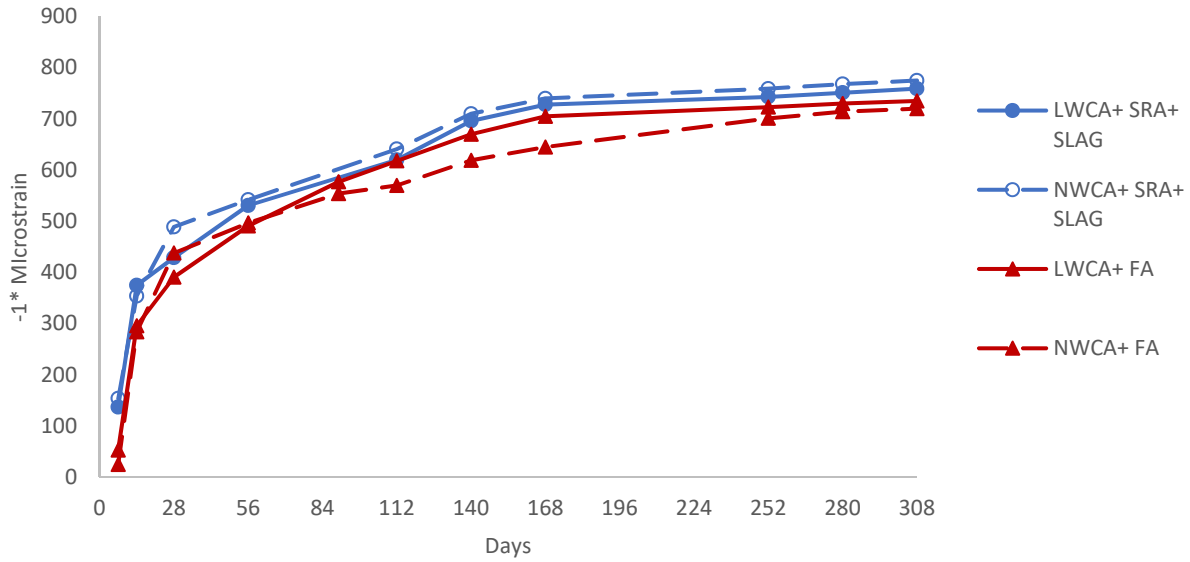

Figure 4-5: Unrestrained Shrinkage of Mixes in Phase II
*NWCA mixes shown in Dashed lines, LWCA mixes shown in solid lines.

4.2.6 Compressive Creep

Figure *4-6* to **Figure *4-9*** show the results of compressive creep testing.

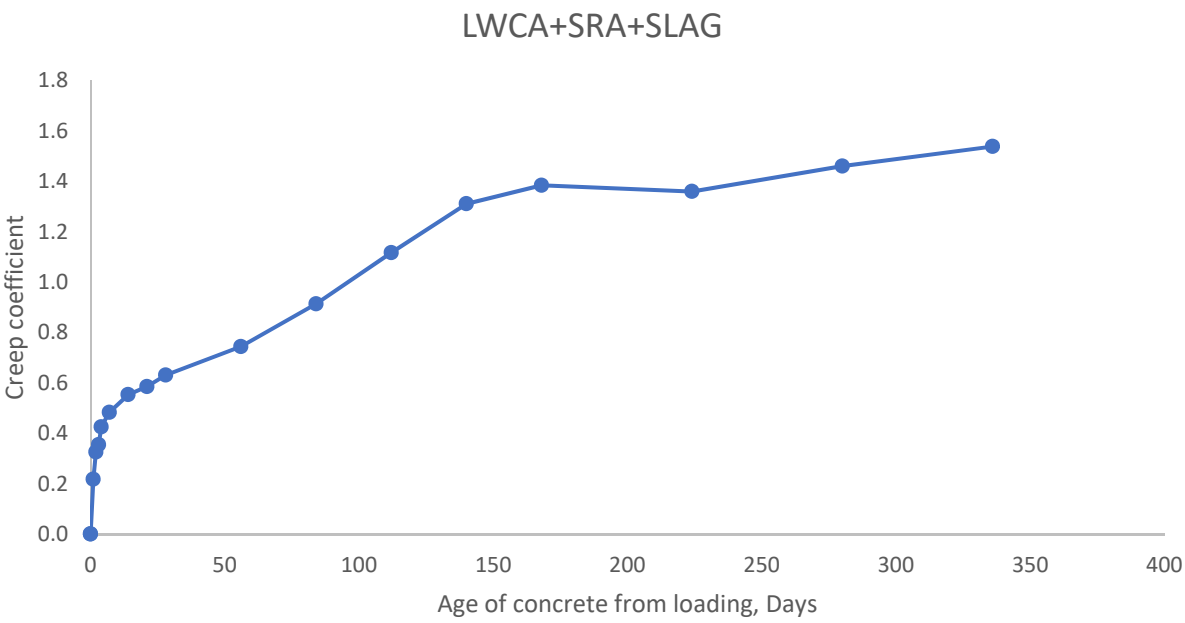

Figure 4-6: Creep Coefficient, LWCA+ SRA+ SLAG

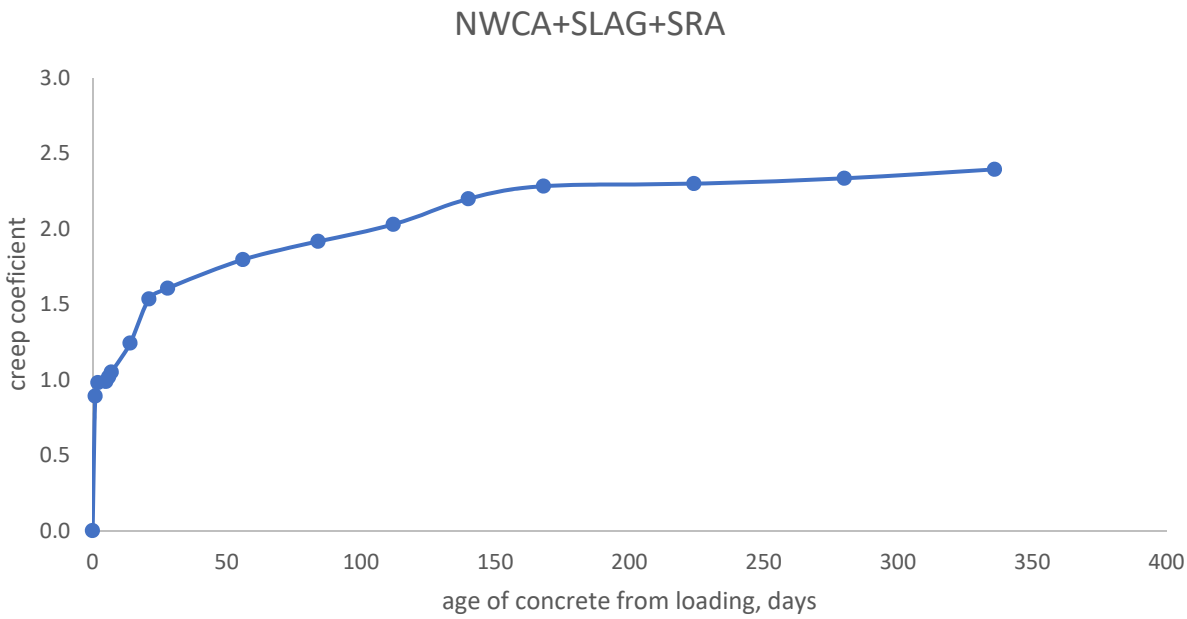

Figure 4-7: Creep Coefficient, NWCA+ SRA+ SLAG

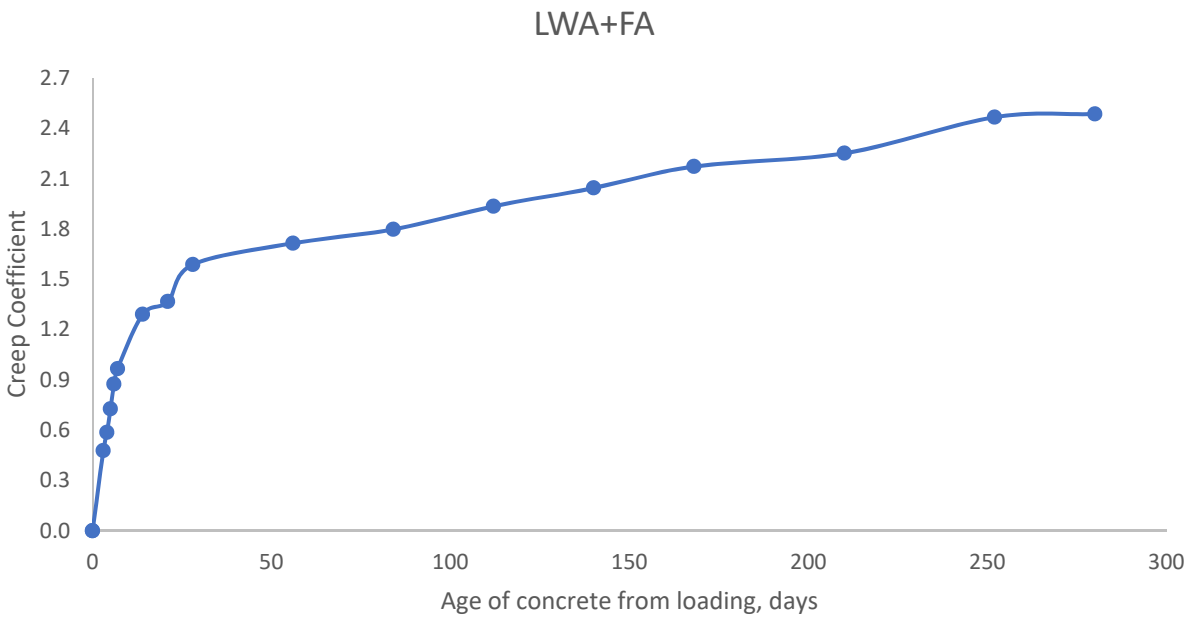

Figure 4-8: Creep Coefficient, LWCA+ FA

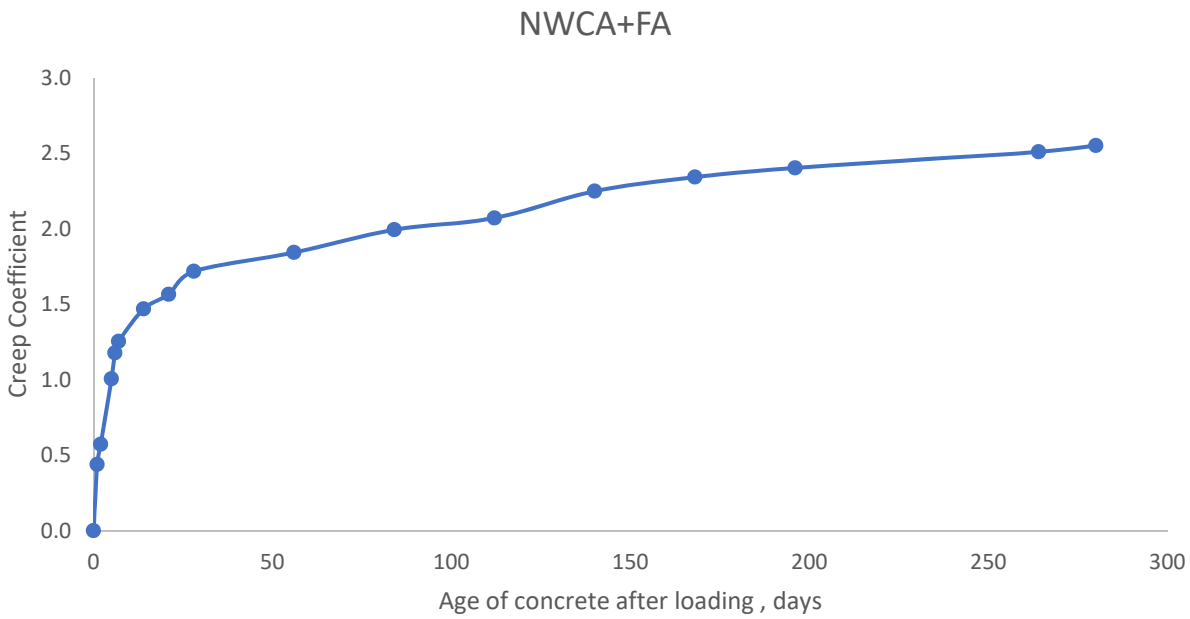

Figure 4-9: Creep Coefficient, NWCA+ FA

4.2.7 Tensile Creep

The tensile creep specimen for LWCA+SRA+SLAG mix broke at an early age while testing, the specimen for NWCA with slag and SRA when loaded to 40% of tensile strength at the day of testing began to shrink even after applying the load. The collection of tensile creep data for these specimens was not continued. Thus, there is no data to help analyze the behavior of concrete subjected to sustained tension.

4.2.8 Age Adjusted Effective Modulus Method

As mentioned in the methods section, based on the results of Phase II, it was determined that the best model to predict creep and shrinkage of the topping concrete mixtures was the ACI 209 model. Therefore this model was used to predict the time dependent properties of the mixtures at 20 years after construction. Based on baseline properties the stresses through the depth of the section were determined. Table 4-15 shows the stresses in the composite section for all the mixes in Phase II. In all the tables, tension is considered positive and compression is considered as negative.

A parametric study was then conducted to determine the influence of saturating the precast element prior to placing the topping concrete. This was accomplished by varying the V/S ratio, with small ratios representing the dry condition, so moisture can leave the topping concrete in two directions. The large ratio represents the saturated condition, so moisture only leaved the topping in one direction.

Table ***4-16*** to Table 4-19 show the calculated stresses in the deck at various levels in the cross section for varying volume to surface ratios of the deck. Variation in V/S ratio of girder has no effect on stresses in the section.

Table 4-15: Stresses in Section for Mixes in Phase II

Depth from bottom		LWCA+SLAG+SRA	NWCA+SRA+SLAG	LWCA+ FA	NWCA+ FA
Stress at top of deck	25	0.241	0.205	0.249	0.217
Stress at center of deck	21.5	0.309	0.263	0.316	0.277
Stress at bottom of deck	18	0.377	0.322	0.384	0.338
Stress at top of beam	18	-0.481	-0.404	-0.493	-0.428
Stress at center of beam	9	-0.090	-0.075	-0.093	-0.08
Stress at bottom of beam	0	0.300	0.254	0.308	0.268

All stresses are in ksi, depth in in,

Table 4-16: Stresses in the Section for Varying V/S Ratio of Deck – LWCA+SLAG+ SRA

Location	Depth from bottom of section, in.	V/S Deck = 2	V/S Deck = 3.5	V/S Deck = 7
Top of deck	25	0.242	0.198	0.112
Mid-height of deck	21.5	0.312	0.262	0.15
Bottom of deck	18	0.383	0.326	0.188
Top of beam	18	-0.486	-0.401	-0.215
Mid-height of beam	9	-0.092	-0.075	-0.037
Bottom of beam	0	0.303	0.252	0.14

All stresses are in ksi, depth in in, V/S in in.

Table 4-17: Stresses in the Section for Varying V/S Ratio of Deck –NLWCA+SLAG+ SRA

	Depth from bottom ofsection, in.	V/S Deck = 2	V/S Deck = 3.5	V/S Deck = 7
Stress at top of deck	25	0.205	0.166	0.092
Stress at center of deck	21.5	0.263	0.219	0.122
Stress at bottom of deck	18	0.322	0.272	0.152
Stress at top of beam	18	-0.404	-0.33	-0.168
Stress at center of beam	9	-0.075	-0.06	-0.028
Stress at bottom of beam	0	0.254	0.209	0.112

All stresses are in ksi, depth in in, V/S in in.

Table 4-18: Stresses in the Section for Varying V/S Ratio of Deck – LWCA+ FA

	Depth from bottom of section, in.	V/S Deck = 2	V/S Deck = 3.5	V/S Deck = 7
Stress at top of deck	25	0.258	0.211	0.121
Stress at center of deck	21.5	0.336	0.282	0.163
Stress at bottom of deck	18	0.413	0.352	0.205
Stress at top of beam	18	-0.525	-0.434	-0.237
Stress at center of beam	9	-0.099	-0.081	-0.042
Stress at bottom of beam	0	0.326	0.271	0.153

All stresses are in ksi, depth in in, V/S in in.

Table 4-19: Stresses in the Section for Varying V/S Ratio of Deck – NWCA+ FA

	Depth from bottom of section	V/S Deck = 2	V/S Deck = 3.5	V/S Deck = 7
Stress at top of deck	25	0.217	0.177	0.099
Stress at center of deck	21.5	0.277	0.232	0.131
Stress at bottom of deck	18	0.338	0.287	0.163
Stress at top of beam	18	-0.428	-0.351	-0.183
Stress at center of beam	9	-0.08	-0.065	-0.031
Stress at bottom of beam	0	0.268	0.222	0.121

All stresses are in ksi, depth in in, V/S in in.

Another parametric study was performed to investigate the influence of slump. Since the mixtures tested had chemical admixtures to increase slump, the actual slump, before the admixtures, was not known. The study was performed to determine how sensitive the results are with respect to slump. Table 4-20 to Table 4-23 shows the stresses and strains at various levels of the cross section for varying slump and a constant V/S ratio of 3.5 and 9 in. for deck and girder respectively.

Table 4-20: Stresses in the Section for Varying Slump – LWCA+SLAG+ SRA

	Depth from Bottom, in.	Slump, in.			
		3	4.5	6	7.5
Stress at top of deck	25	0.189	0.202	0.214	0.225
Stress at center of deck	21.5	0.253	0.266	0.278	0.290
Stress at bottom of deck	18	0.317	0.330	0.342	0.354
Stress at top of beam	18	-0.387	-0.408	-0.429	-0.448
Stress at center of beam	9	-0.072	-0.076	-0.08	-0.084
Stress at bottom of beam	0	0.243	0.256	0.268	0.280

All stresses are in ksi,

Table 4-21: Stresses in the Section for Varying Slump– NWCA+SLAG+ SRA

	Depth from Bottom, in.	Slump, in.			
		3	4.5	6	7.5
Stress at top of deck	25	0.159	0.170	0.180	0.190
Stress at center of deck	21.5	0.212	0.223	0.233	0.244
Stress at bottom of deck	18	0.264	0.276	0.287	0.297
Stress at top of beam	18	-0.318	-0.336	-0.355	-0.372
Stress at center of beam	9	-0.058	-0.062	-0.065	-0.069
Stress at bottom of beam	0	0.202	0.213	0.224	0.235

All stresses are in ksi,

Table 4-22: Stresses in the Section for Varying Slump – LWCA+ FA

	Depth from Bottom, in.	Slump, in.			
		3	4.5	6	7.5
Stress at top of deck	25	0.196	0.208	0.22	0.232
Stress at center of deck	21.5	0.258	0.271	0.282	0.293
Stress at bottom of deck	18	0.321	0.333	0.344	0.355
Stress at top of beam	18	-0.395	-0.416	-0.436	-0.455
Stress at center of beam	9	-0.073	-0.078	-0.082	-0.085
Stress at bottom of beam	0	0.248	0.261	0.273	0.285

All stresses are in ksi,

Table 4-23: Stresses in the Section for Varying Slump – NWCA+ FA

	Depth from Bottom, in.	Slump, in.			
		3	4.5	6	7.5
Stress at top of deck	25	0.169	0.181	0.191	0.202
Stress at center of deck	21.5	0.224	0.236	0.246	0.257
Stress at bottom of deck	18	0.279	0.291	0.301	0.312
Stress at top of beam	18	-0.339	-0.358	-0.376	-0.394
Stress at center of beam	9	-0.062	-0.066	-0.07	-0.073
Stress at bottom of beam	0	0.214	0.226	0.237	0.248

All stresses are in ksi,

5 RESULT AND DISCUSSIONS

5.1 Phase I

5.1.1 Compressive Strength

All the design mixes had a compressive strength more than 4000 psi at 28 days. The addition of fly ash reduces the early age strength and increases the later age strength. The mixes with fly ash had lower strength at 28 days compared to other mixes. Mixes with slag performed better compared to mixes with fly ash in terms of compressive strength. The strength of mixes with LWCA is lower than that of NWCA mixes. Using LWCA and, slag resulted in higher strength concrete.

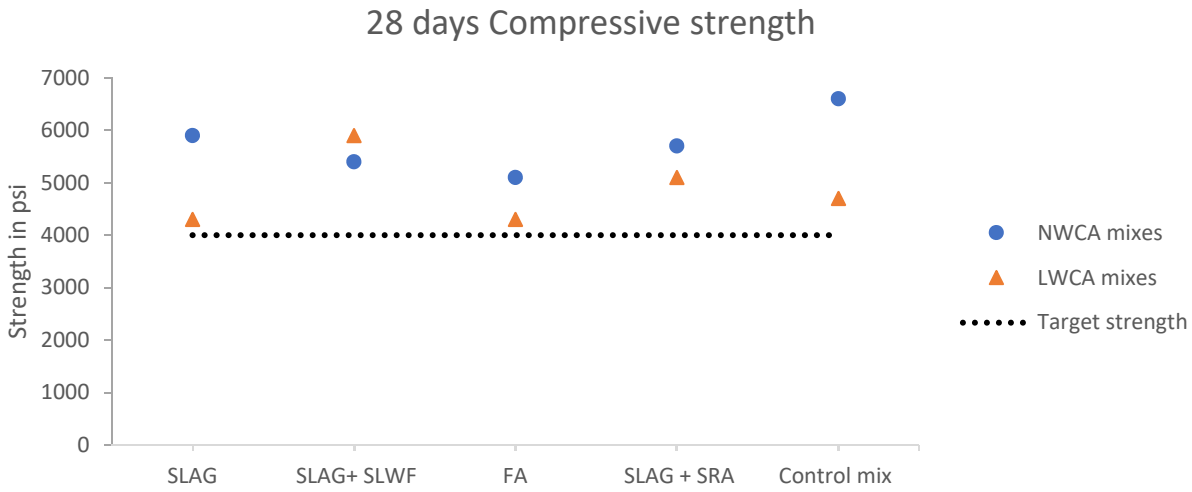

Figure 5-1: Comparison of 28-day Compressive Strength- Phase I

5.1.2 Splitting Tensile Strength

Figure 5-2 shows the comparison of LWCA and NWCA mixes. Figure 5-3 to Figure 5-12 compare the measured tensile strength to the value given by ACI 318-14 (ACI 318, 2014).

$$f_t = 6.7 * \sqrt{f_c} \qquad \text{Equation 5-1}$$

where f_c is the mean compressive strength on the day of testing.

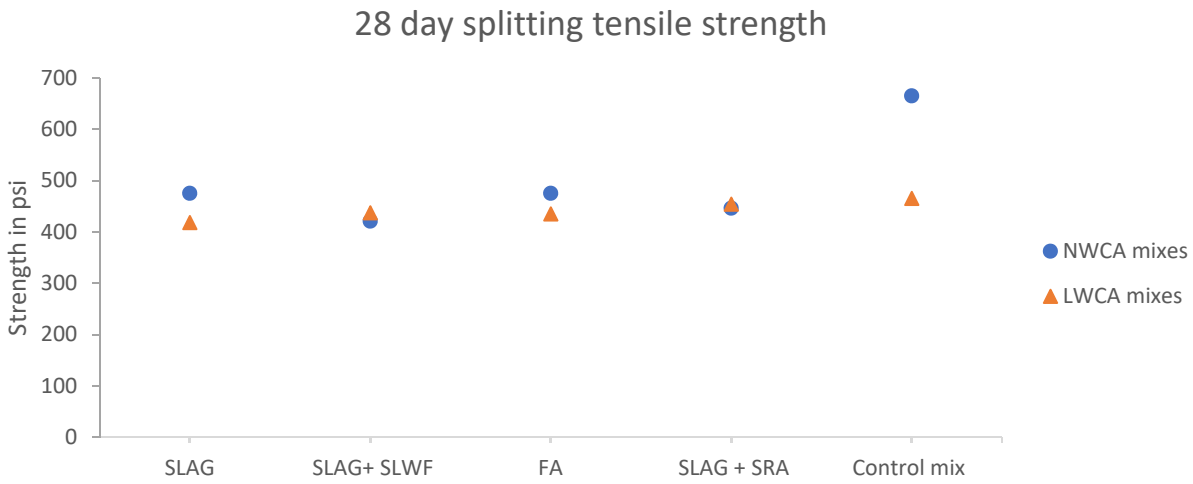

Figure 5-2: Comparison of 28-day Splitting Tensile Strength, Phase I

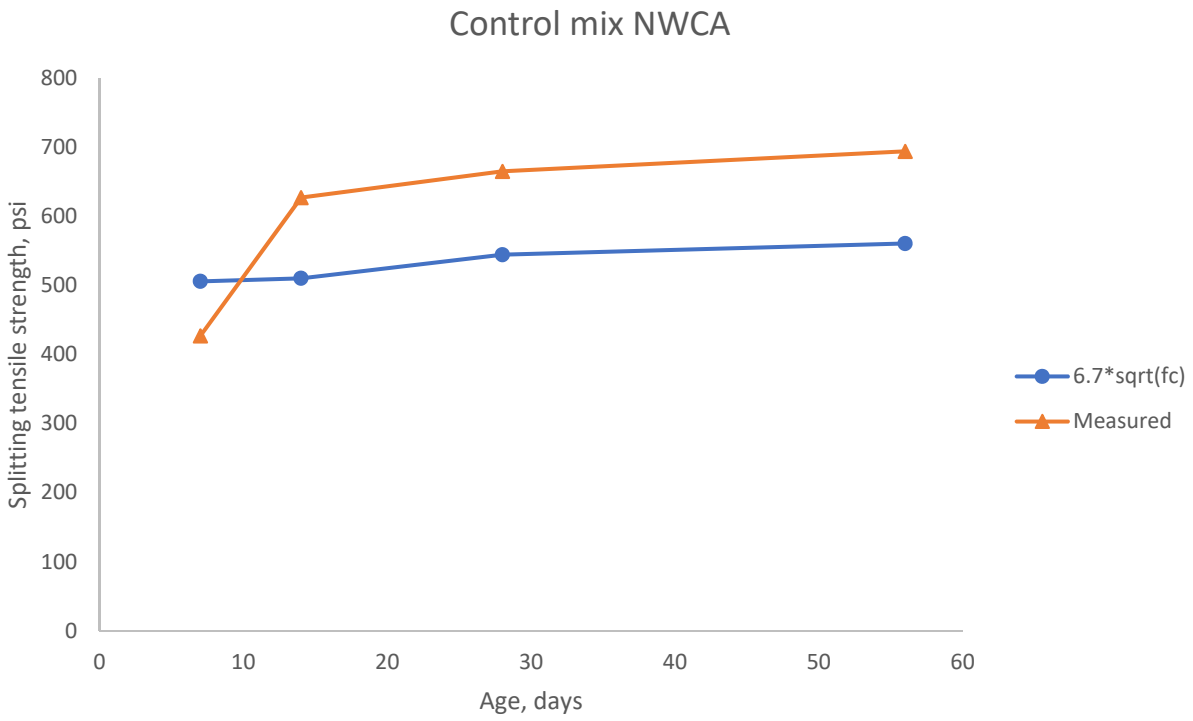

Figure 5-3: Splitting Tensile Strength Control Mix NWCA

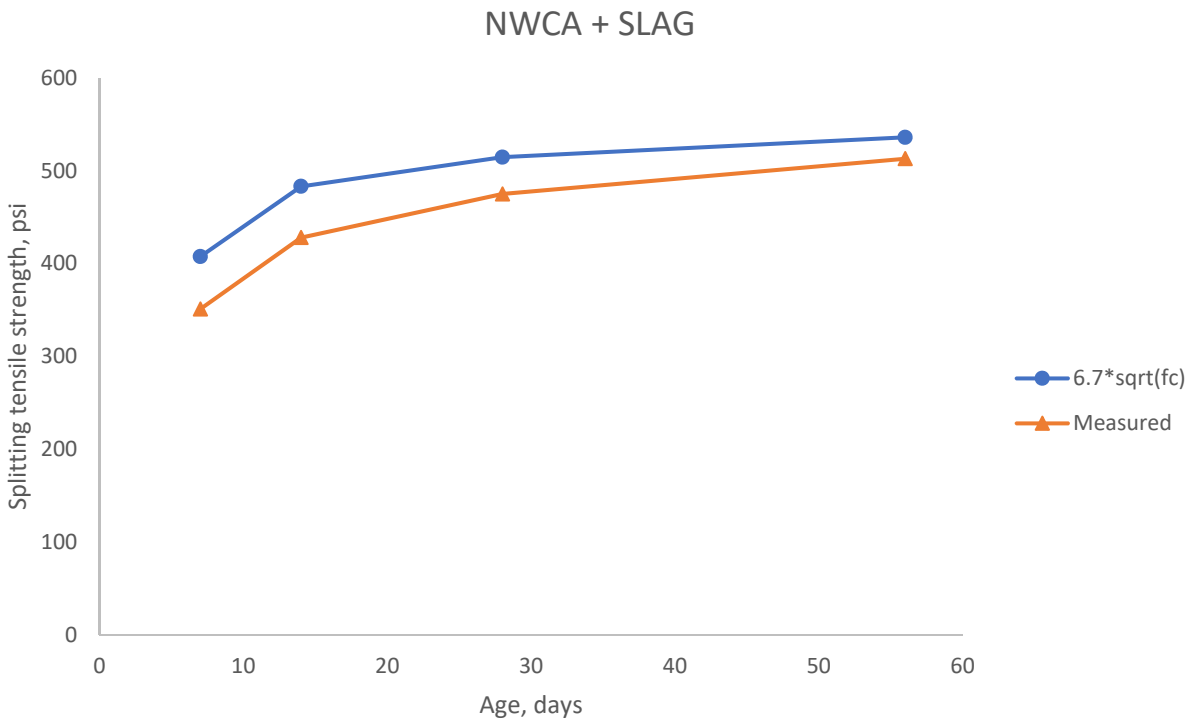

Figure 5-4: Splitting Tensile Strength NWCA + SLAG

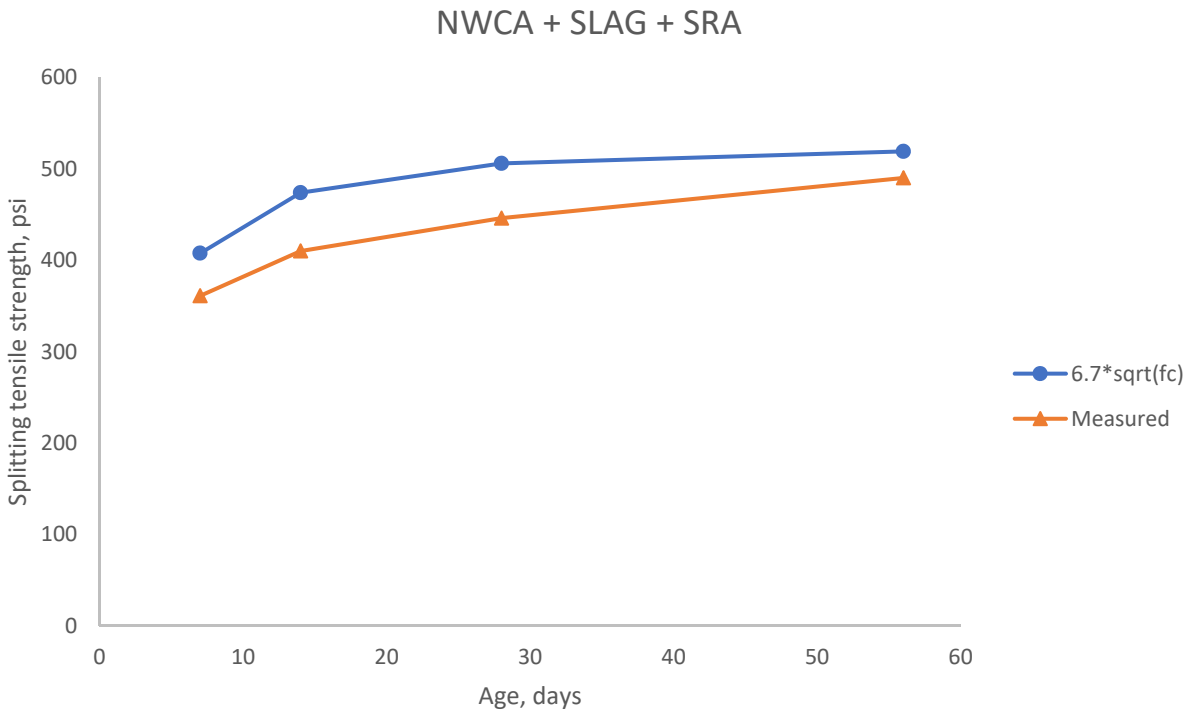

Figure 5-5: Splitting Tensile Strength NWCA +SLAG + SRA

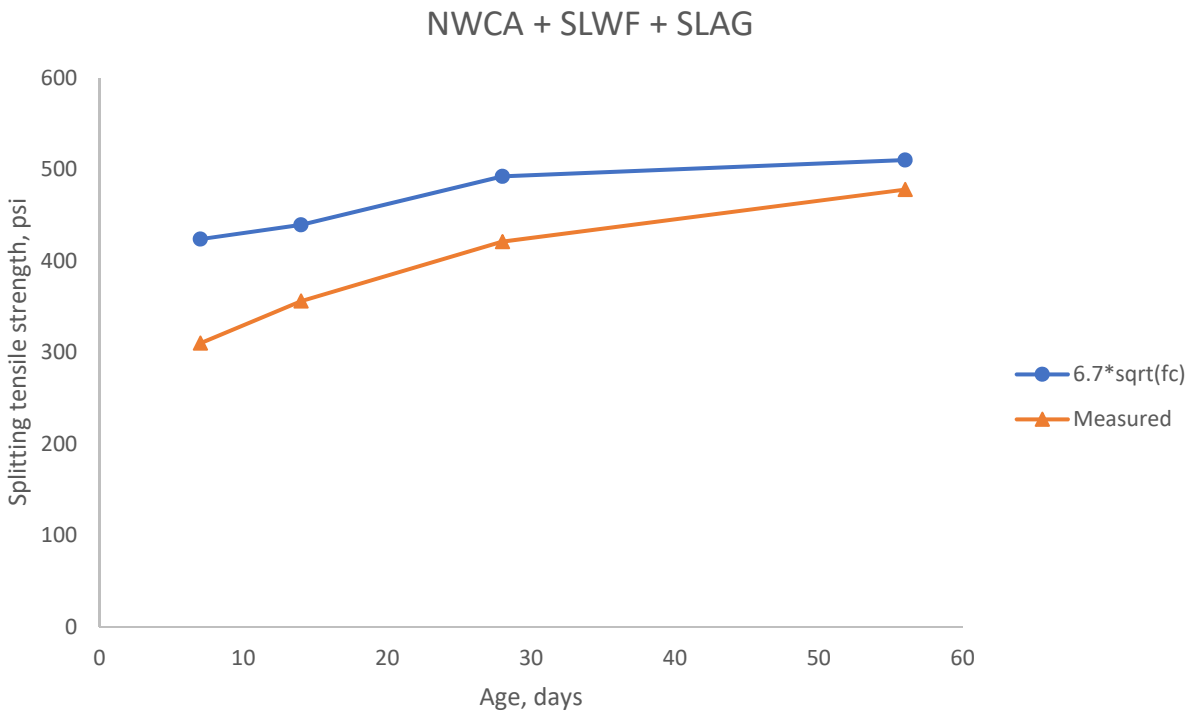

Figure 5-6: Splitting Tensile Strength NWCA +SLWF+ SLAG

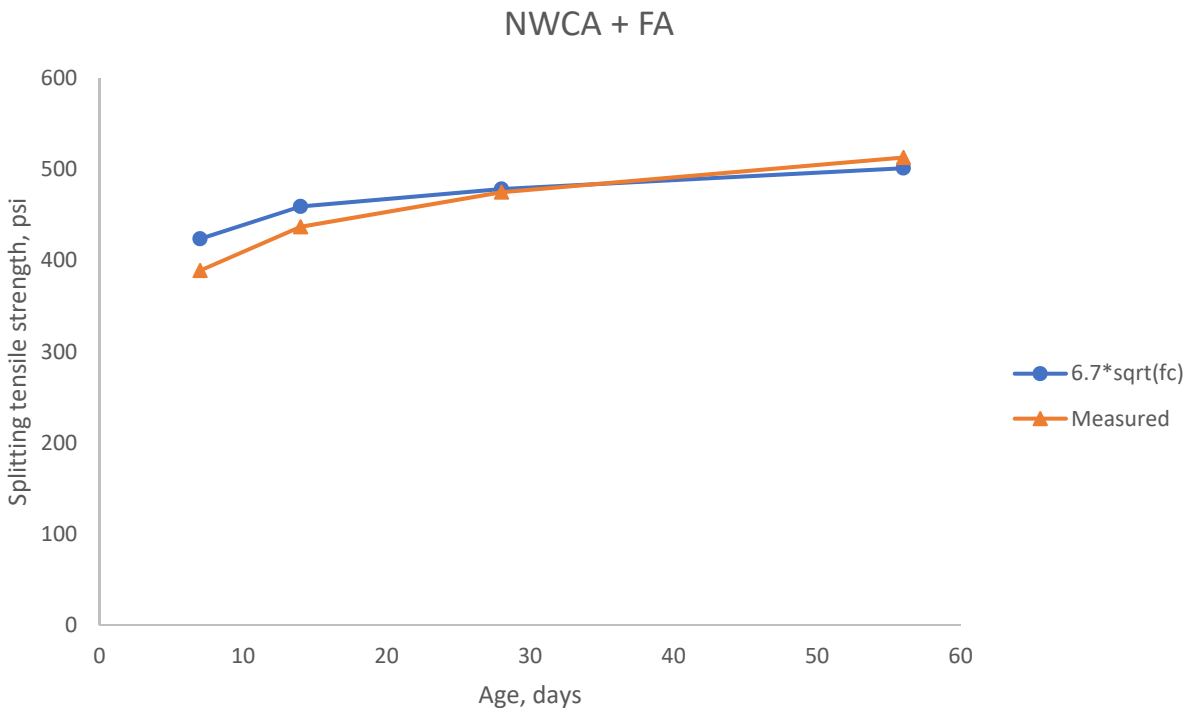

Figure 5-7: Splitting Tensile Strength NWCA +FA

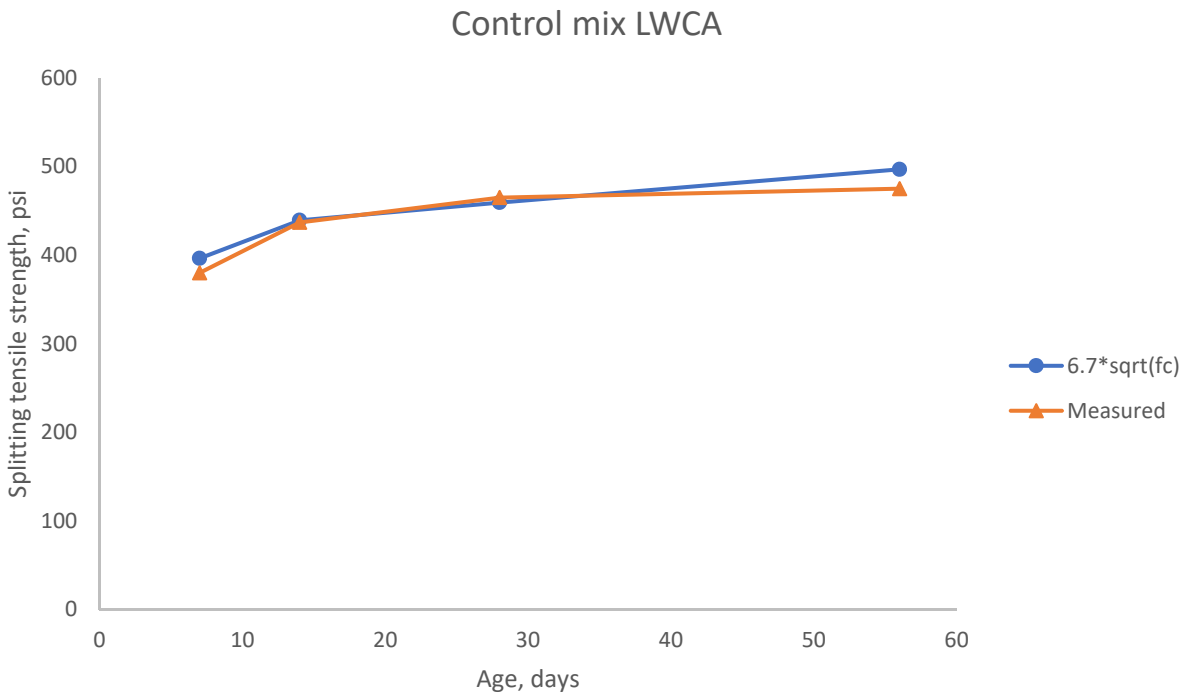

Figure 5-8: Splitting Tensile Strength Control Mix LWCA

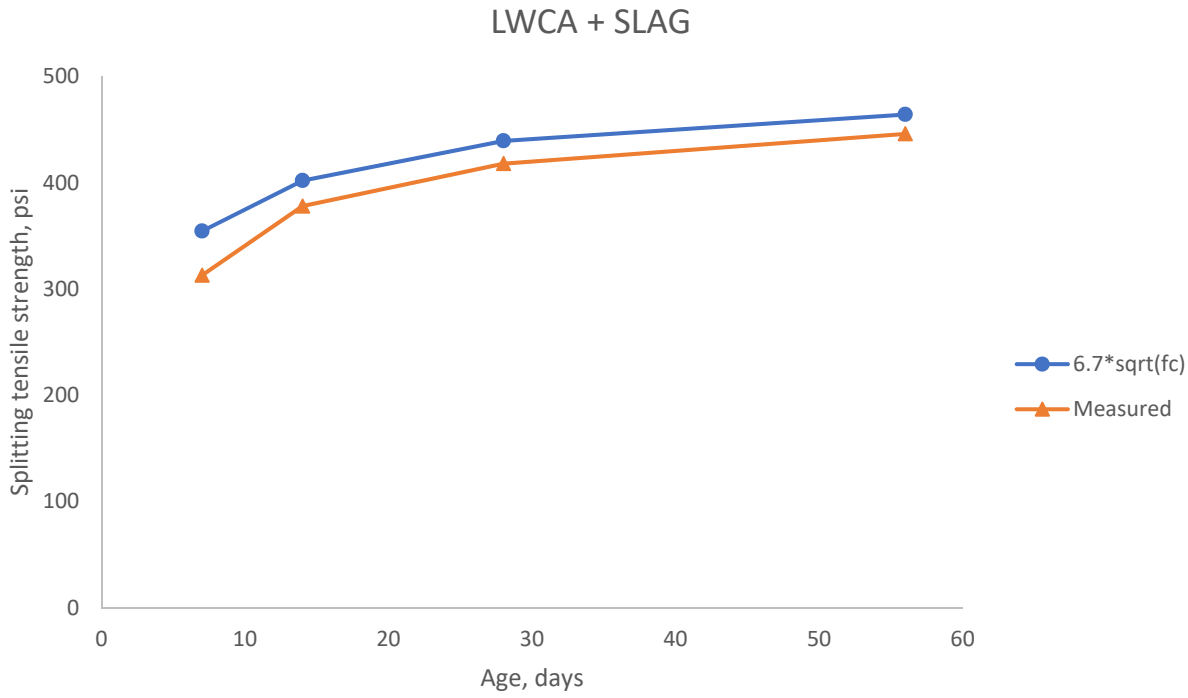

Figure 5-9: Splitting Tensile Strength LWCA + SLAG

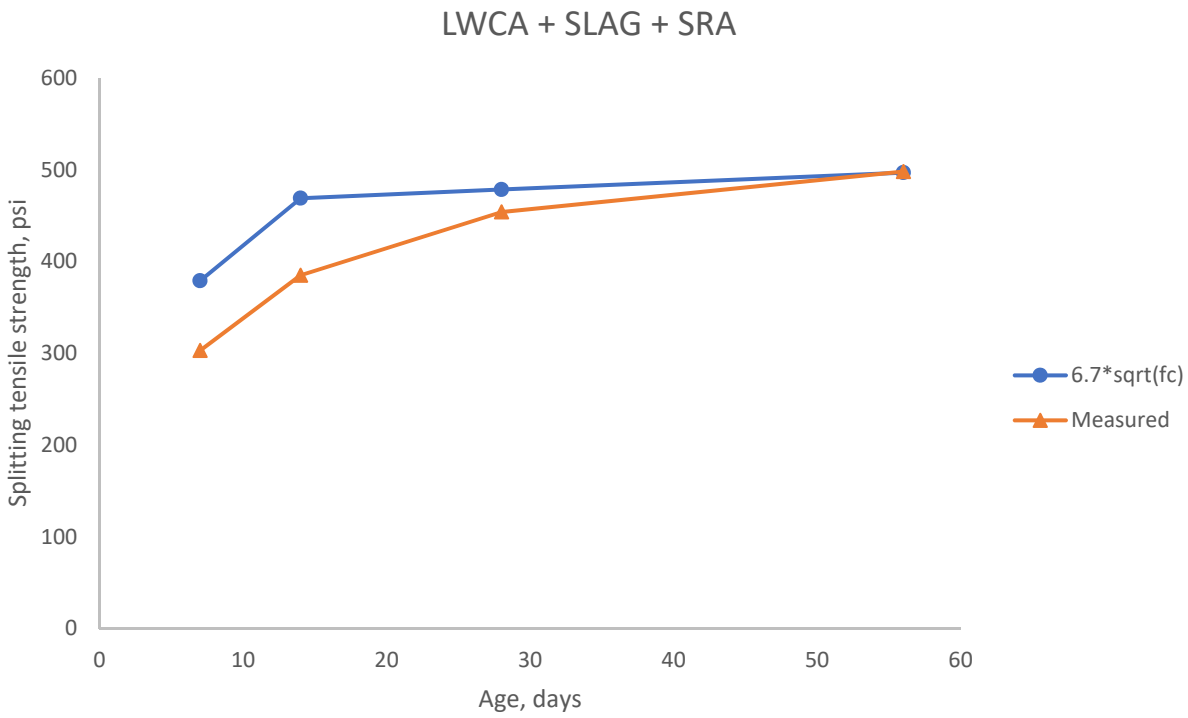

Figure 5-10: Splitting Tensile Strength LWCA + SLAG+ SRA

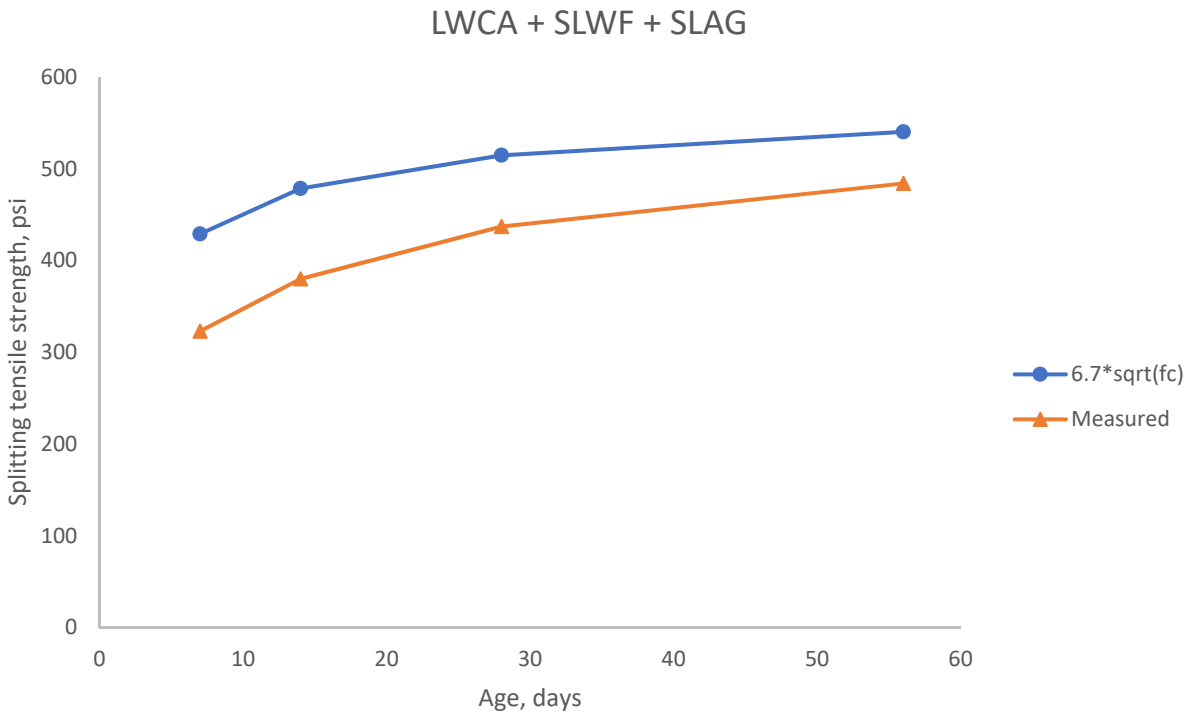

Figure 5-11: Splitting Tensile Strength LWCA + SLWF + SLAG

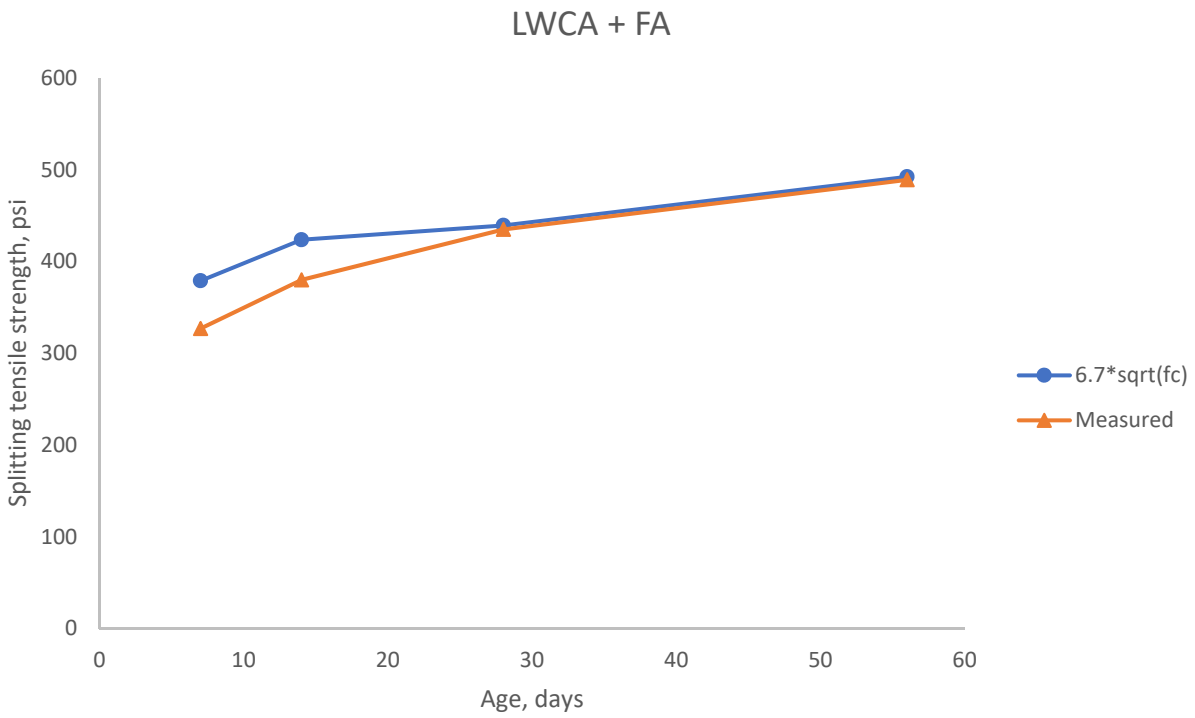

Figure 5-12: Splitting Tensile Strength LWCA + FA

As expected, the mixes with LWCA had lower splitting tensile strength than the mixes with NWCA. The mixes with slag as SCM showed lower tensile strength than the calculated tensile strength using Equation 5-1. Mixes with fly ash as SCM displayed strengths consistent with the calculated strength. Their strength was lower initially but then increased with age of concrete. This is attributed to the lower early age compressive strength of mixes with fly ash.

The control mix with no SCM and with NWCA displayed higher tensile strength than calculated, while the control mix with no SCM and with LWCA exhibited tensile strengths very similar to the calculated values.

5.1.3 Modulus of Elasticity

Figure 5-13 shows the comparison between modulus of elasticity of LWCA and NWCA mixes. Figure 5-14 to Figure 5-23 compare the measured modulus of elasticity to the value given by ACI 318-14.

$$E = 33.3 * w^{1.5} * \sqrt{f_c} \qquad \text{Equation 5-2}$$

where f_c is the mean compressive strength on the day of testing, w is the unit weight in lb/yd^3.

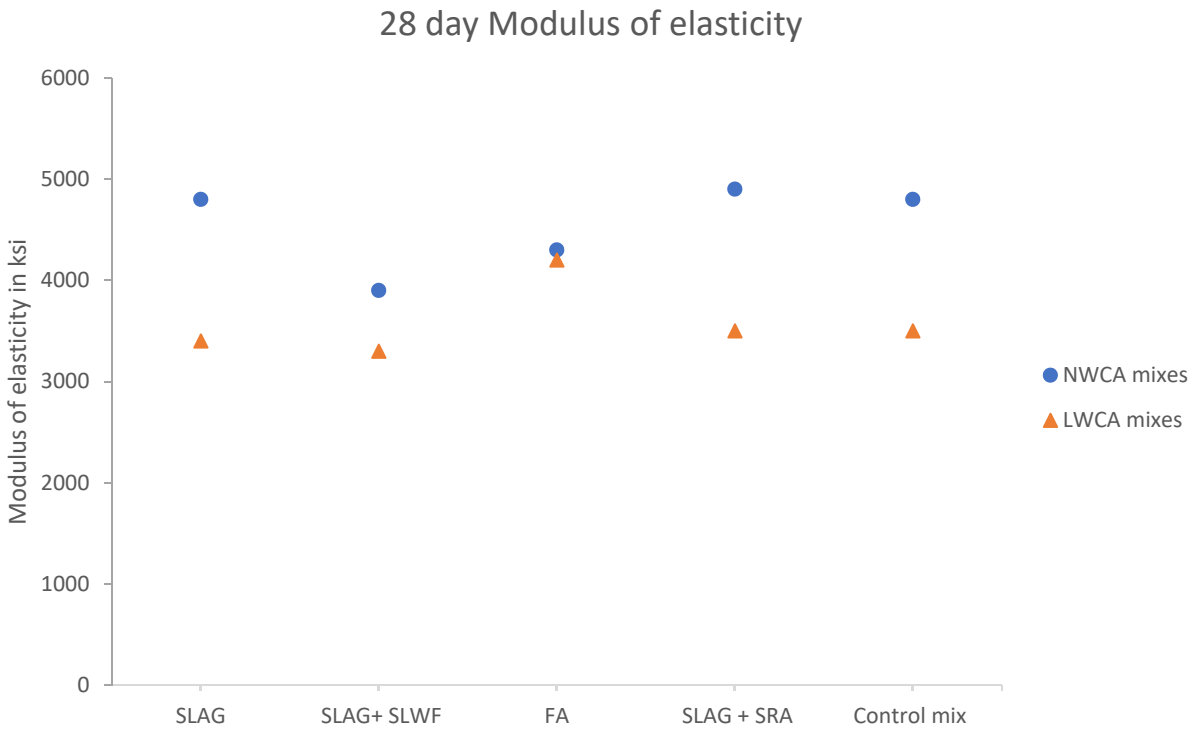

Figure 5-13: Comparison of 28-day Modulus of Elasticity, Phase I

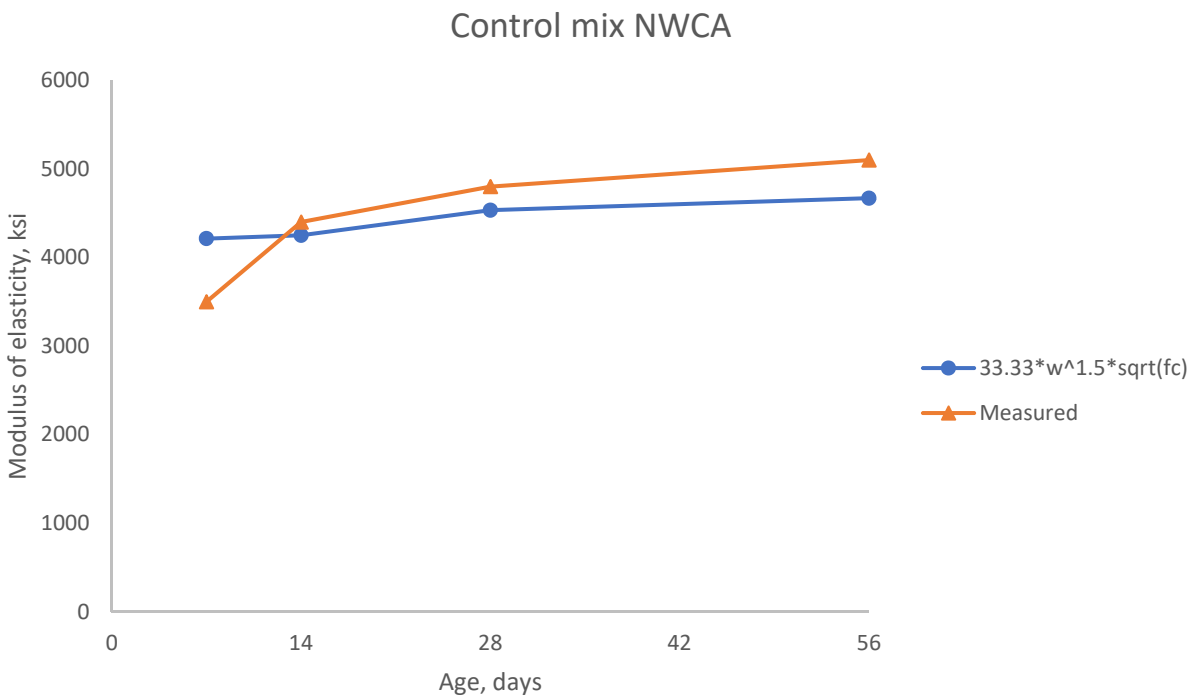

Figure 5-14: Modulus of Elasticity, Control Mix NWCA

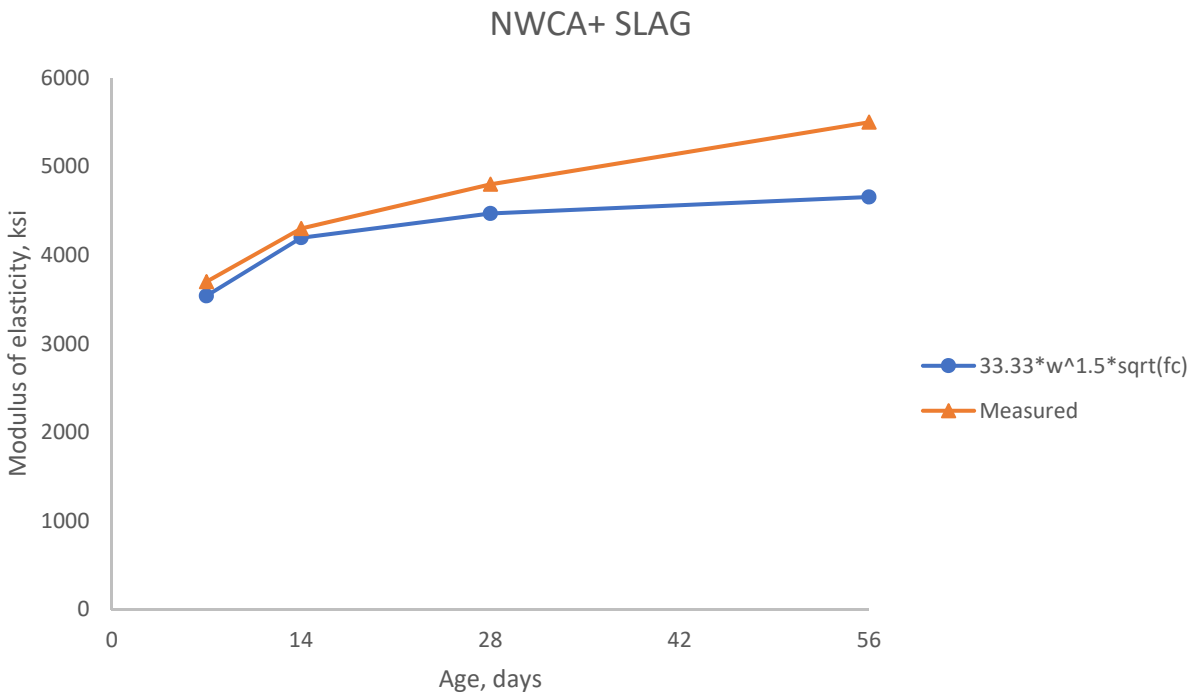

Figure 5-15: Modulus of Elasticity, NWCA+ SLAG

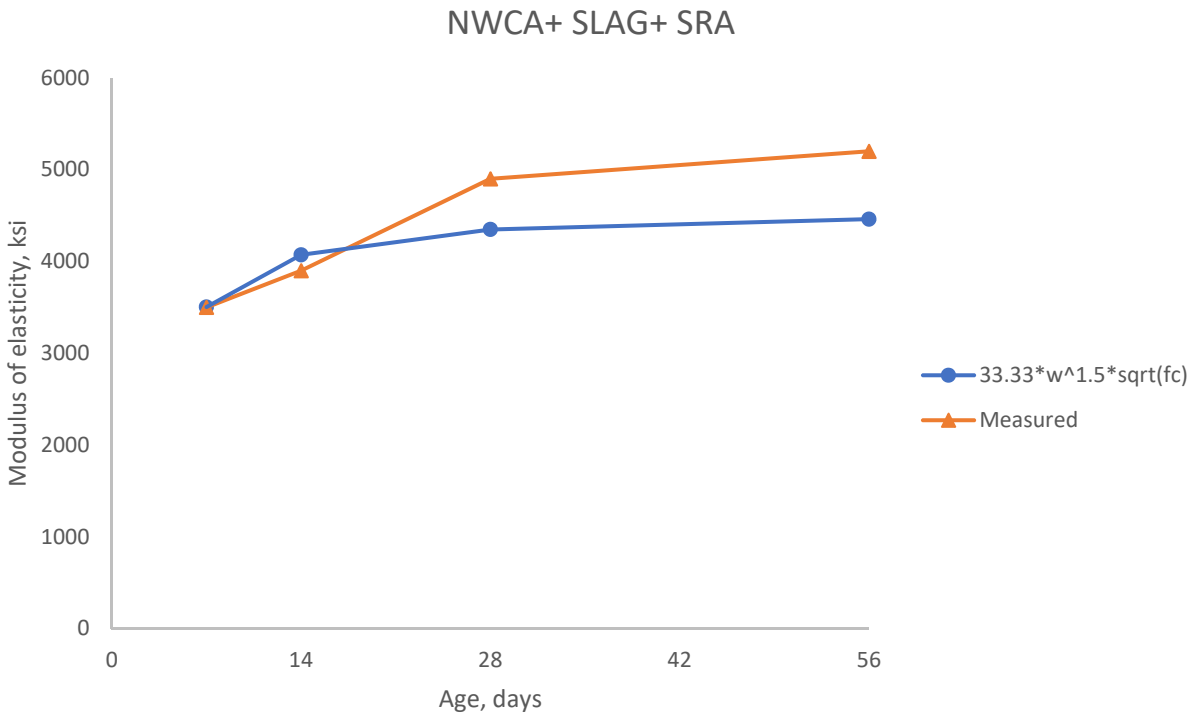

Figure 5-16: Modulus of Elasticity, NWCA+ SLAG+ SRA

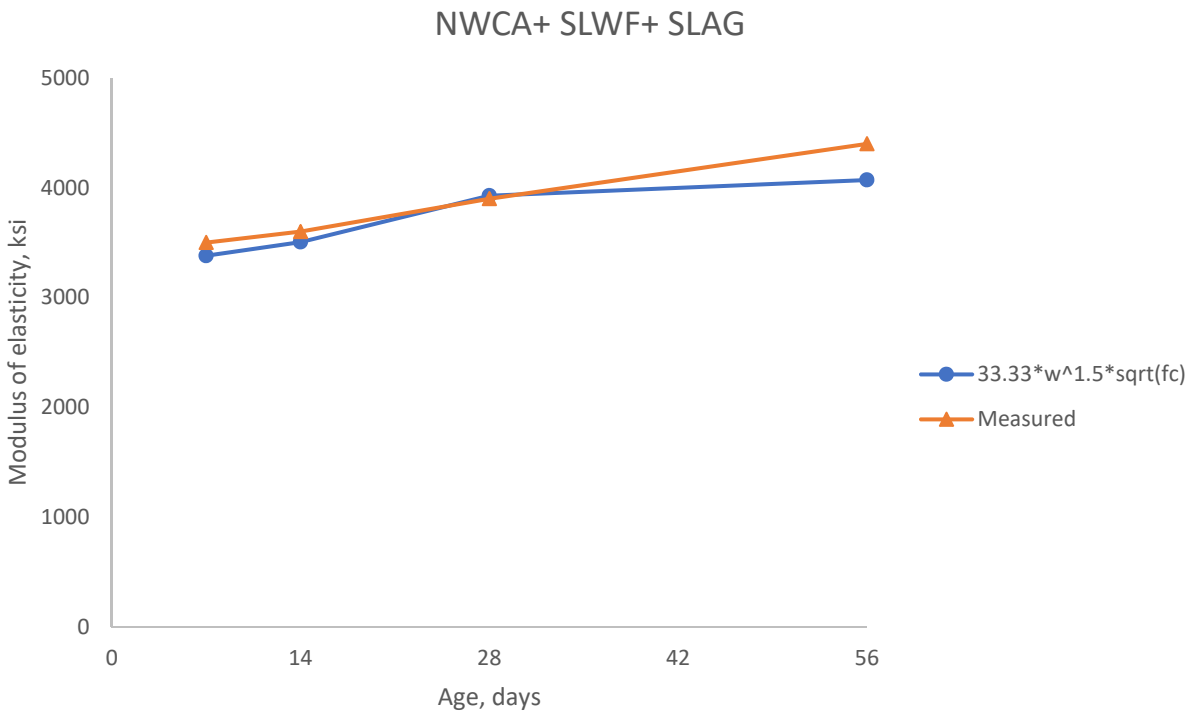

Figure 5-17: Modulus of Elasticity, NWCA+ SLWF+ SLAG

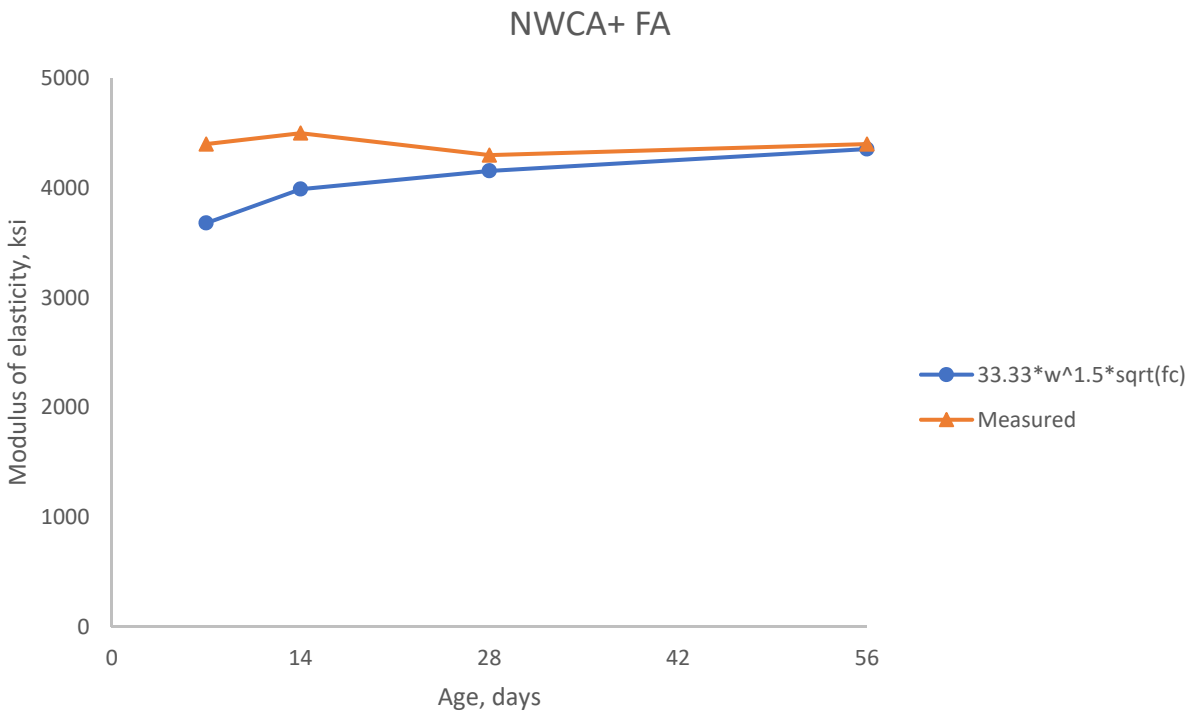

Figure 5-18: Modulus of Elasticity, NWCA+ FA

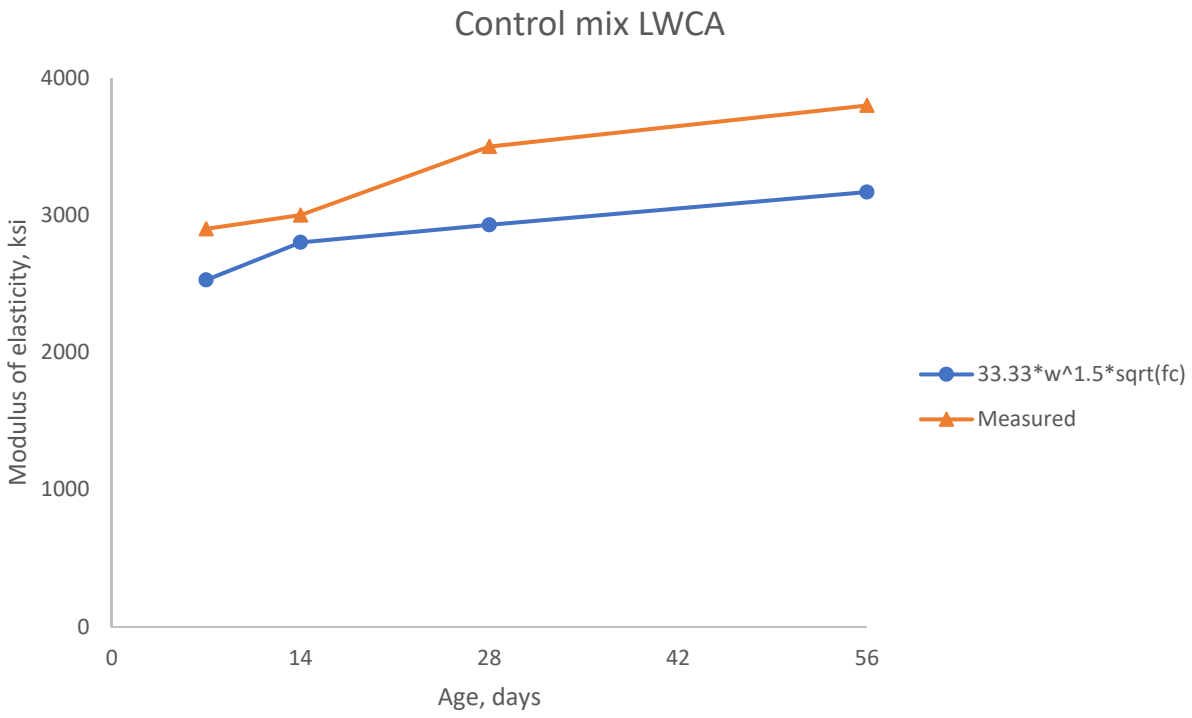

Figure 5-19: Modulus of Elasticity, Control mix LWCA

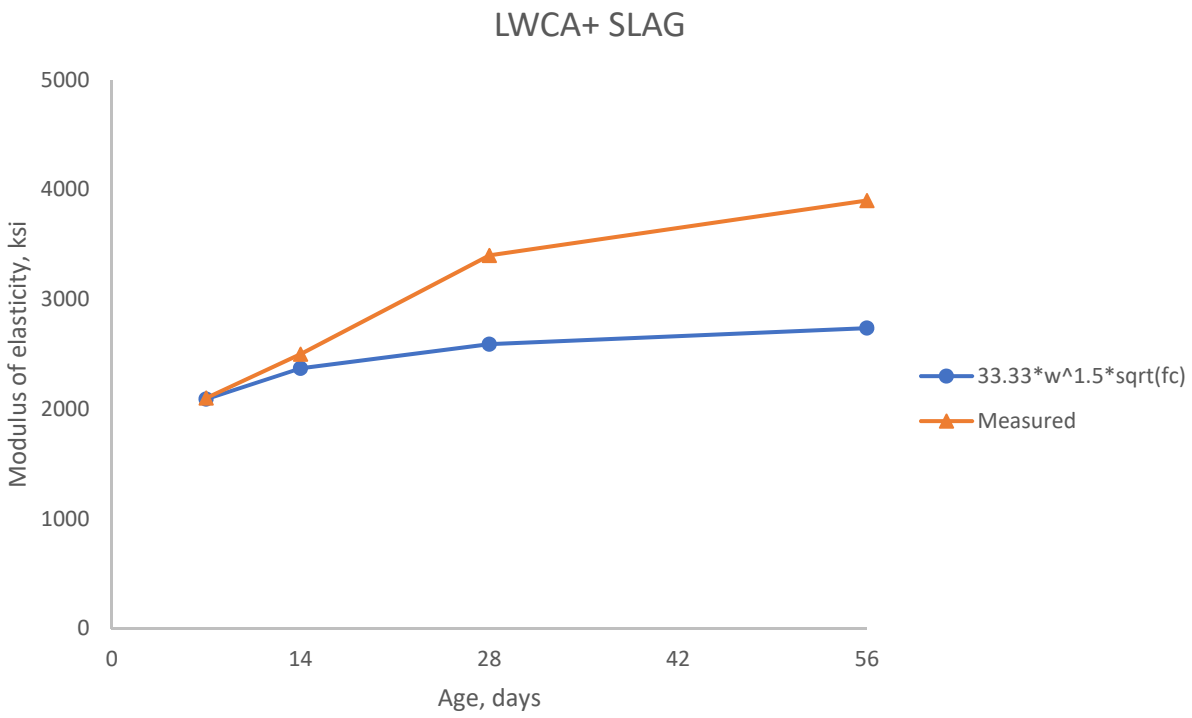

Figure 5-20: Modulus of Elasticity, LWCA+ SLAG

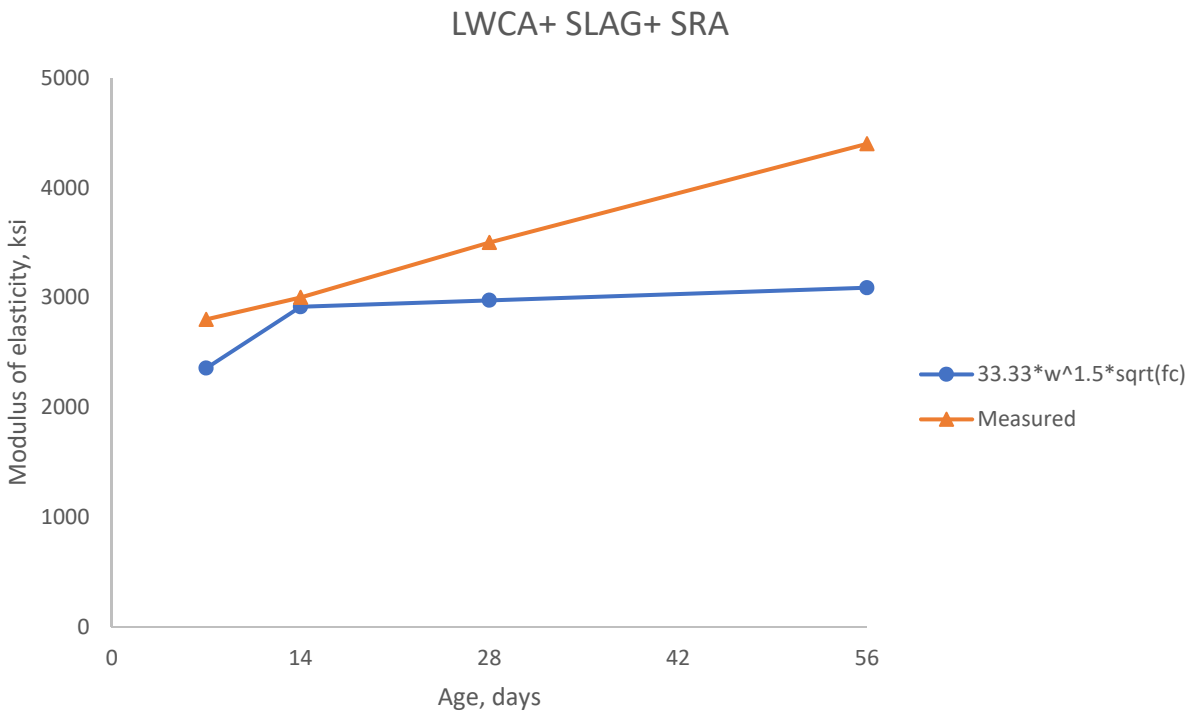

Figure 5-21: Modulus of Elasticity, LWCA+ SLAG+ SRA

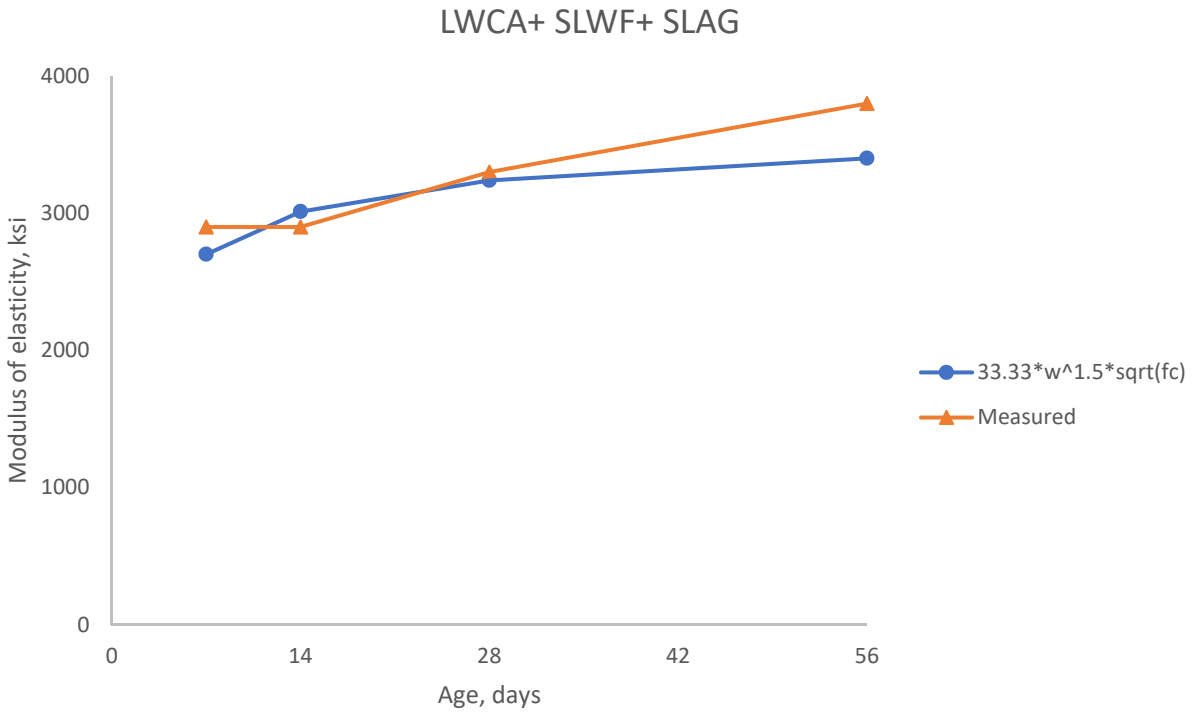

Figure 5-22: Modulus of Elasticity, LWCA+ SLWF+ SRA

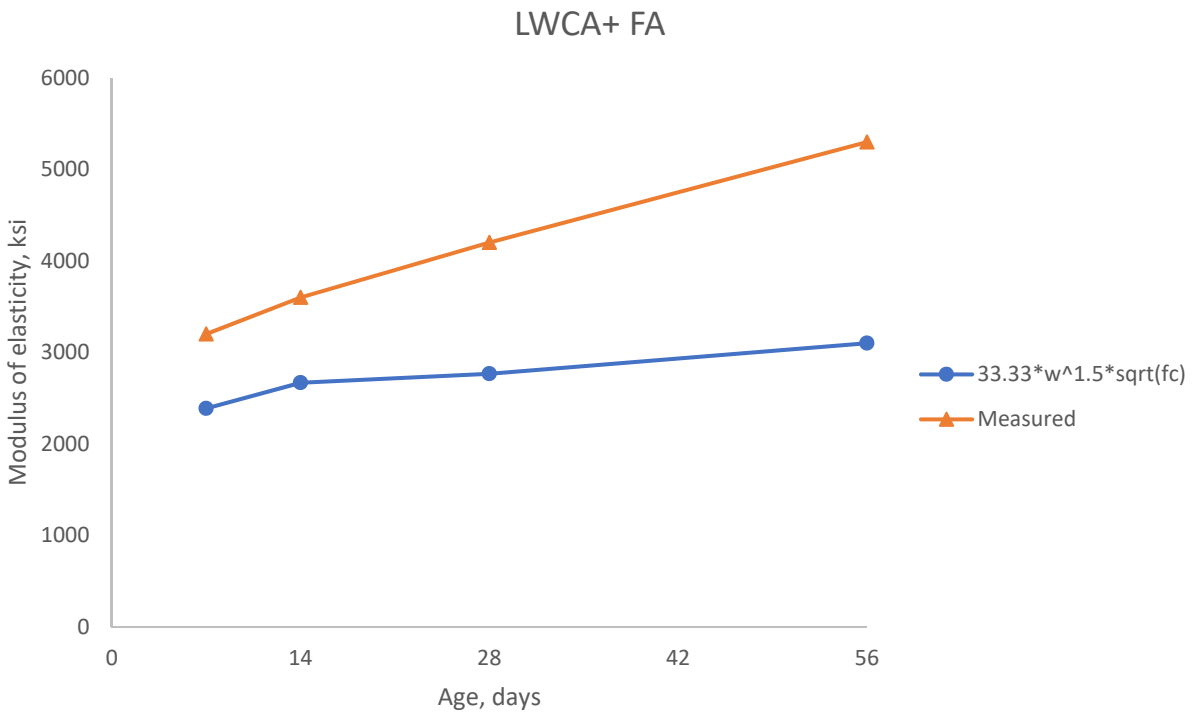

Figure 5-23: Modulus of Elasticity, LWCA+ FA

As expected, the mixes with LWCA generally have lower modulus of elasticity than the mixes with NWCA. All the mixes exhibited higher moduli than the calculated value using Equation 5-2.

5.1.4 Unrestrained Shrinkage

Figure 5-24 shows the comparison of unrestrained shrinkage of NWCA and LWCA mixes in Phase I.

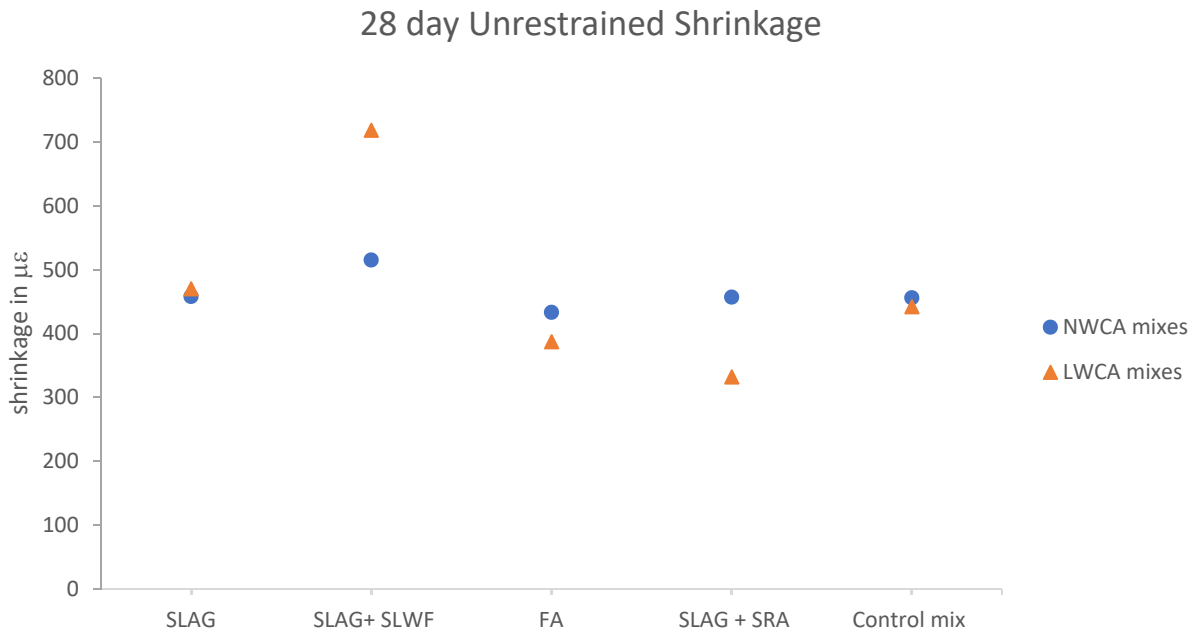

Figure 5-24: Comparison of 28-day Unrestrained Shrinkage, Phase I

The mixtures with SLWF had the highest shrinkage, which could be due to more water in the mix. This excess water is due to an unsuccessful effort to attain saturated surface dry condition of the SLWF, and hence more drying shrinkage. Mixtures with LWCA performed better than their NWCA companion, as expected. This is due to addition of LWCA which helps in internal curing. Mixtures with SRA performed better than the same mix without SRA in the case of LWCA mixes. It is also observed that addition of SRA had little effect in the mix with NWCA. The mixes with fly ash as the SCM performed better than all the other mixes. These results were primary in selection of mixes for phase II for further investigation of long term time dependent properties.

5.2 Phase II

As mentioned in the results section, based on the results obtained in Phase I, the four best performing mix designs were selected based on their compressive strength and unrestrained shrinkage performance. The four mixtures selected were:

- LWCA+SLAG+SRA
- NWCA+SLAG+SRA
- LWCA+FA
- NWCA+FA

This section provides additional discussion of the results of the Phase II testing program.

5.2.1 Compressive Strength

Figure 5-25 compares the compressive strength of mixes in Phase II and Figure 5-27 to Figure 5-30 show the comparison of the performance of the mixes in Phase II with their performance in Phase I.

The mixes with slag performed better than the mixes with fly ash. Mixes with NWCA performed better than the mixes with LWCA. The compressive strength of the mix with NWCA+ SLAG+ SRA attained a strength of 6800 psi at 28 days, this can be attributed to lower air content in the mix. Overall, all the mixes performed better than the required strength of 4000 psi at 28 days.

Comparing the performances in Phase I and II, it is observed that the mixes with fly ash showed little difference in the strength. The mixes with slag showed higher strengths in Phase II than in Phase I. This is attributed to the difference in air content of the mixes in each phase. As seen in section 4.1.1 and 4.2.1 the air content in mix with slag in Phase I was 6.5% whereas, it was 5.5 % in Phase II. Overall, compressive strengths measured in Phase I and Phase II were relatively consistent.

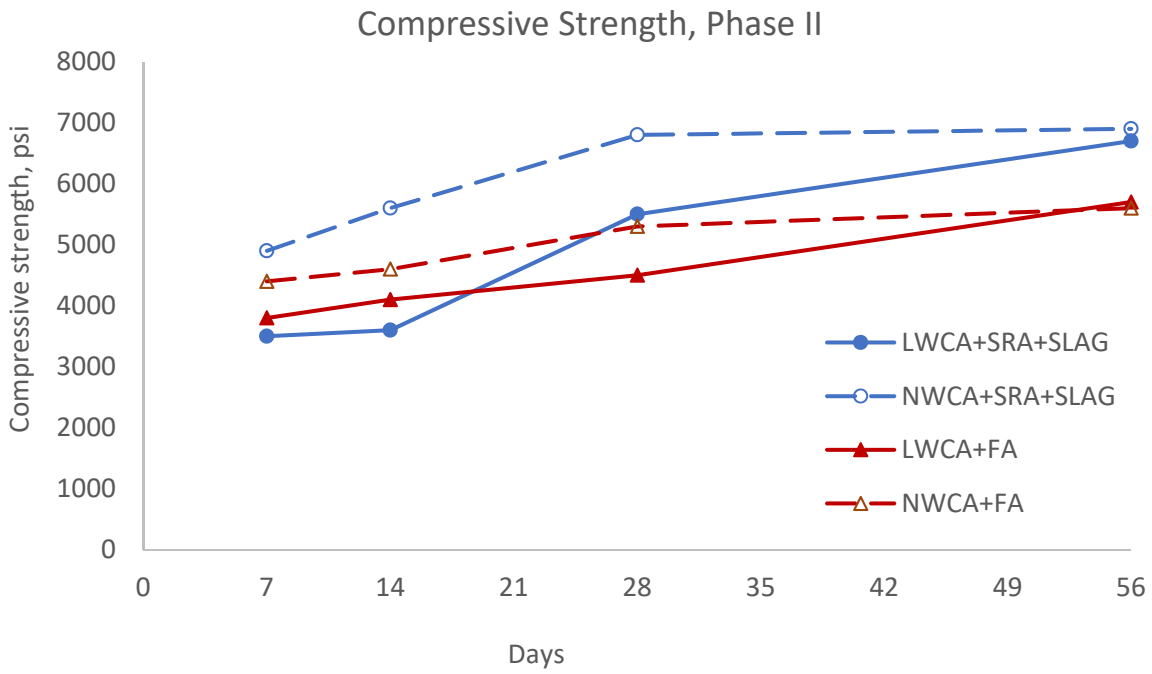

Figure 5-25: Compressive Strength of Mixes in Phase II
*NWCA mixes shown in Dashed lines, LWCA mixes shown in solid lines.

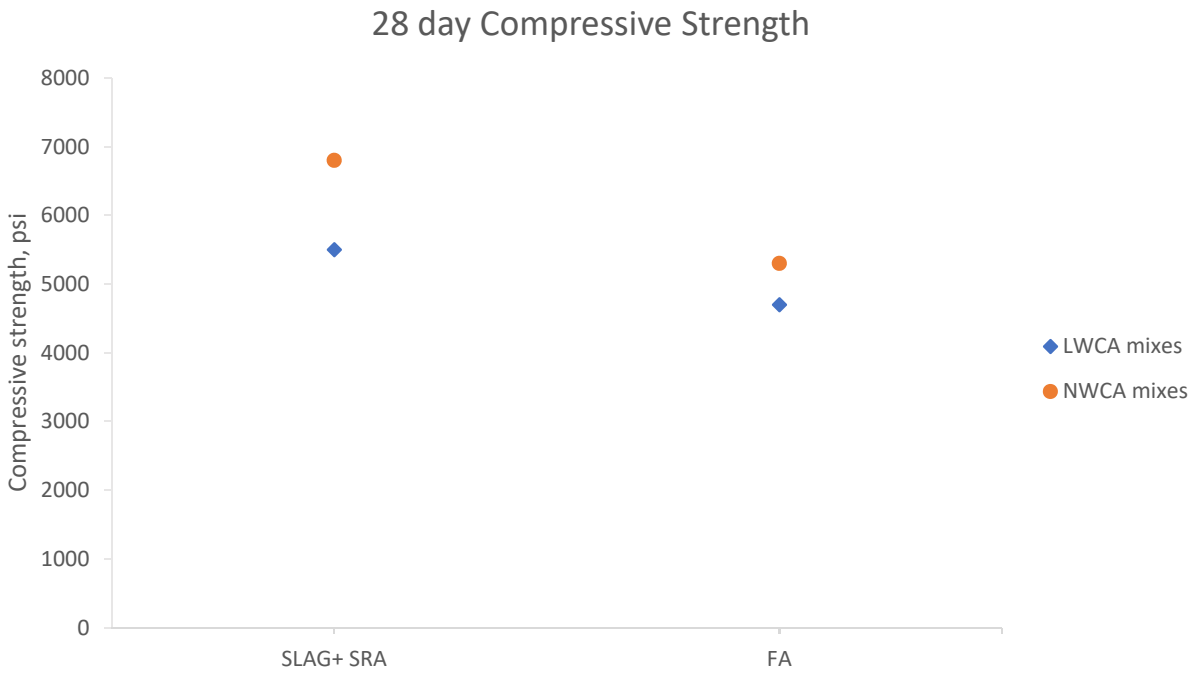

Figure 5-26: Comparison of 28-day Compressive Strength, Phase II

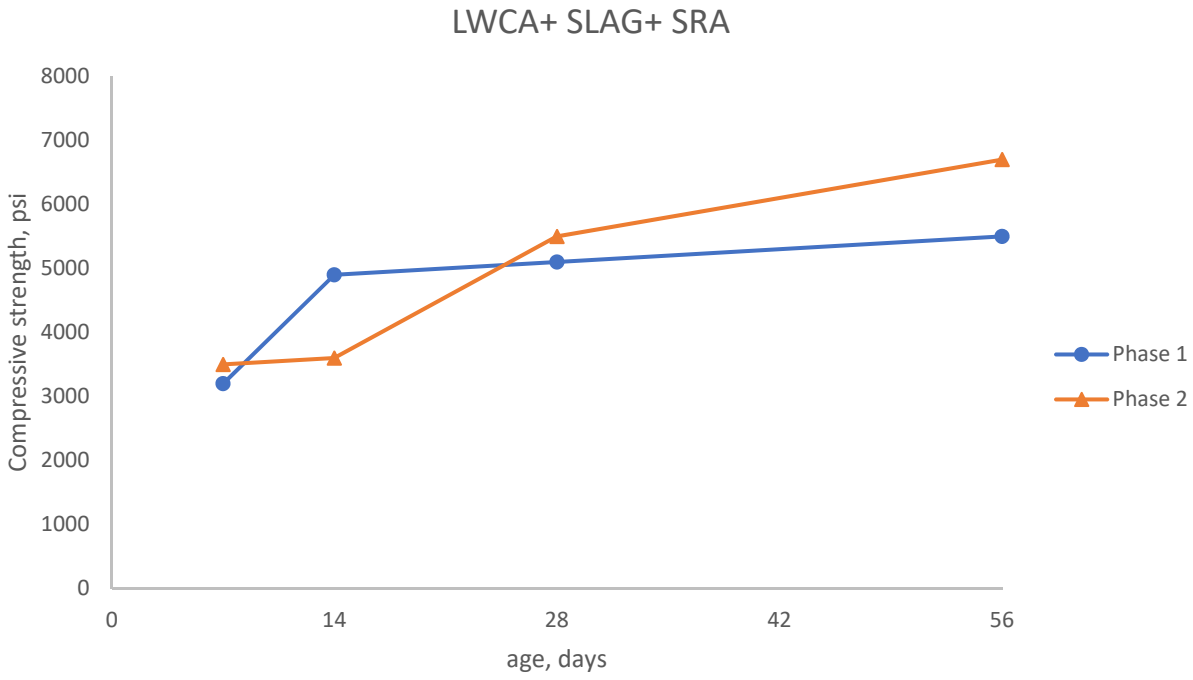

Figure 5-27: Comparison of Compressive Strength of LWCA+ SLAG+ SRA Mix in Phase I and Phase II

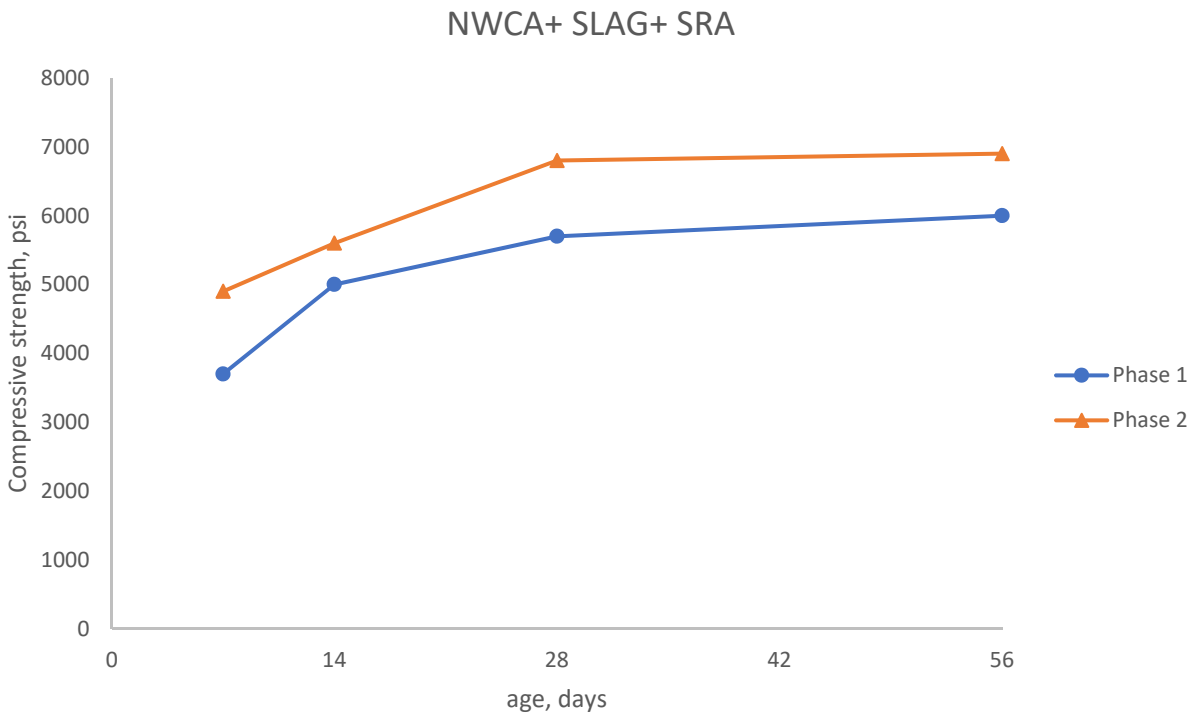

Figure 5-28: Comparison of Compressive Strength of NWCA+ SLAG+ SRA Mix in Phase I and Phase II

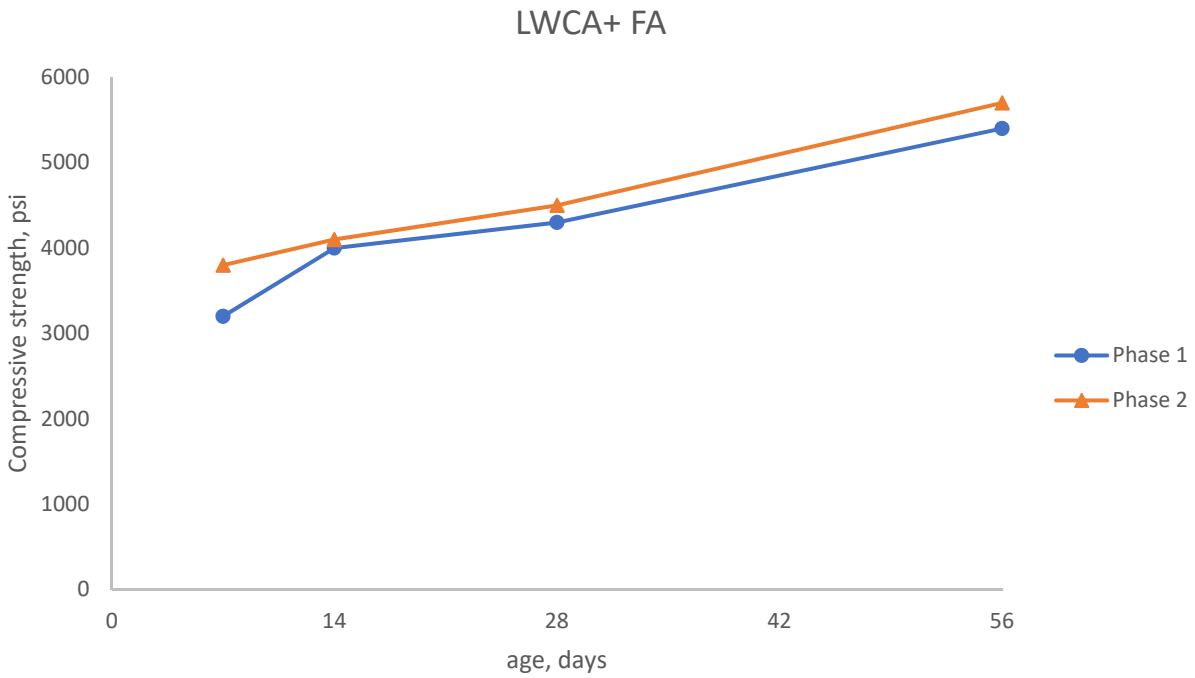

Figure 5-29: Comparison of Compressive Strength of LWCA+ FA Mix in Phase I and Phase II

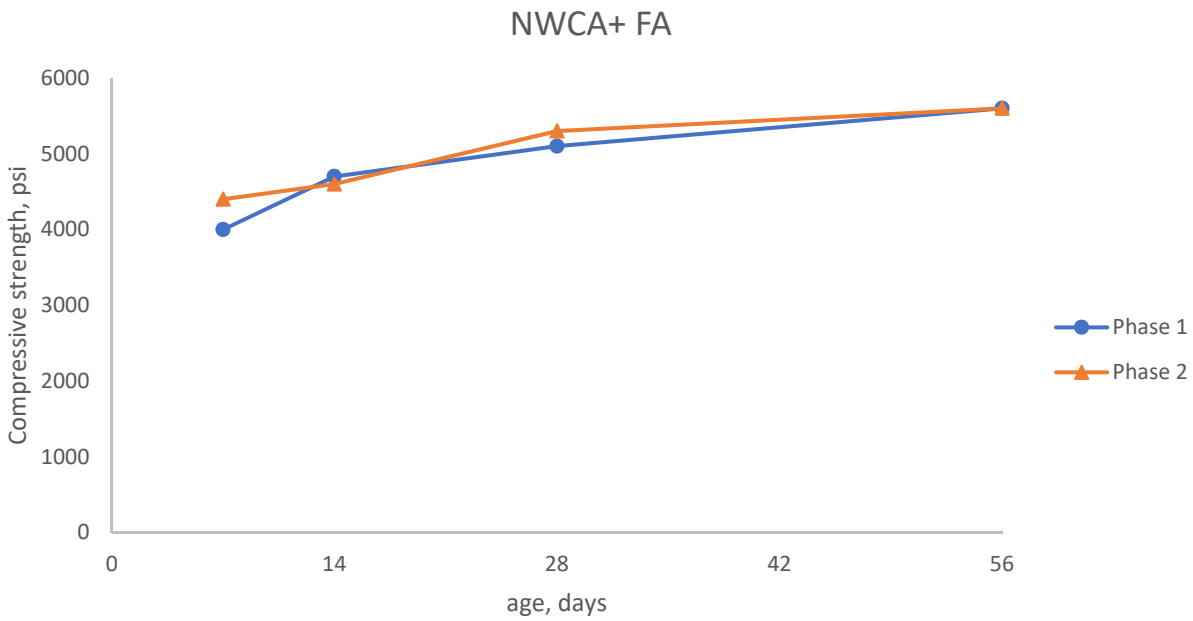

Figure 5-30: Comparison of Compressive Strength of NWCA+ FA Mix in Phase I and Phase II

5.2.2 Splitting Tensile Strength

Figure 5-31 shows the tensile strength of mixes in Phase II. Figure 5-32 to Figure 5-35 gives the comparison between tensile strength measured and the splitting tensile strength obtained by using the value given by Equation 5-1.

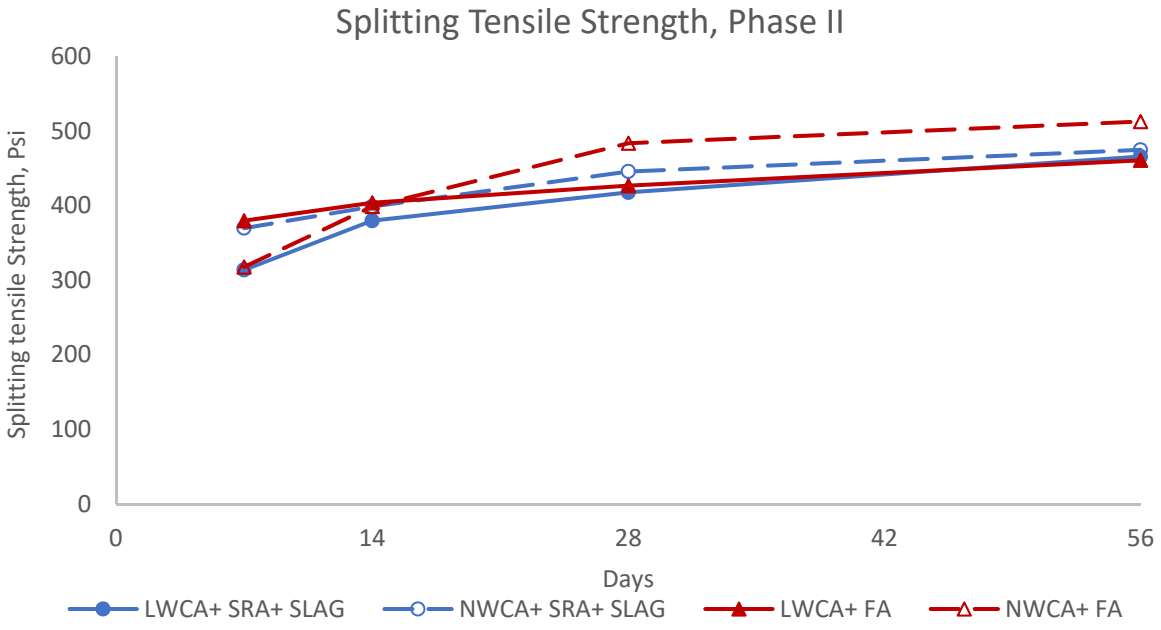

Figure 5-31: Splitting Tensile Strength of Mixes in Phase II
*NWCA mixes shown in Dashed lines, LWCA mixes shown in solid lines.

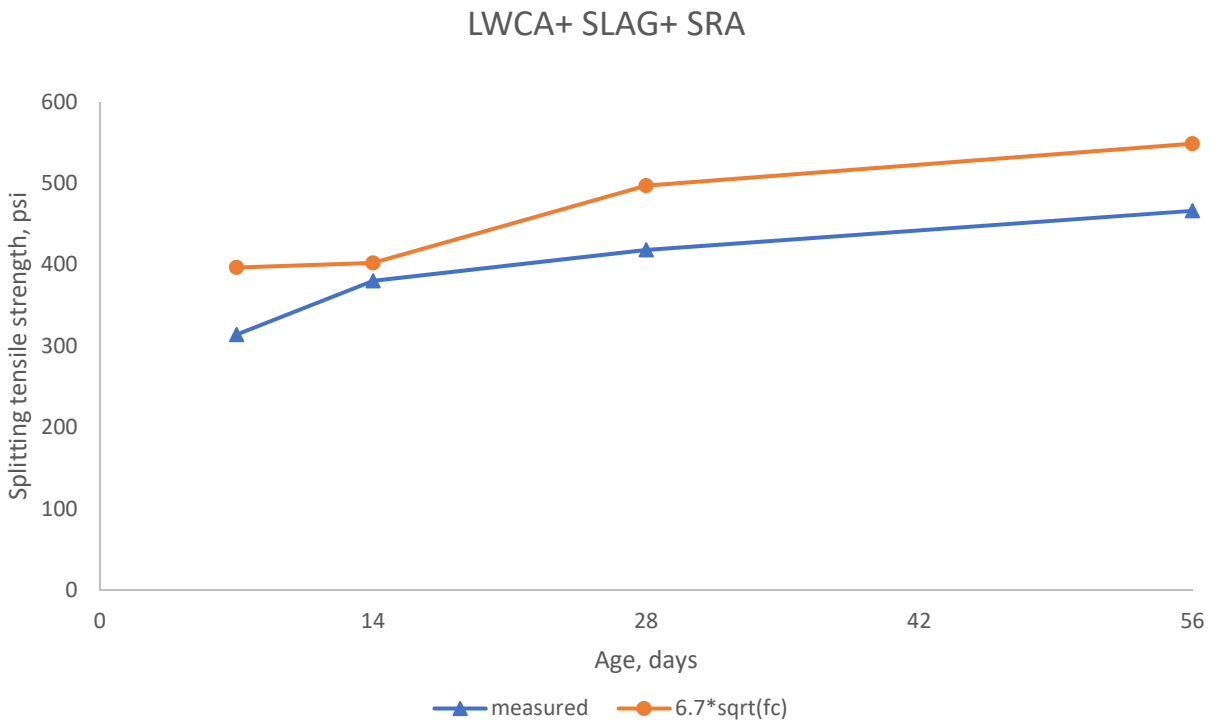

Figure 5-32: Splitting Tensile Strength of LWCA+ SLAG+ SRA

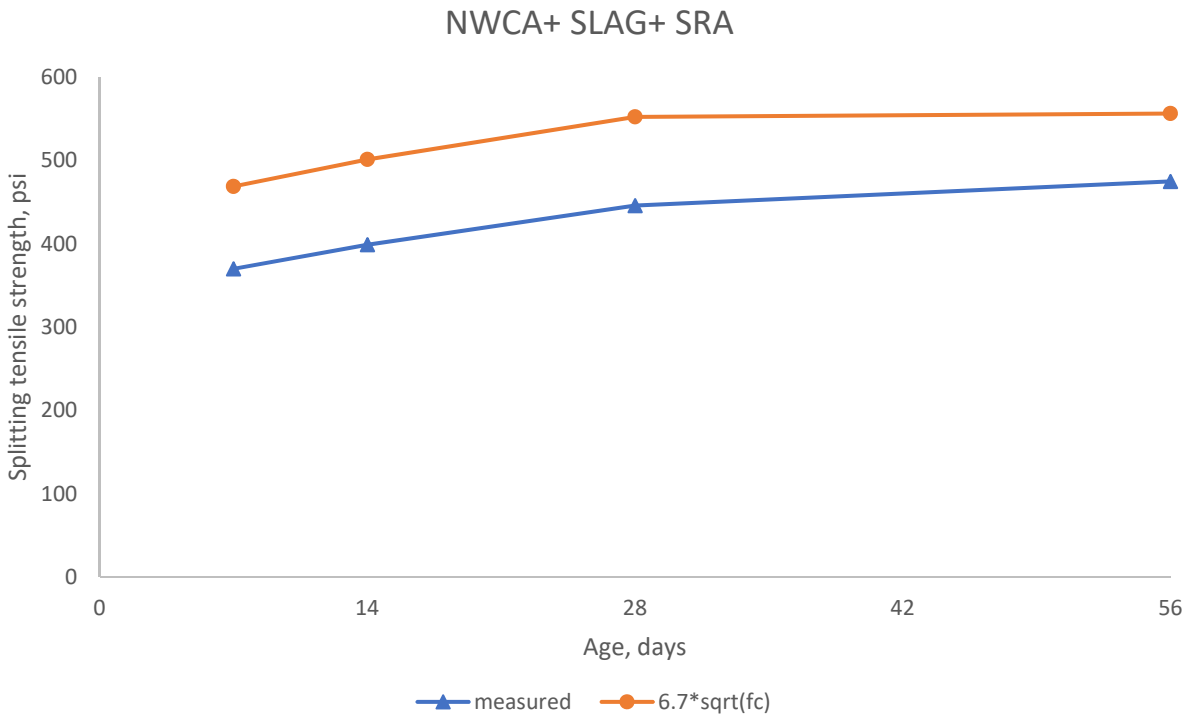

Figure 5-33: Splitting Tensile Strength of NWCA+ SLAG+ SRA

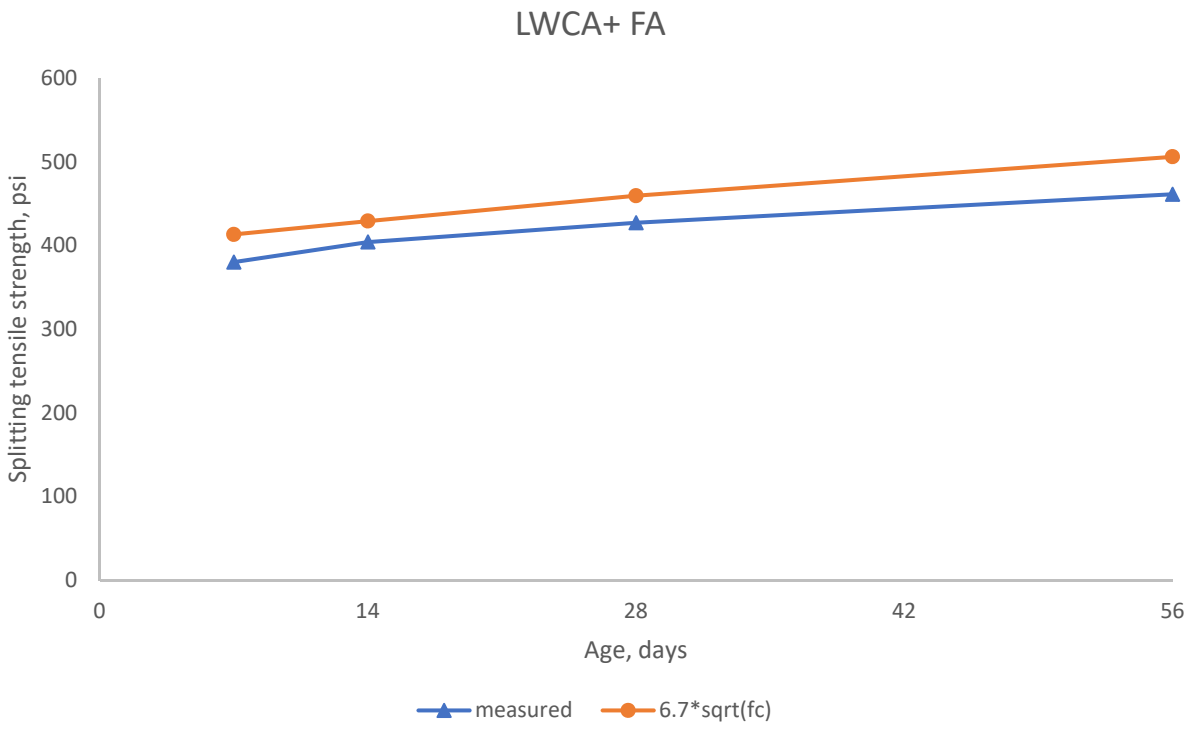

Figure 5-34: Splitting Tensile Strength of LWCA+ FA

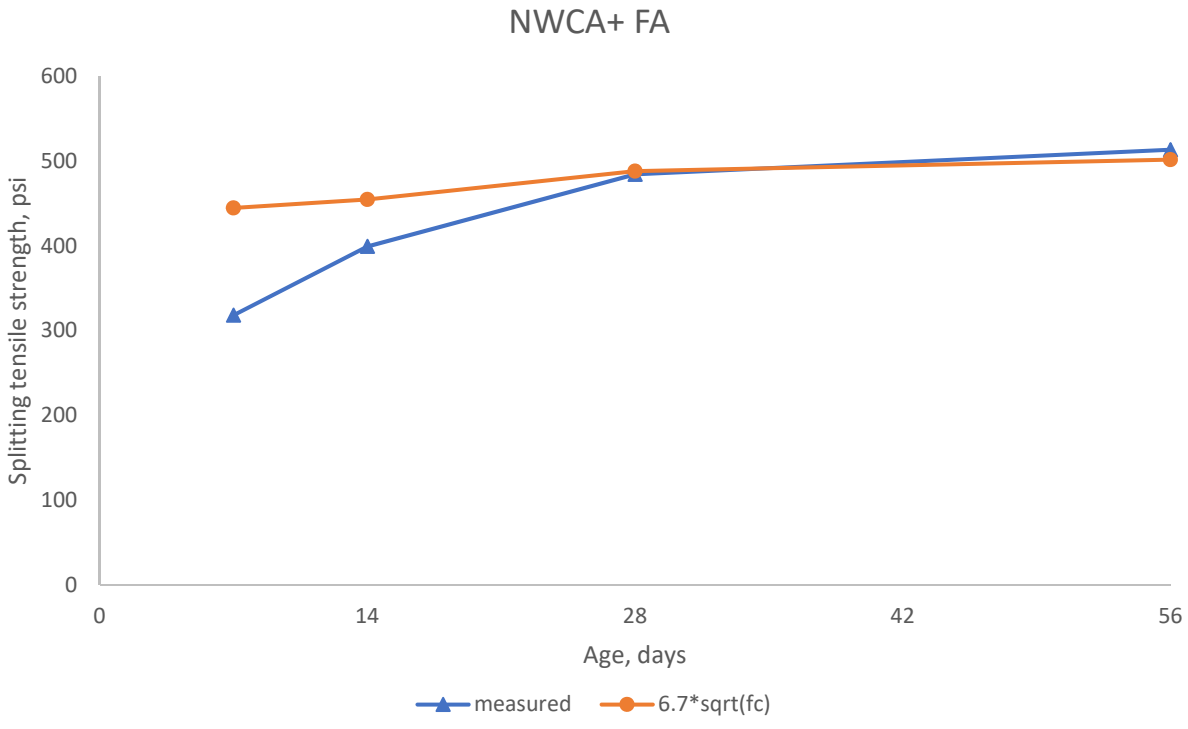

Figure 5-35: Splitting Tensile Strength of NWCA+ FA

As expected, the mixes with NWCA performed better than the mixes with LWCA in terms of splitting tensile strength. The mixes with slag and SRA exhibited lower tensile strengths than the calculated value given by Equation 5-1. Mixes with fly ash had tensile strengths close to the calculated value.

The splitting tensile strength of mixes in Phase I and Phase II were very similar as seen in Figure 5-36 to Figure 5-39.

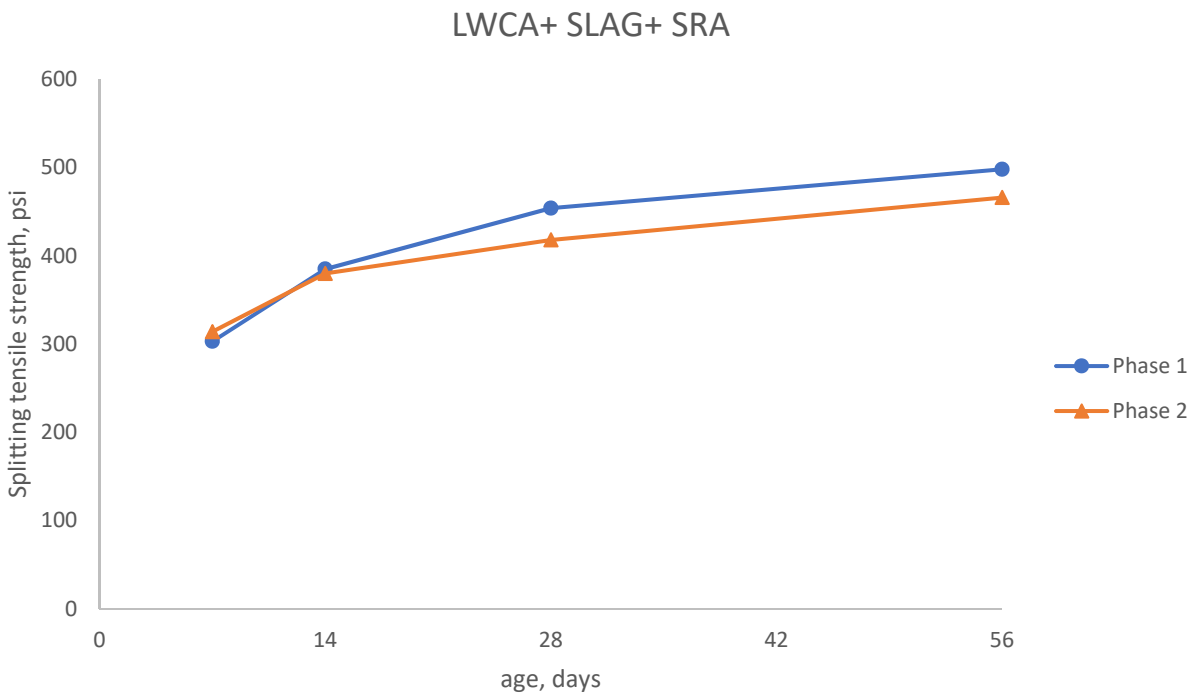

Figure 5-36: Comparison of Splitting Tensile Strength of LWCA+ SLAG+ SRA Mix in Phase I and Phase II

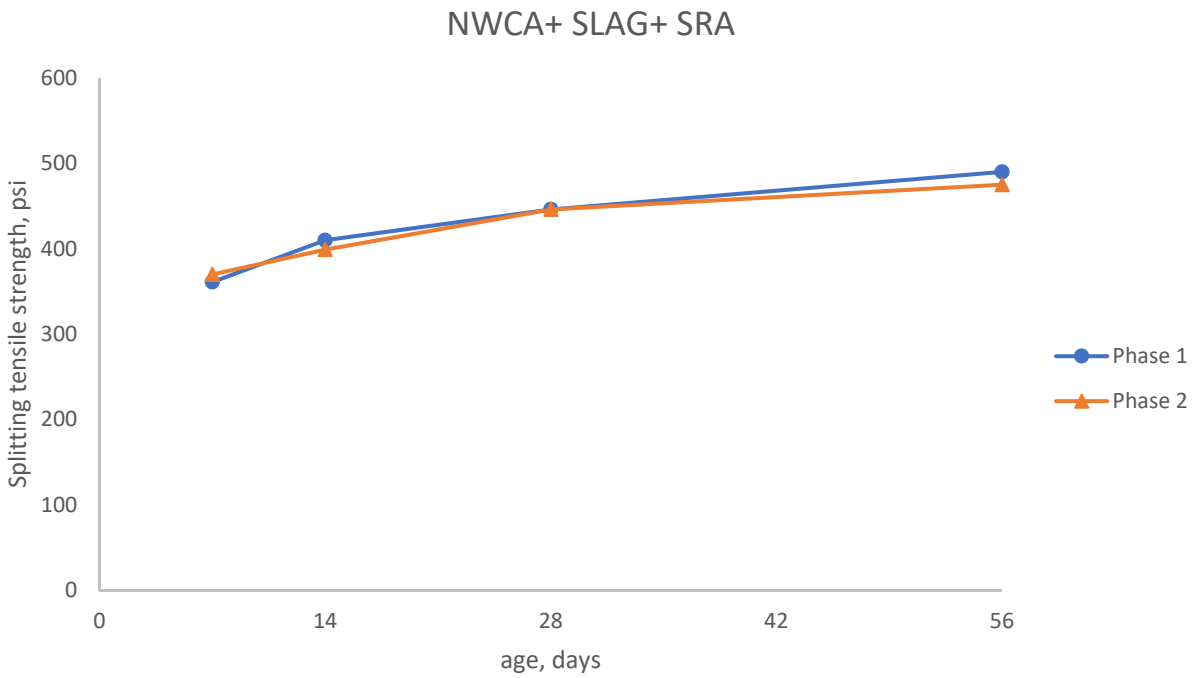

Figure 5-37: Comparison of Splitting Tensile Strength of NWCA+ SLAG + SRA mix in Phase I and Phase II

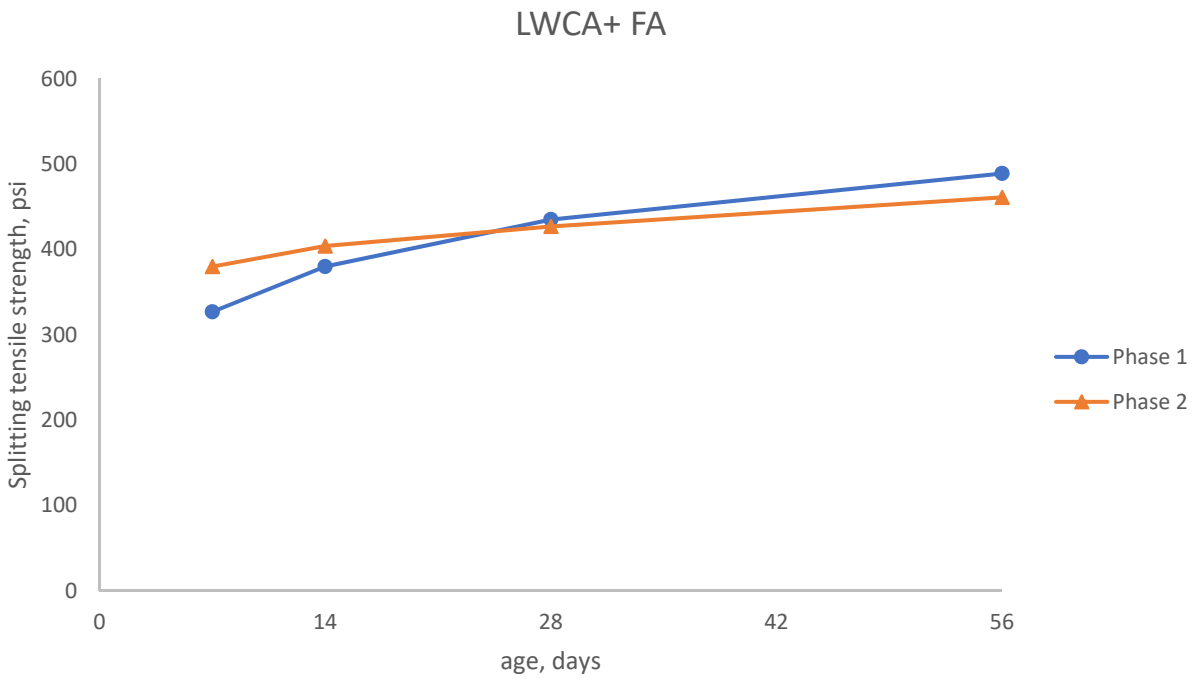

Figure 5-38: Comparison of Splitting Tensile Strength of LWCA+ FA Mix in Phase I and Phase II

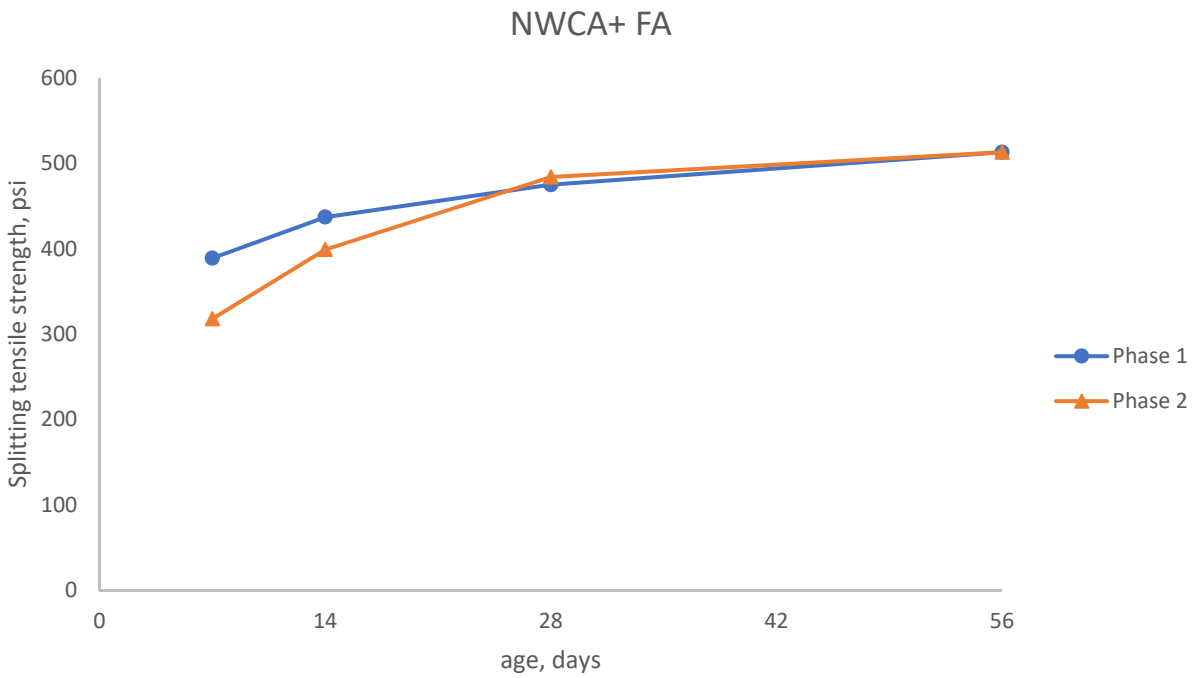

Figure 5-39: Comparison of Splitting Tensile Strength of NWCA+ FA Mix in Phase I and Phase II

5.2.3 Modulus of Elasticity

Figure 5-40 shows the modulus of elasticity of mixes in Phase II and Figure 5-41 to Figure 5-44 gives the comparison between modulus of elasticity measured and the modulus obtained by using the value given by Equation 5-2.

As seen in Figure 5-40, the modulus of NWCA mixes was higher than the mixes with LWCA as expected. All the mixes had measured moduli of elasticity similar to those predicted using the formula given by ACI 318 – Equation 5-2. It is observed that the LWCA mixes in phase II had lower modulus when compared to Phase I, but they were above what is expected as given by Equation 5-2. NWCA mixes performed better in Phase II.

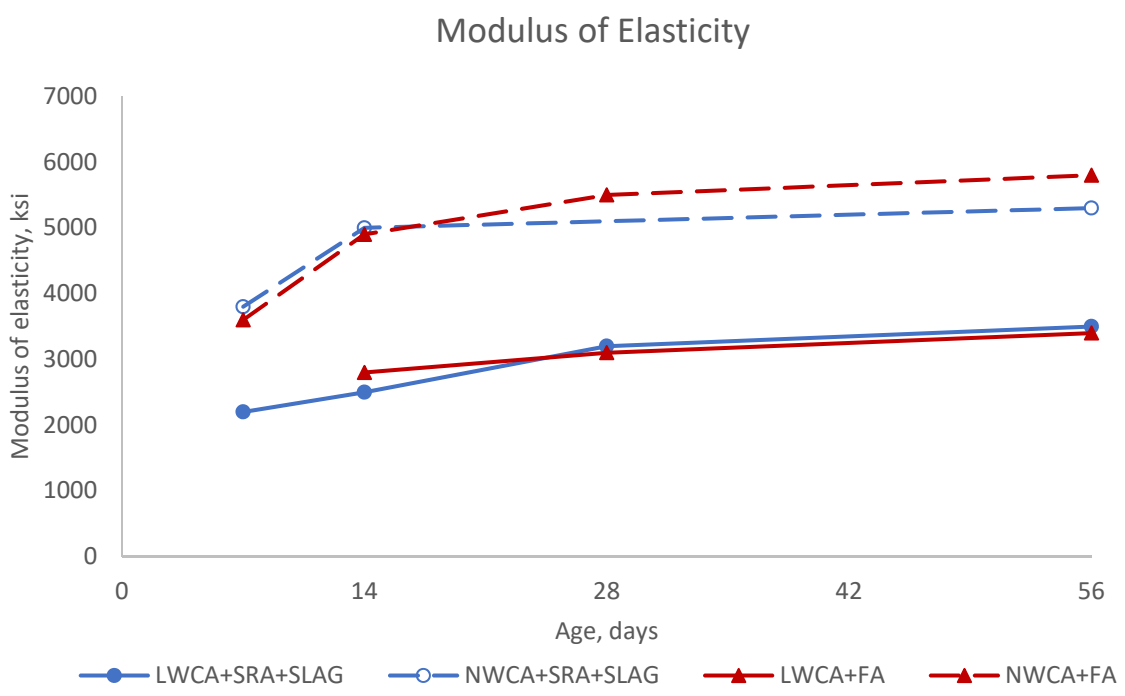

Figure 5-40: Modulus of Elasticity of Mixes in Phase II
*NWCA mixes shown in Dashed lines, LWCA mixes shown in solid lines.

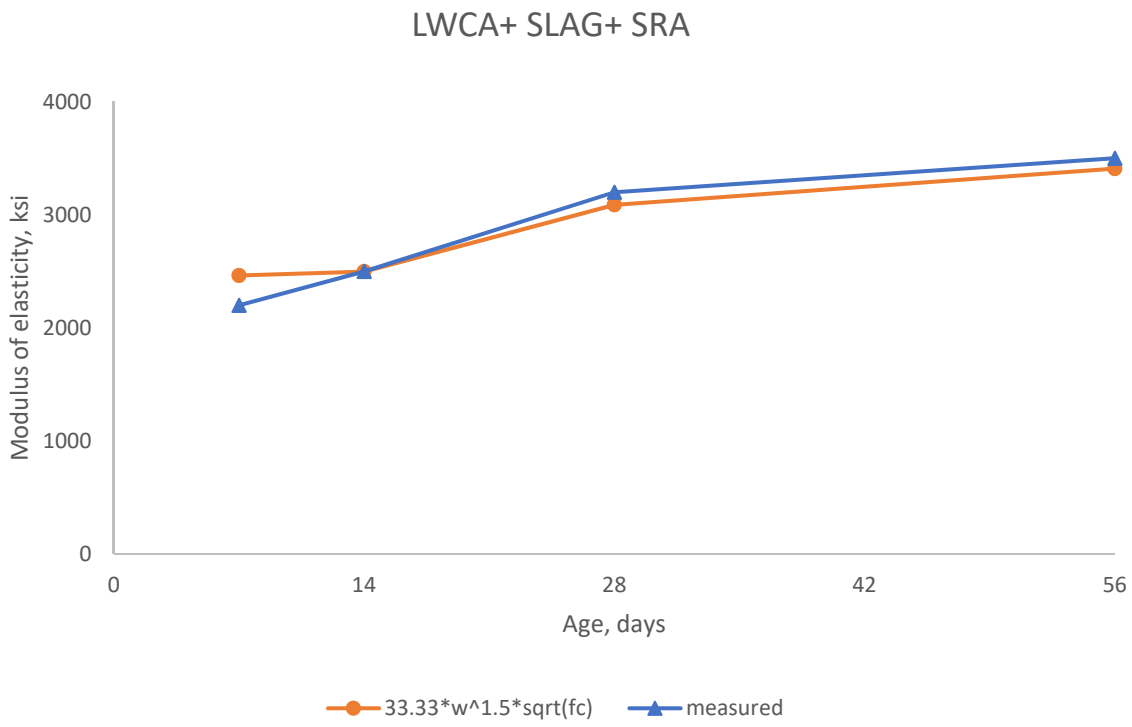

Figure 5-41: Modulus of Elasticity, LWCA+ SLAG+ SRA

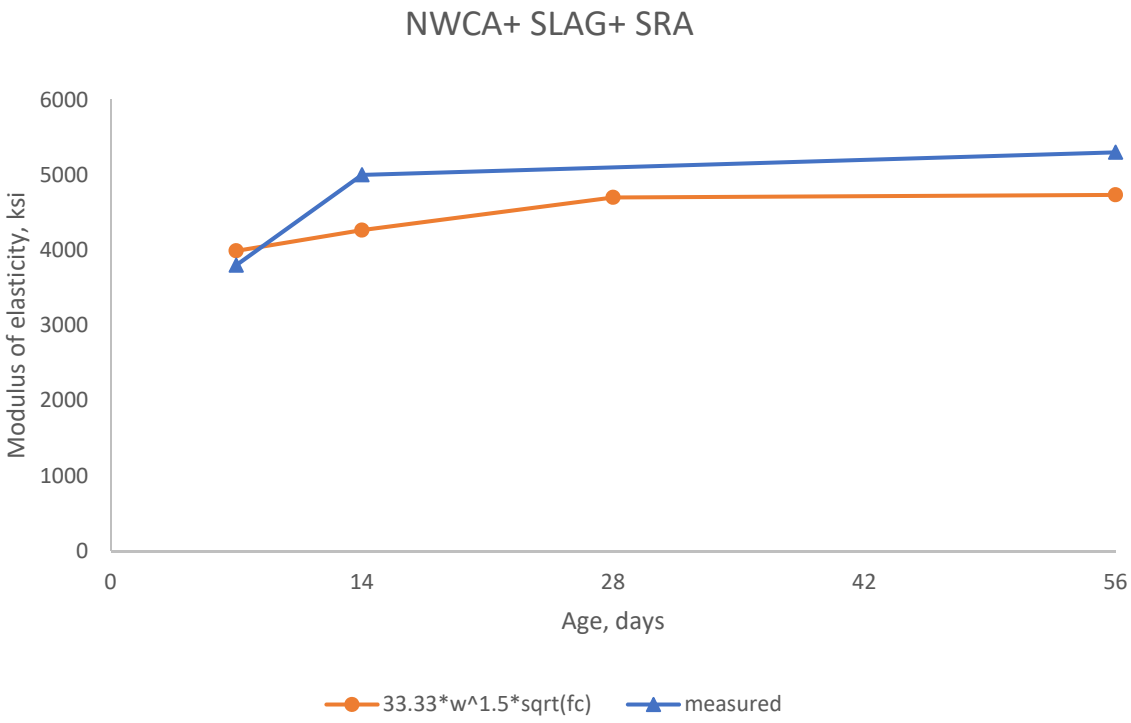

Figure 5-42: Modulus of Elasticity, NWCA+ SLAG+ SRA

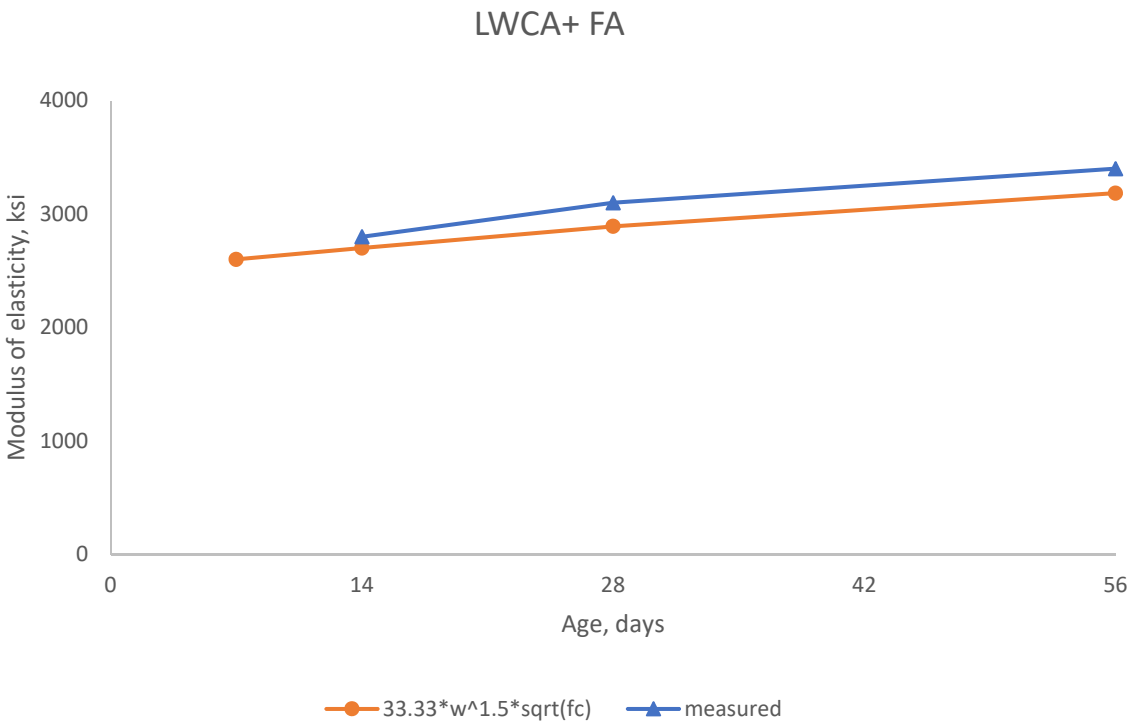

Figure 5-43: Modulus of Elasticity, LWCA+ FA

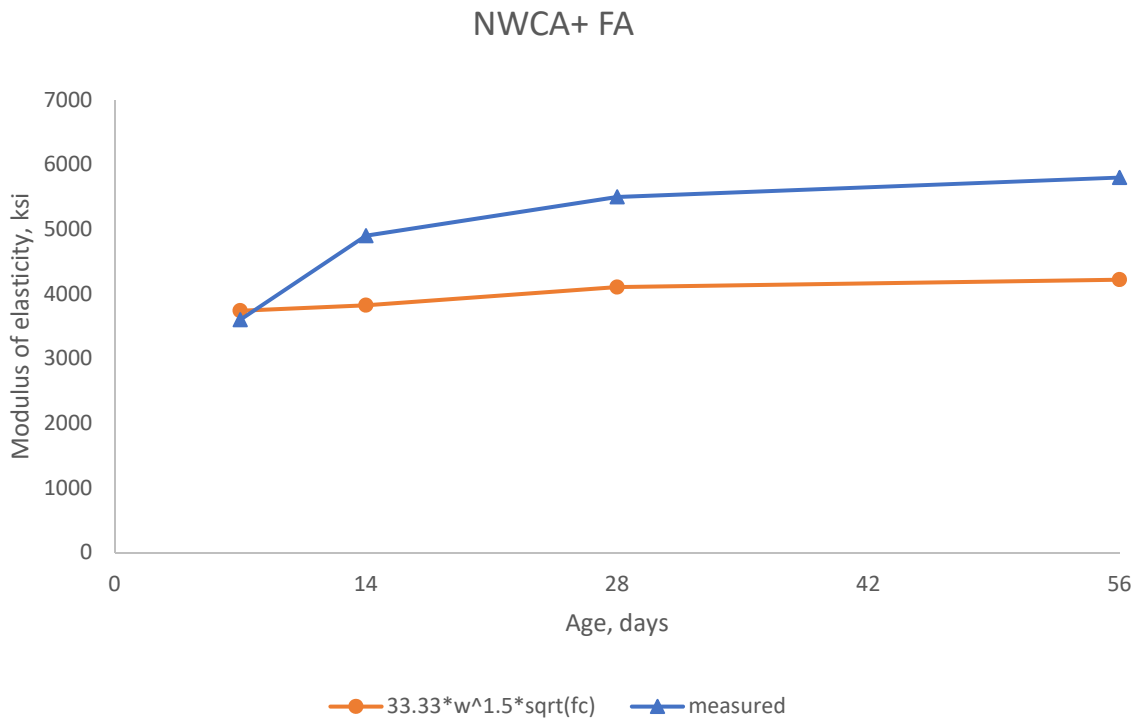

Figure 5-44: Modulus of Elasticity, NWCA+ FA

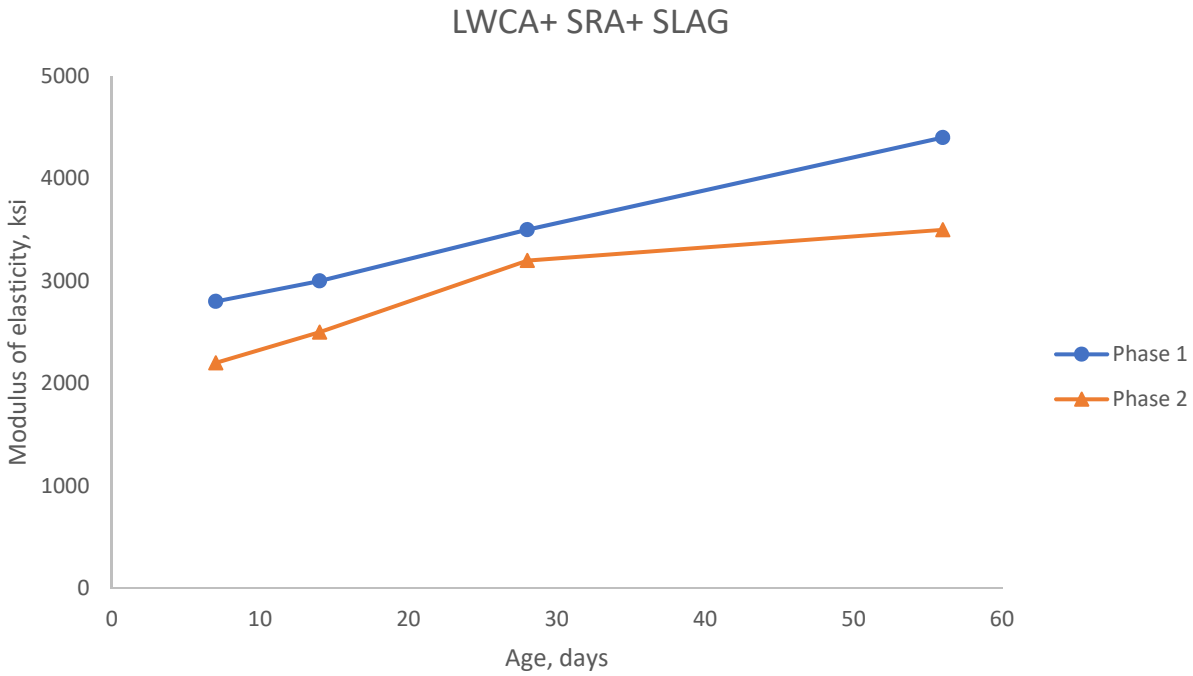

Figure 5-45: Comparison of Modulus of Elasticity of LWCA+ SRA+ SLAG Mix in Phase I and Phase II

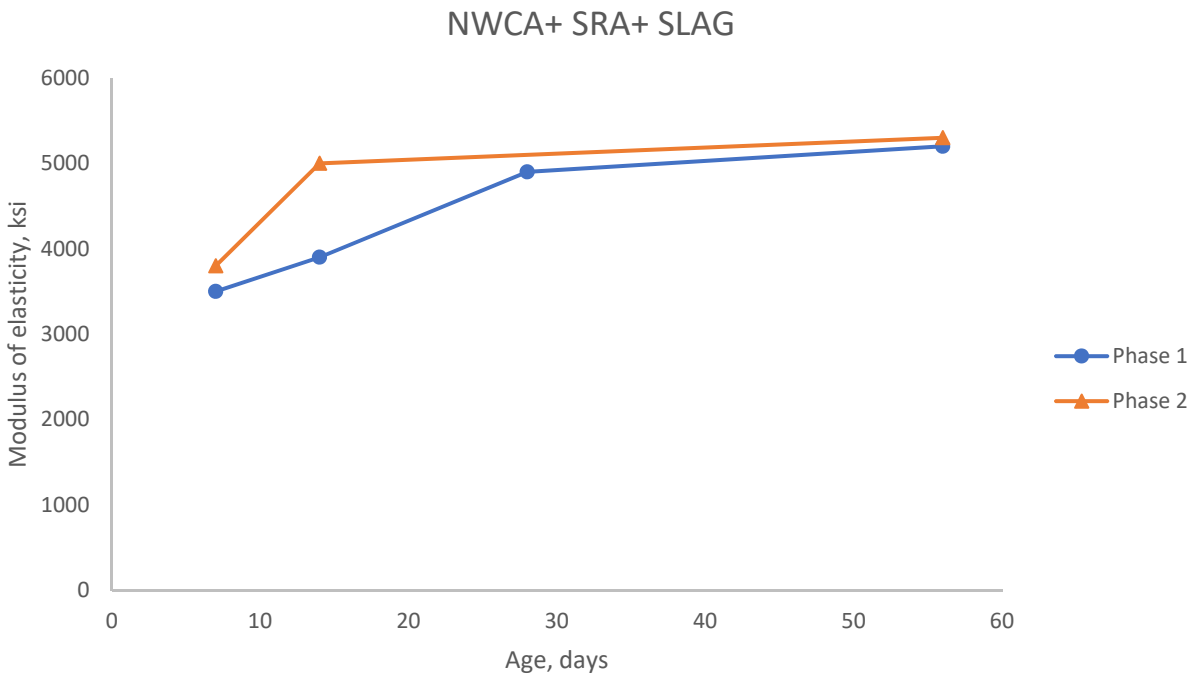

Figure 5-46: Comparison of Modulus of Elasticity of NWCA+ SRA+ SLAG Mix in Phase I and Phase II

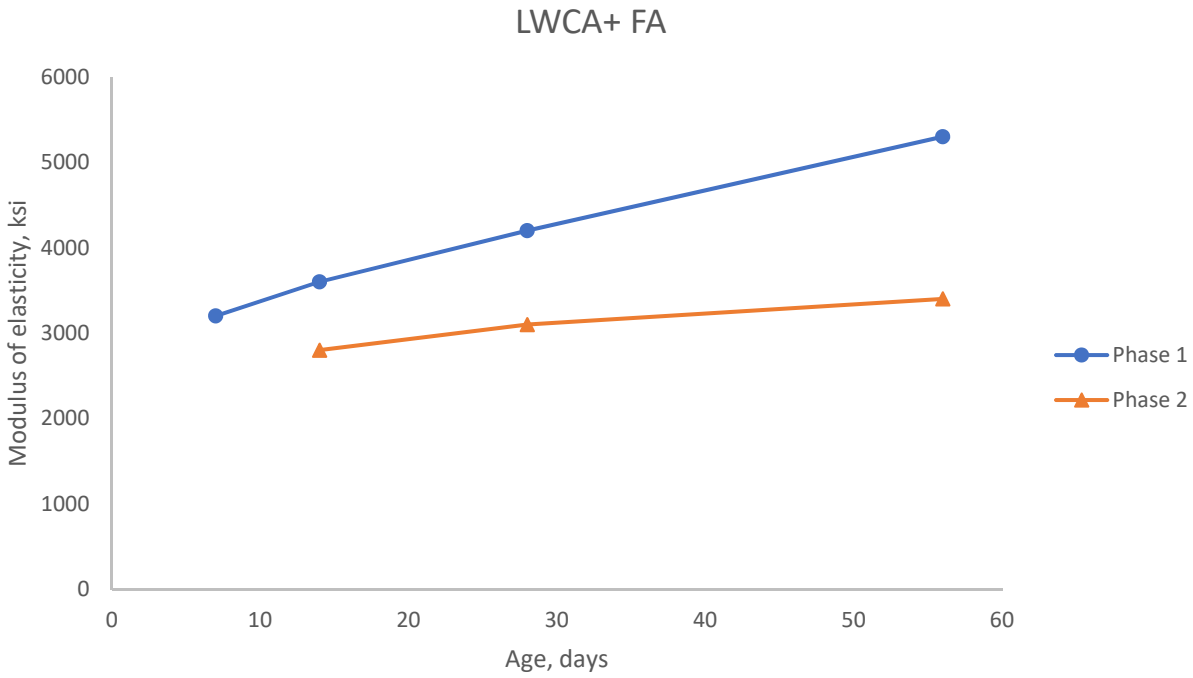

Figure 5-47: Comparison of Modulus of Elasticity of LWCA+ FA Mix in Phase I and Phase II

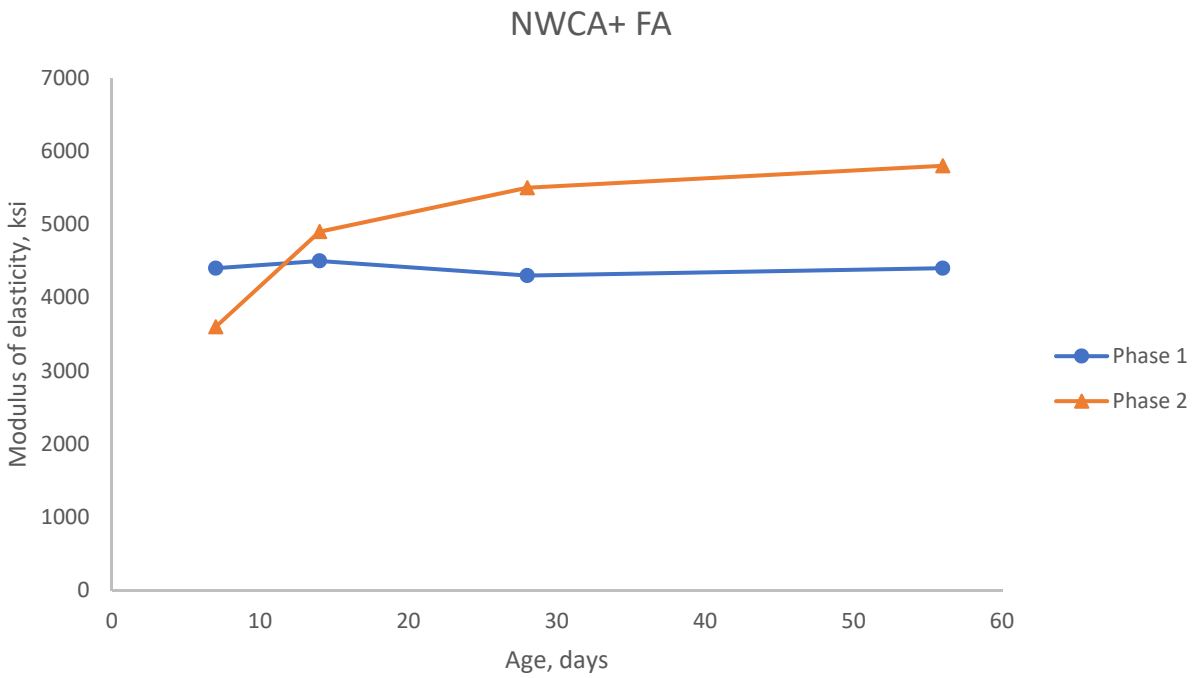

Figure 5-48: Comparison of Modulus of Elasticity of NWCA+ FA Mix in Phase I and Phase II

5.2.4 Unrestrained shrinkage

Figure 4-5 shows the data for unrestrained shrinkage measured for the mixes in Phase II. Figure 5-49 to Figure 5-52 shows the comparison of measured shrinkage to that of the shrinkage predicted using the three models, ACI 209R, AASHTO model, CEB MC90-99 models.

When considering computational effort AASHTO is the easiest, while the CEB model requires more computational effort and time. LWCA+ SRA+ SLAG mix shrinkage is best predicted by ACI in early age but is then inclined to the shrinkage predicted by AASHTO for later age as shown in Figure 5-49. All the three models under predicted the shrinkage at later ages for NWCA+ SRA+ SLAG mix but CEB model over predicted the shrinkage at early age. Out of the three, shrinkage predicted by ACI model was close to the measured shrinkage for mixes with slag as SCM.

The early age shrinkage of LWCA+ FA was very similar to that predicted by ACI and AASHTO models, where the CEB model overestimated the shrinkage for the same, as shown in Figure 5-51. In later ages the shrinkage measured was inclined more towards CEB model, while ACI and AASHTO over predicted the later age shrinkage. For the mix with NWCA+ FA, measured shrinkage was fairly close to that predicted by ACI. AASHTO over predicted it whereas, CEB model under predicted as shown in Figure 5-52.

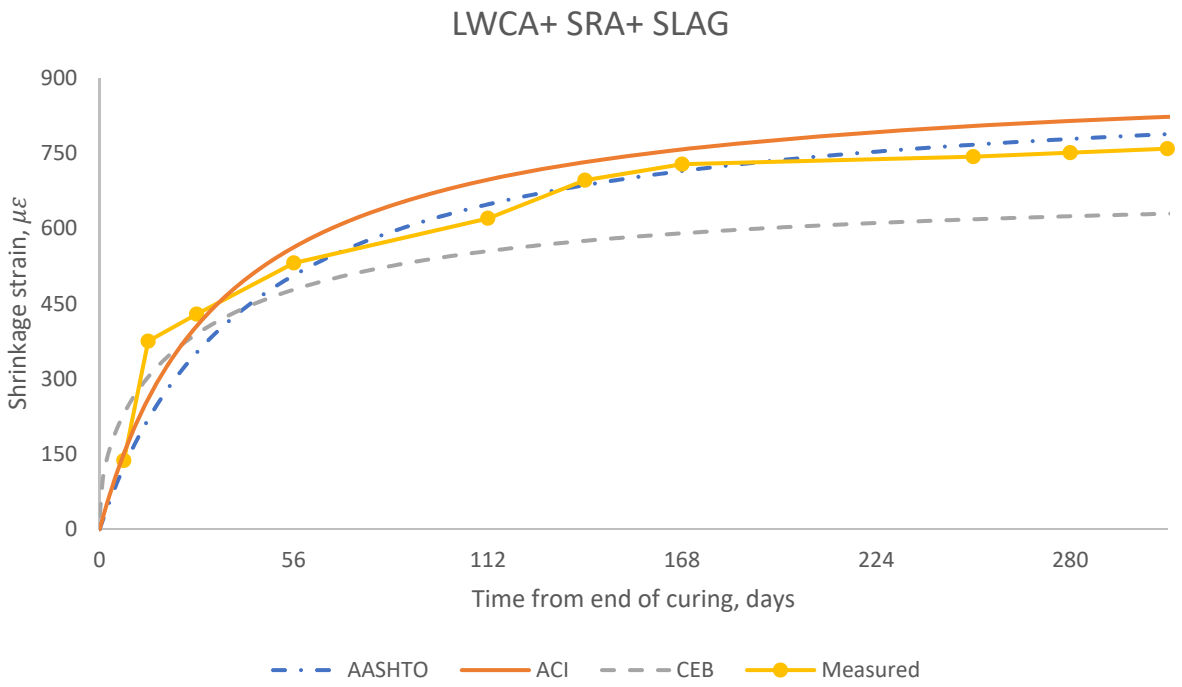

Figure 5-49: Comparison of Measured Shrinkage with Models for LWCA+SLAG+SRA Mix

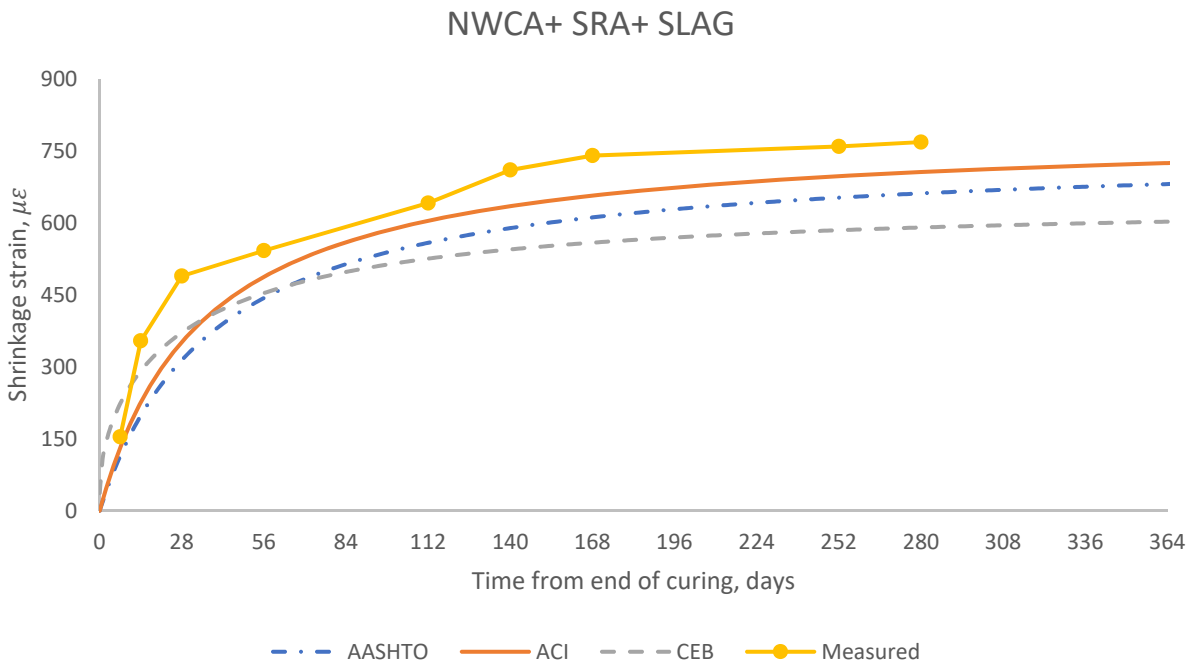

Figure 5-50: Comparison of Measured shrinkage with Models for NWCA+SLAG+SRA Mix

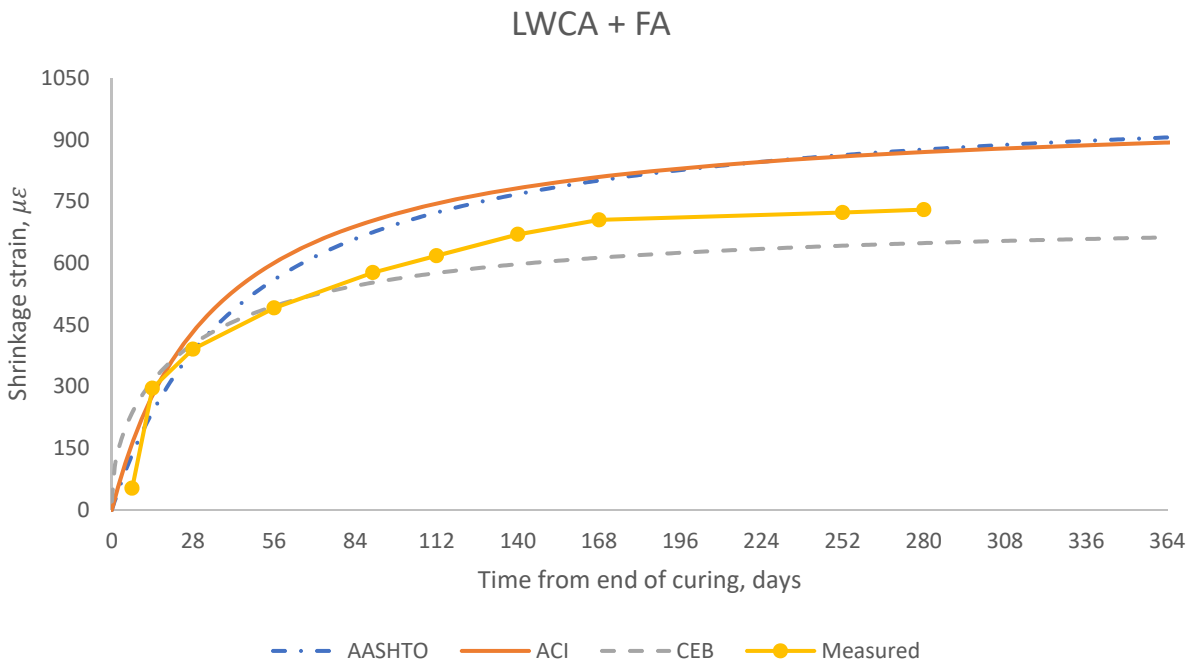

Figure 5-51: Comparison of Measured Shrinkage with Models of LWCA+ FA Mix

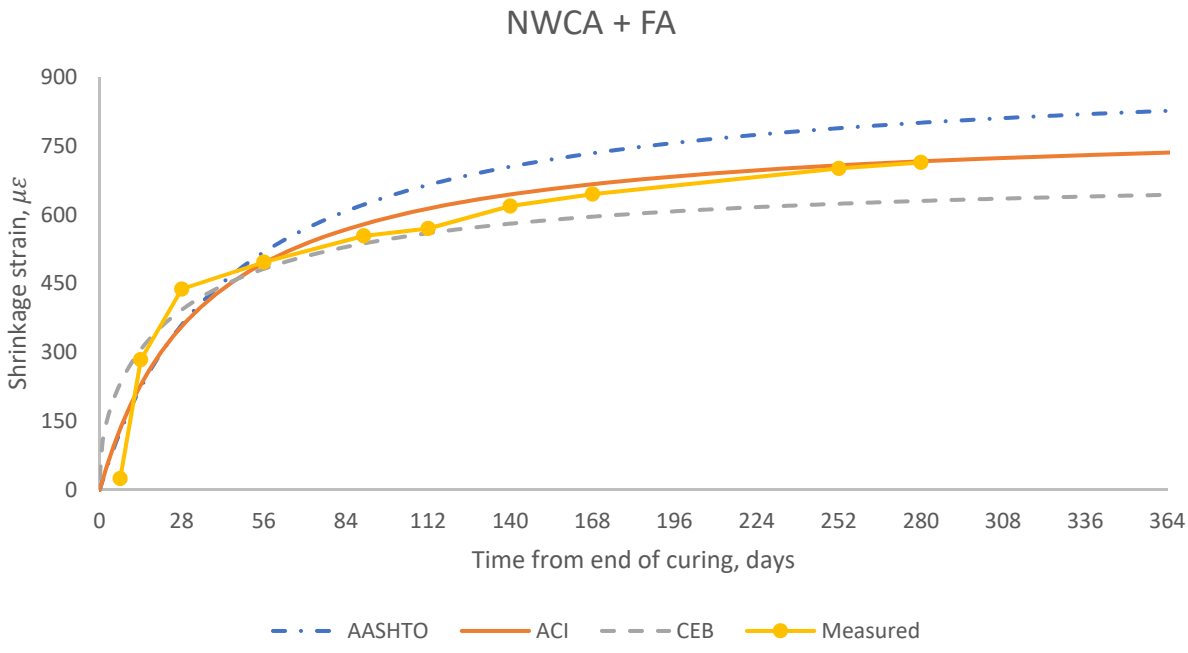

Figure 5-52: Comparison of Measured Shrinkage with Models of NWCA+ FA Mix

5.2.5 Compressive creep

Figure 5-53 shows the creep coefficient calculated using the data obtained from compressive creep test, Figure 5-54 to Figure 5-57 shows the comparison of calculated creep coefficient to that of the coefficient predicted using the three models, ACI 209R, AASHTO model, CEB MC90-99 models. When considering computational effort, AASHTO is the easiest, while the CEB model requires more computational effort and time. It is observed that the mix with LWCA and Slag and SRA exhibited the lowest creep. Mixes with fly ash exhibited more creep compared to mixes with slag as SCM. The NWCA mixes exhibited more creep than the mixes with LWCA. Over all, the mix with NWCA and fly ash exhibited the highest creep out of the four mixes tested.

For the LWCA+SRA+ SLAG mix AASHTO, CEB and ACI models over predicted the creep coefficient as seen in Figure 5-54. Out of the three models, the AASHTO model predicted closest to the creep coefficient calculated from measured data. The creep coefficient of NWCA+SRA+SLAG is under predicted by all the three models but is close to the coefficient predicted by CEB model as shown in Figure 5-55. The creep coefficient for LWCA with fly ash is under predicted by AASHTO model and over predicted by CEB model at all ages, while the early age creep is under predicted by ACI model, but the later age creep predicted by ACI model is fairly accurate as shown in Figure 5-56. The creep coefficient of NWCA with fly ash is under predicted by ACI and AASHTO models but is closely represented by CEB model as shown in Figure 5-57.

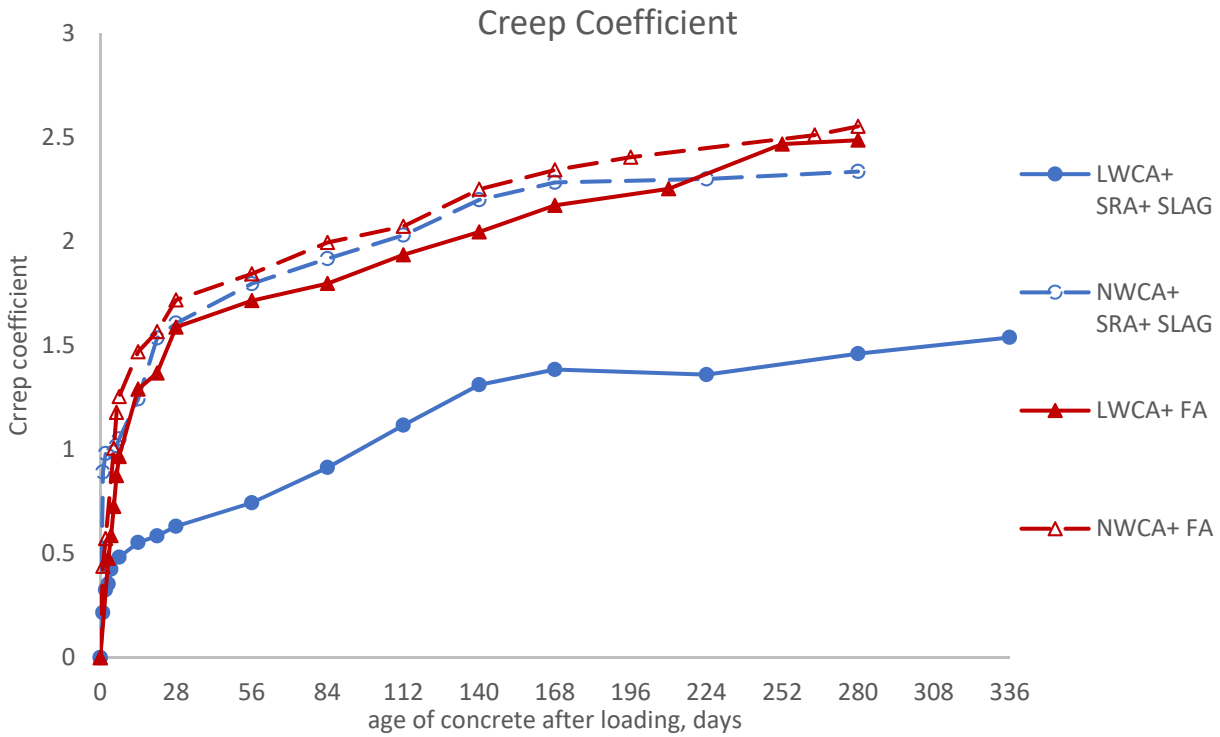

Figure 5-53: Creep Coefficient for Mixes in Phase II

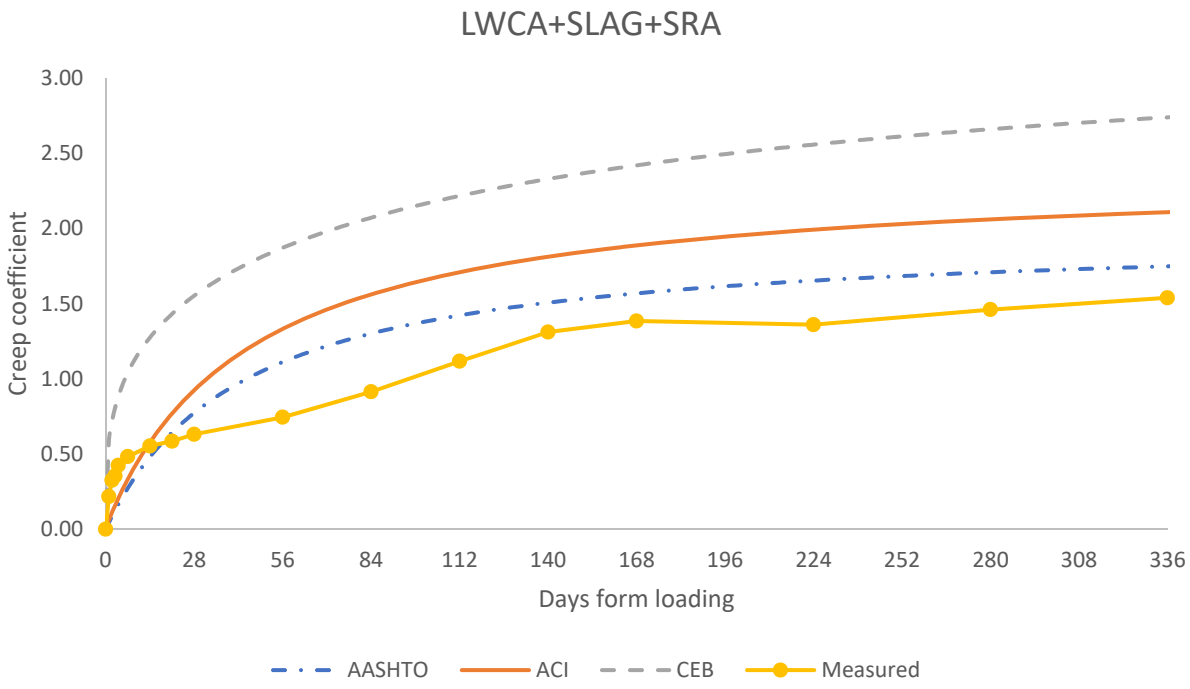

Figure 5-54: Comparison of Creep Coefficient Calculated with Models for LWCA+SLAG+SRA Mix

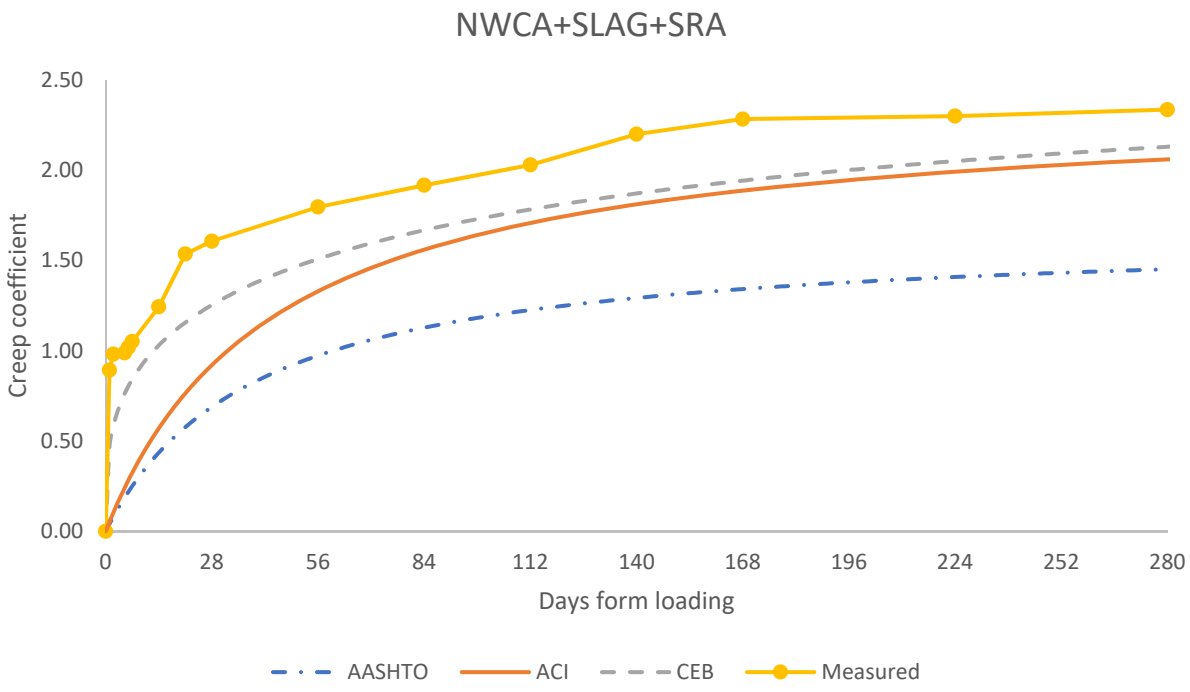

Figure 5-55: Comparison of Creep Coefficient Calculated with Models for NWCA+SLAG+SRA Mix

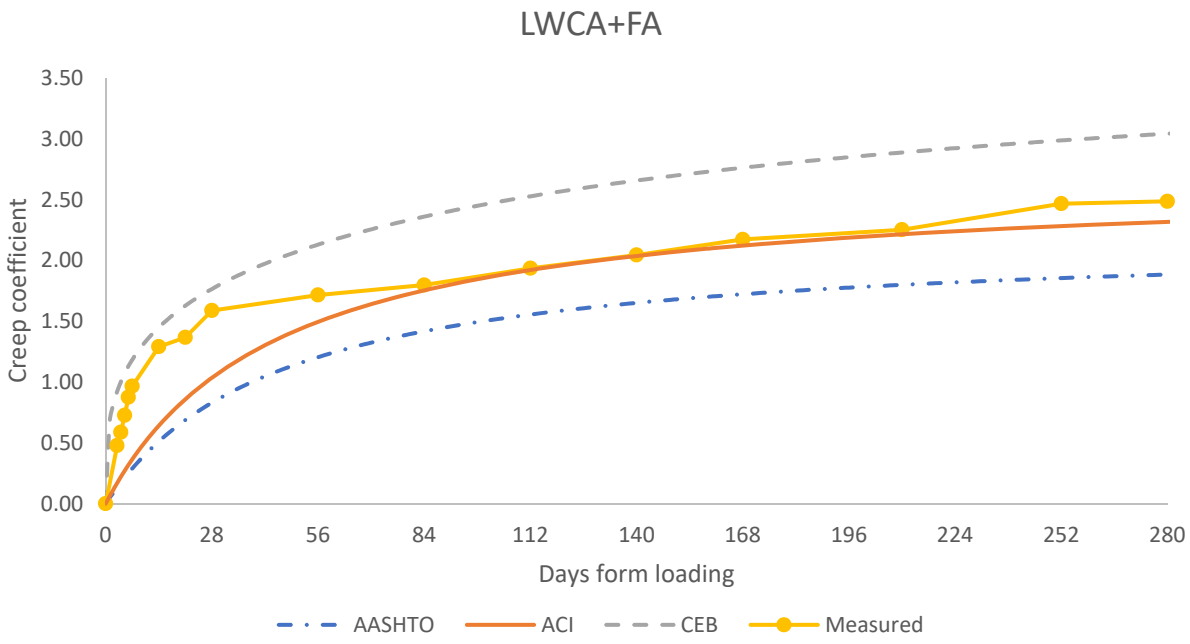

Figure 5-56: Comparison of Creep Coefficient Calculated with Models for LWCA+ FA Mix

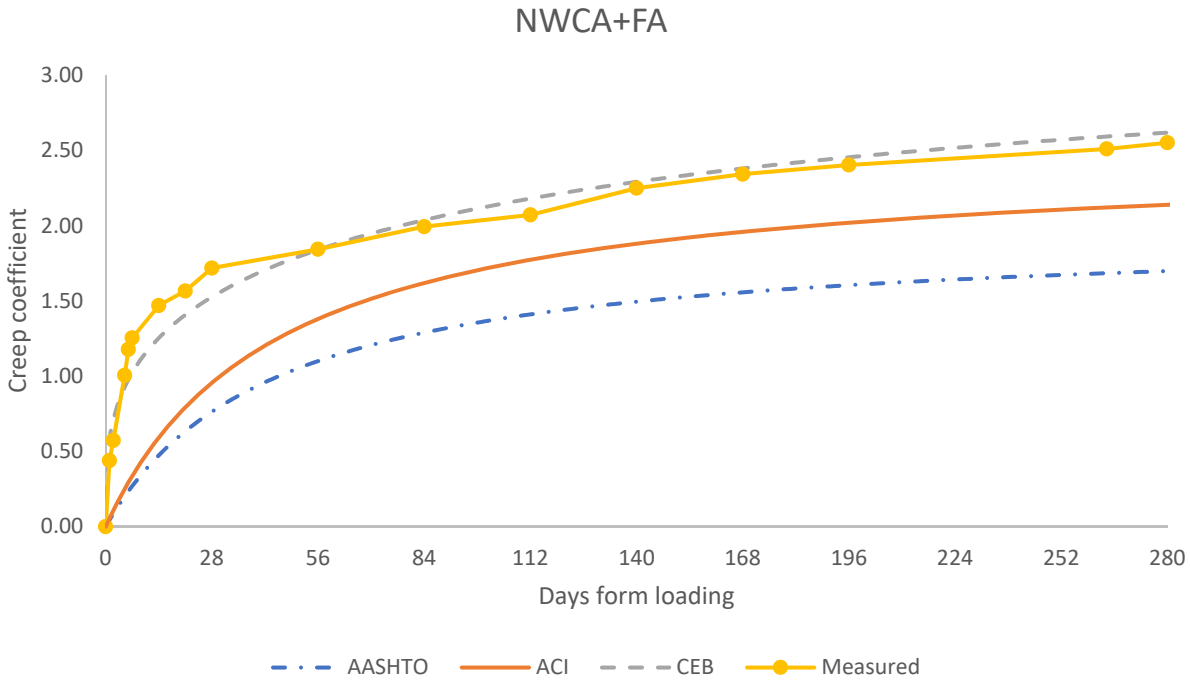

Figure 5-57: Comparison of Creep Coefficient Calculated with Models for NWCA+ FA Mix

5.2.6 Tensile Creep

As discussed earlier, no useful data was obtained from the tensile creep testing. Therefore, for the AAEM analysis, it is assumed that the creep behavior of concrete is the same in compression and tension.

5.2.7 AAEM analysis

Figure 5-58 shows the variation of stresses through the depth of the cross section for mixes in Phase II due to the change in time dependent properties of concrete. The time dependent properties for the topping mixtures were calculated using the ACI 209 model. For the precast beam mixtures, the time dependent properties were calculated using AASHTO. The stresses were calculated at 20 years after construction. Figure 5-59 compares the stress at bottom of deck to that of the tensile strength of concrete given by Equation 5-3, where f`c is the compressive strength of concrete at 28 days.

$$f_r = 7.5 * \sqrt{f`c} \qquad \text{Equation 5-3}$$

It is observed that, all the mixtures tested in Phase II developed stresses smaller than the cracking stress of 4000 psi concrete which is 474 psi obtained using Equation 5-3. It is observed that the stress at bottom of deck for LWCA, NWCA mix with slag and SRA was 309 psi, 263 psi respectively. The stress at bottom of deck for LWCA, NWCA mix with fly ash was 316 psi, 277 psi respectively. The mix with LWCA and fly ash had the highest stress at the bottom of deck while the mix with NWCA developed a smaller stress.

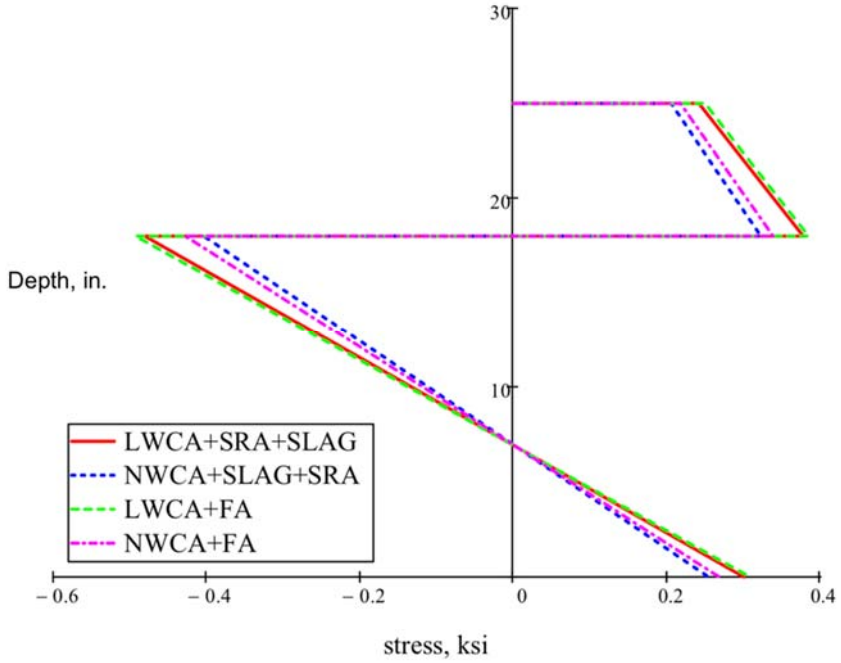

Figure 5-58: Stresses in the Composite Section for Mixes in Phase II

Figure 5-60 to Figure 5-63 show the variation of stresses in deck with varying volume to surface ratio of the deck. The variation of volume to surface ratio of the beam had no effect on the stresses and strains in the section. However, variation in volume to surface ratio of the deck had a significant influence on the stresses. It is observed that the mixes with LWCA had higher stresses at the bottom of deck irrespective of volume to surface ratio. The higher the volume to surface ratio lower the stresses for each mix. This means that if the precast beam surface is saturated prior to casting the topping, the likelihood of cracking will be diminished.

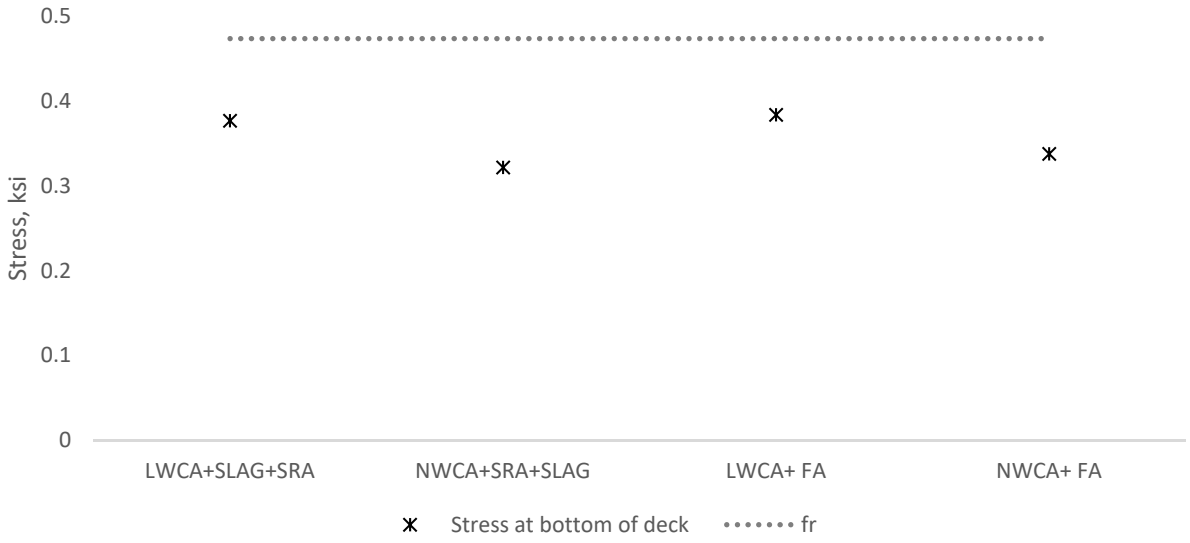

Figure 5-59: Stresses at Bottom of the Deck for Mixes in Phase II

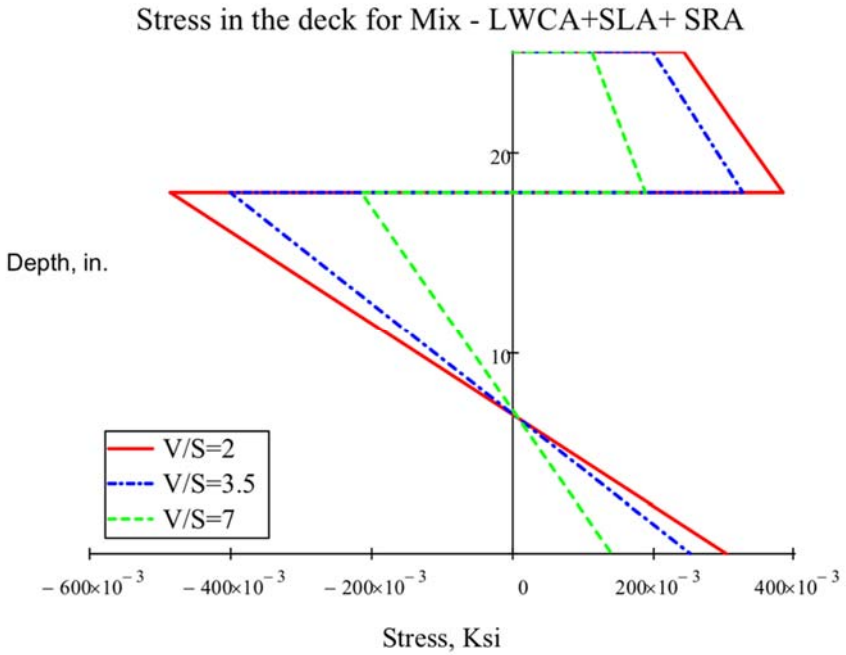

Figure 5-60: Stresses in the Composite Section for Varying V/S Ratios – LWCA+ SRA+ SLAG

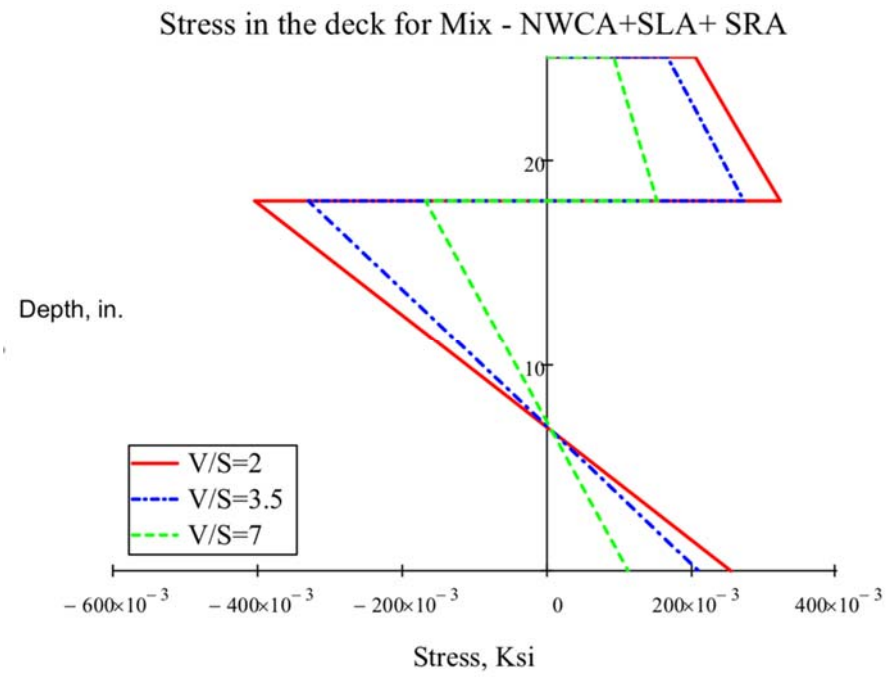

Figure 5-61: Stresses in the Composite Section for Varying V/S Ratios – NWCA+ SRA+ SLAG

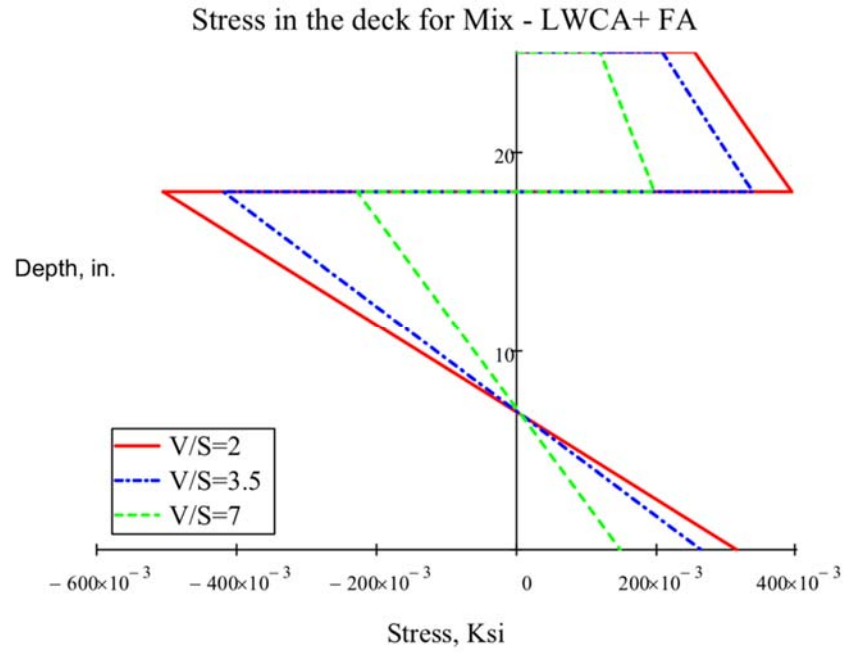

Figure 5-62: Stresses in the Composite Section for Varying V/S Ratios – LWCA+ FA

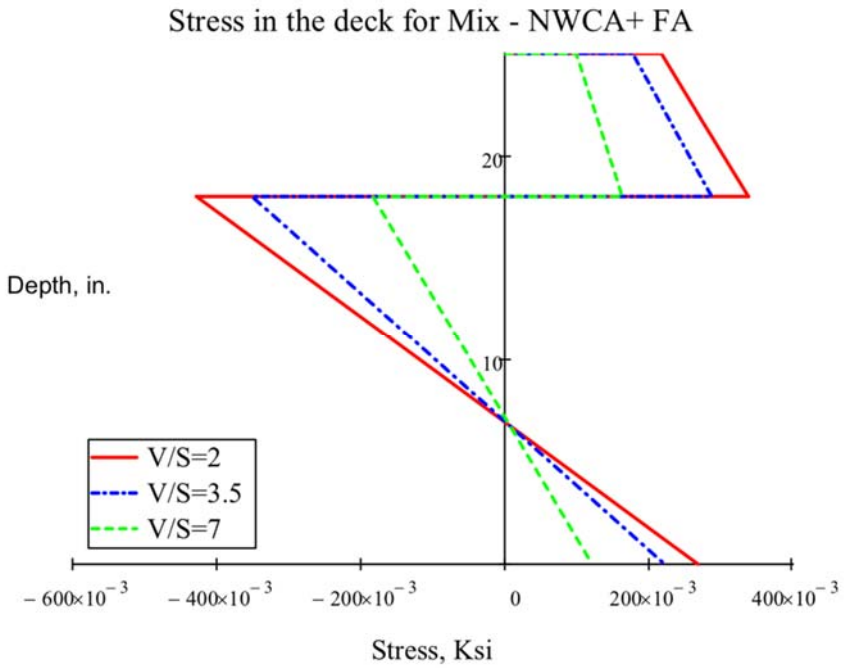

Figure 5-63: Stresses in the Composite for Varying V/S Ratios – LWCA+ FA

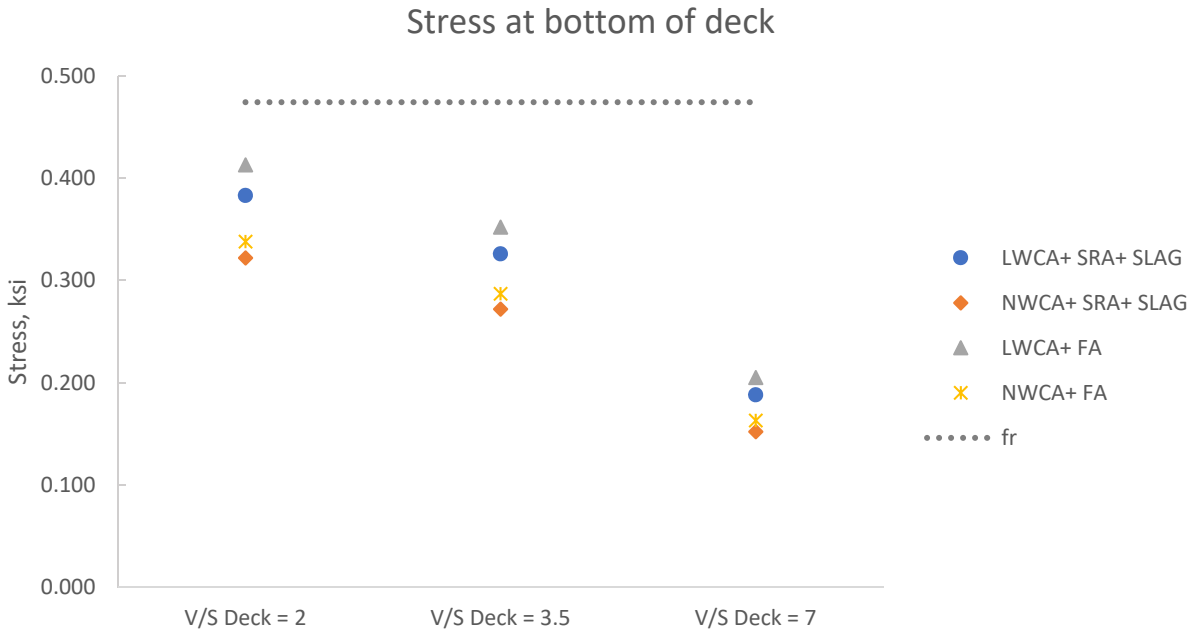

Figure 5-64: Stresses at Bottom of Deck for Varying V/S Ratio of the Deck

Figure 5-64 compares the stresses at bottom of deck for different volume to surface ratios of the deck where f_r is the tensile strength of concrete given by Equation 5-3. It is observed that all the stresses are below cracking stress of concrete but there is a significant decrease in stress with increase in V/S ratio. This points out the significance of saturating the surface of the girder before placement of new concrete.

Figure 5-65 to Figure 5-68 shows the variation of stresses in the cross section for varying slump of the deck mix. It is observed that the stresses at any particular section increased with increase in the slump of concrete. It is observed that the mixes with LWCA developed higher stresses than the corresponding mixes with NWCA. Figure 5-69 compares the stresses at bottom of deck for different slump of the deck concrete where f_r is the tensile strength of concrete given by Equation 5-3. LWCA mixes had higher stresses irrespective of the slump whereas, the mixes with NWCA developed lower stresses for the same slump. Overall, the slump did not have a large impact on the stresses in the cross-section.

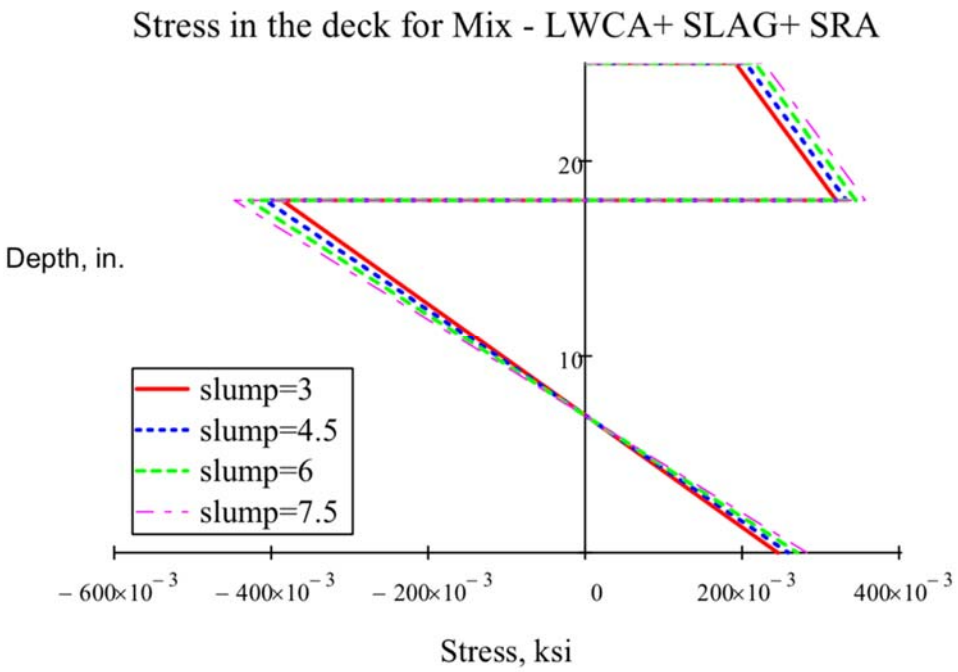

Figure 5-65: Stresses in the Composite Section for Varying Slump of the Deck Mix – LWCA+SRA+SLAG

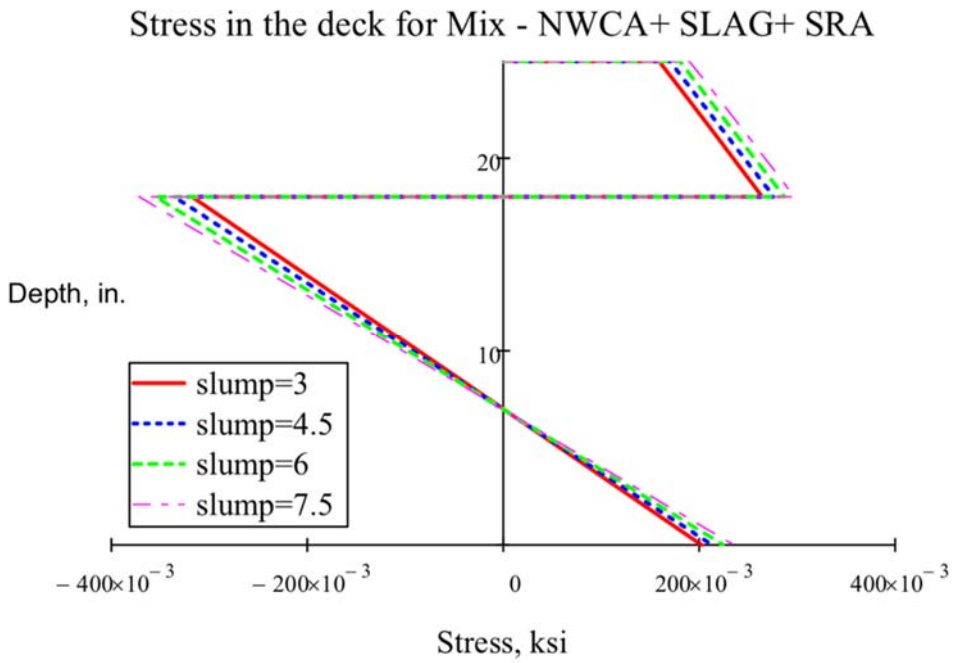

Figure 5-66: Stresses in the Composite Section for Varying Slump of the Deck Mix – NWCA+SRA+SLAG

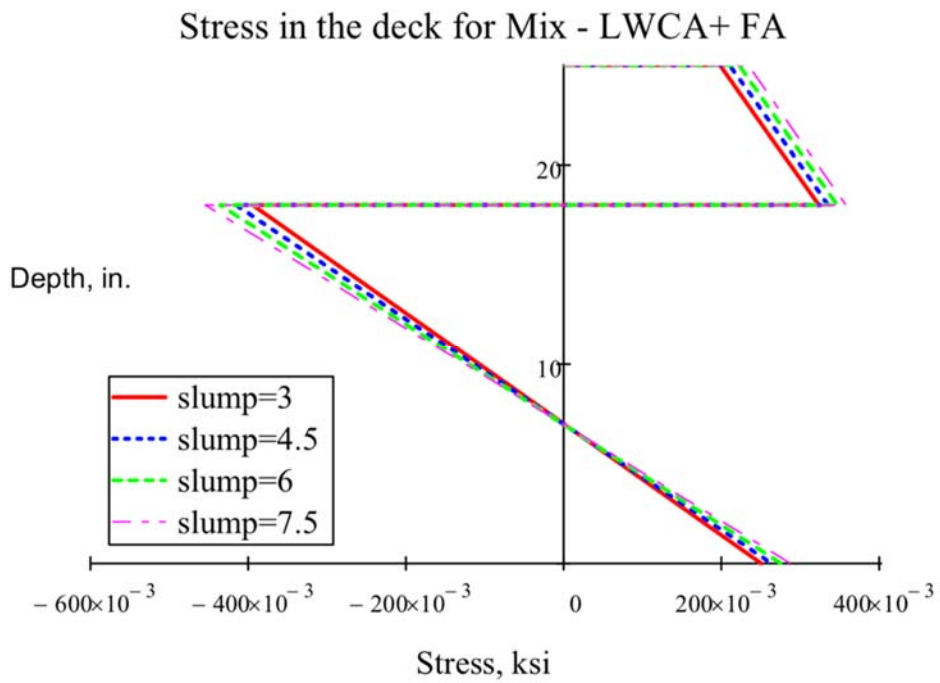

Figure 5-67: Stresses in the Composite Section for Varying Slump of the Deck Mix – LWCA+FA

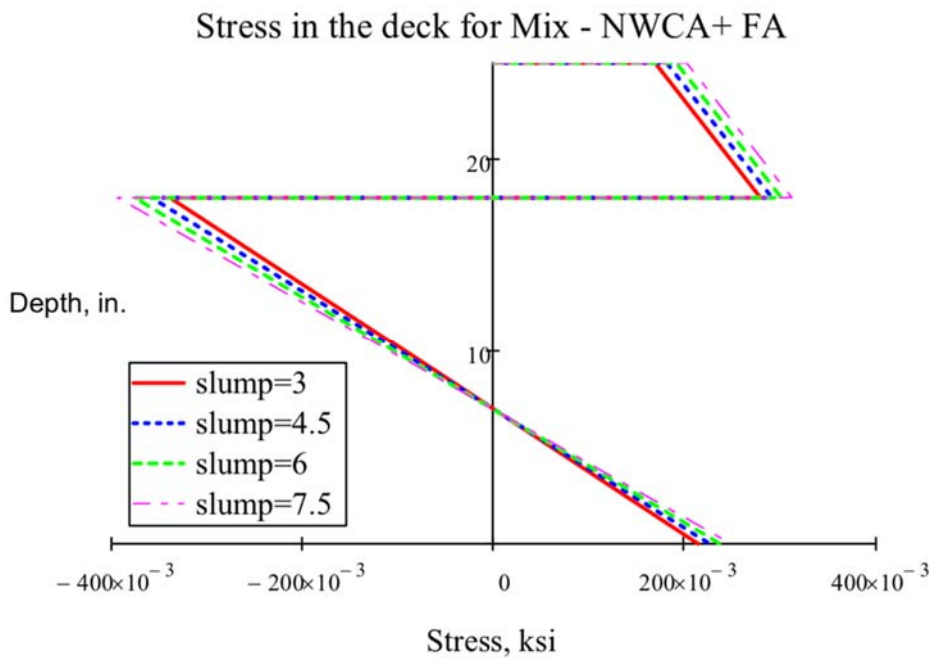

Figure 5-68: Stresses in the Composite Section for Varying Slump of the Deck Mix – NWCA+FA

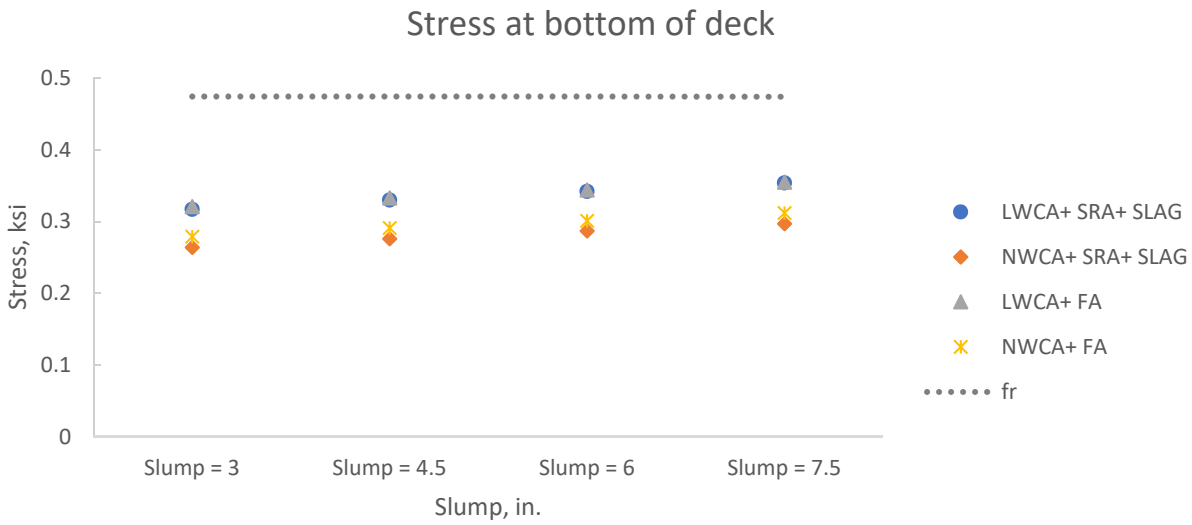

Figure 5-69: Stresses at Bottom of the Deck for Varying Slump of Deck Concrete

6 CONCLUSIONS AND RECOMMENDATIONS

The research presented herein investigated mix designs for the cast-in-place topping for the inverted T-beam system which have lower shrinkage and increased creep behavior in order to increase the service life of the bridge. With the inverted T-beam system, due to the shape of the beam, stress concentrates on the corners of the beam and thus the interface between the deck and beam is susceptible to cracking. This research focused on the section where there is less concrete on top of beam i.e. the section through the web of the beam where the beam is of 18 in. thick and the deck is 7 in. thick. This section presents the conclusions from this project and also recommendations for future study, in this area.

6.1 Conclusions

The scope of this project included ten design mixes initially, narrowed down to four best performing mixes for long term analysis. In Phase I, all ten mixes were treated equally in terms of casting curing and storage. All the mixes performed as required in terms of compressive strength, tensile strength and modulus of elasticity. It can be concluded from the data that, mixes with LWCA showed lower shrinkage compared to mixes with NWCA. Use of SLWF did not prove to reduce shrinkage due to the difficulty in attaining SSD condition. The use of SRA reduced the shrinkage of LWCA concrete but not NWCA concrete (Table 6-1). Mixes with fly ash as the SCM and mixes with SRA out performed all other mixes in terms of shrinkage.

Table 6-1: Shrinkage comparison with/ without SRA

28 – day shrinkage		
LWCA+ SLAG	With SRA	332
	Without SRA	470
NWCA+ SLAG	With SRA	457
	Without SRA	458

All values are -1 x micro strain.

It can be concluded from the data that higher creep can be obtained by using NWCA over LWCA and using fly ash as the SCM. Shrinkage can be reduced by the use of LWCA over NWCA but there was not a large difference when fly ash was used as SCM with NWCA mixes (Table 6-2). The shrinkage of LWCA with slag and SRA in phase I was 332 micro strain, shrinkage in Phase II was 429 micro strain. The reason for this difference in shrinkage of same mix in two phases is unknown.

The mixes in Phase II were tested for their shrinkage and creep performance. The data, obtained for over a year, was compared against ACI 209, AASHTO, CEB MC 90-99 models to determine which model best predicts the behavior of concrete in terms of shrinkage and creep.

From the prediction models it can be concluded that the ACI 209 model was the best predictor of creep and shrinkage in most of the cases for mixes in Phase II (Table 6-3). Thus, the ACI model was used to predict the shrinkage and creep for all mixes in the parametric study

conducted using AAEM method. The creep coefficient of the NWCA and fly ash mix was better predicted by CEB model.

Table 6-2: 28- day Shrinkage and 90- day Creep Coefficient

	28-day shrinkage Phase I	28-day Shrinkage Phase II	Creep Coefficient
LWCA+SRA+SLAG	332	429	0.91
NWCA+SRA+SLAG	457	489	1.92
LWCA+ FA	387	391	1.80
NWCA+ FA	433	438	1.99

Shrinkage values in -1* Micro strain.

Table 6-3: Selecting Best Prediction Model for Shrinkage and Creep

Mix	Shrinkage Prediction			Creep Coefficient Prediction		
	Early age	Later age	Overall	Early age	Later age	Overall
LWCA+SRA+SLAG	ACI	AASHTO/ ACI	ACI	ACI	AASHTO	ACI
NWCA+SRA+SLAG	ACI	ACI	ACI	CEB	CEB/ACI	ACI
LWCA+ FA	ACI	ACI/ CEB	ACI	CEB	ACI	ACI
NWCA+ FA	ACI	ACI	ACI	CEB	CEB	CEB

The parametric study was conducted in the transverse direction of the section to analyze the effect of increasing creep and reducing shrinkage of concrete deck topping. Stresses in all the cases were less than tensile strength, f_r , of 4000 psi concrete given by Equation 5-3. It was observed that the mixes with LWCA developed higher stresses than the mixes with NWCA (Table 6-4). This is attributed to the lower creep in those mixes. The parametric study was then extended to analyze the sensitivity of the stresses in the cross section to variation in slump of the deck mix and variation in V/S ratio of the deck and beam.

Varying slump of the deck topping had minimal effect on the magnitude of the stresses developed in the cross section, but the stresses increased slightly with increasing slump (Table 6-5). Varying the volume to surface ratio of the beam had no effect on the stresses developed in the cross section. However, varying the volume to surface ratio of the deck had a significant impact on the stresses developed. The stresses were much higher when the V/S ratio was assumed to be 2 in. compared to V/S ratio of 7 in. (Table 6-6). This means that in former case, water has to travel a smaller distance to be evaporated and thus more shrinkage occurs, resulting in higher stresses. Thus, it is important to keep the surface of the girder saturated before placement of the new concrete topping.

Table 6-4: Stresses at Bottom of Deck Baseline Study

Mix	Stress at bottom of deck
LWCA+ SRA+ SLAG	0.309
NWCA+ SRA+ SLAG	0.263
LWCA+ FA	0.316
NWCA+ FA	0.277

All stress values are in ksi.

Table 6-5: Stresses at Bottom of Deck for Varying Slump of Deck Topping

Mix	Slump = 3	Slump = 4.5	Slump = 6	Slump = 7.5
LWCA+ SRA+ SLAG	0.317	0.330	0.342	0.354
NWCA+ SRA+ SLAG	0.264	0.276	0.287	0.297
LWCA+ FA	0.321	0.333	0.344	0.355
NWCA+ FA	0.279	0.291	0.301	0.312

All stress values are in ksi, slump in in.

Table 6-6: Stresses at the Bottom of Deck for Varying V/S Ratio of Deck

MIX	V/S Deck = 2	V/S Deck = 3.5	V/S Deck = 7
LWCA+ SRA+ SLAG	0.383	0.326	0.188
NWCA+ SRA+ SLAG	0.322	0.272	0.152
LWCA+ FA	0.413	0.352	0.205
NWCA+ FA	0.338	0.287	0.163

All stress values are in ksi, V/S in in.

From this parametric study, it can be concluded that the mixes with NWCA will develop smaller stresses compared to the mixes with LWCA. Further, the difference in the magnitude of stresses between mixes with fly ash and slag is minimum but considering the performance in terms of shrinkage and creep, fly ash is found to be better at reducing the tendency to crack compared to slag.

6.2 Recommendations

1. Based on the parametric study, a mixture with 28 – day shrinkage around 500 micro strain and 90 – day creep coefficient close to 2.0 should result in stresses at bottom of deck less than the cracking strength of concrete, preventing formation of cracks, thus increasing the service life of the bridge.
2. The following are the properties recommended for a mix that is used as a deck topping:
    a. Compressive strength – 4000 psi
    b. Slump – as needed for proper consolidation
    c. Air content – 6.5 % ± 1.5 %
    d. Shrinkage – < 500 με at 28 days
    e. Creep Coefficient – > 1.8 at 90 days

f. Cementitious content – Less than 600 lb/ft^3 for NWC, less than 650 lb/ft^3 for LWC.
g. Water cement ratio – 0.45

3. Three of the four mixtures used in the Phase II testing satisfy these requirements. Only LWCA+SRA+SLAG would not be recommended, without further testing, due to the low creep coefficient.
4. The following placement techniques are highly recommended to help reduce the possibility of restrained shrinkage cracking:
    a. Surface of precast beam should be in the saturated surface dry condition before placing the topping concrete.
    b. The deck is moist cured for at least 7 days.

6.3 Future investigation

Further investigation is needed to analyze behavior of concrete creep in tension, optimize the quantity of shrinkage reducing admixtures used. The AAEM analysis was done assuming the top surface of the beam is sufficiently saturated before the placement of deck. Further sensitivity analysis can be conducted assuming partial saturation of the beam surface to better represent a practical scenario of the beam.

REFERENCES

232.1R-12, A. (2012). Report on the Use of Raw or Processed Natural Pozzolans in Concrete. *ACI*, 15-19.

AASHTO. (2014). *AASHTO lRFD bridge design specifications, seventh edition, 2014.* Washington D.C: American Association of State Highway and Transportation Officials.

ACI 318, c. (2014). *Building code requirements for structural concrete : (ACI 318-14) ; and commentary (ACI 318R-14).* ACI.

ACI-209. (2008). *Guide for Modeling and Calculating Shrinkage and Creep in Hardened Concrete.* Farmington Hills, MI: American Concrete Institute.

Akkaya, C. O. (2007). Effect of supplementary cementitious materials on shrinkage and crack development in concrete. *Cement & Concrete Composites 29*, 117–123.

al., R. e. (2005). *Prefabricated Bridge Elements and Systems in Japan and Europe – International Technology Exchange Program.* US Department of Transportation Federal Highway Administration.

Banerjee, S. P. (1971). *Differential shrinkage effects in composite structures.* IABSE publications.

Bazant, Z. P. (1972). Prediction of concrete creep effects using age-adjusted effective modulus method. *ACI*, 212-217.

Bell, C. S. (2006). *Application of Precast Decks and other Elements to Bridge Structures - Mn/DOT Technical Report No. MN/RC 2006-37, 2006.* Saint Paul, MN: Minnesota Department of Transportation.

C192, A. (2007). *Standard Practice for Making and Curing Concrete Test Specimens in the Laboratory.* ASTM international.

Mokarem, D, (2003). *DEVELOPMENT OF CONCRETE SHRINKAGE PERFORMANCE SPECIFICATIONS.* The Virginia Transportation Research Council, VTRC 04-CR1.

Dilger, W. (2005). Time Dependent Effects in Concrete Structures. *Draft Document, ACI Committee 209 – Creep and Shrinkage in Concrete.*

Dimaculangan, M. C. (2010). *Minnesota's Precast Composite Slab Span System.* Aspire.

Hagen, E. F. (2005). *Development and Construction of a Precast Inverted T System for Expediting Minnesota Slab Span Bridge Projects.* Concrete Bridge Conference.

Halverson, M. F. (2012). *Full-Depth Precast Concrete Bridge Deck System: Phase II, Mn/DOT Technical Report No. MN/RC 2012-30.* Saint Paul, MN: Minnesota Department of Transportation.

Harikrishnan Nair, C. O. (2016). USE OF LIGHTWEIGHT CONCRETE FOR REDUCING CRACKS IN BRIDGE DECKS. *Virginia Transportation Research Council*.

Henkensiefken, R. D. (2009). Volume change and cracking in internally cured mixtures made with saturated lightweight aggregate under sealed and unsealed conditions. *Cement & Concrete Composites*, 427-437.

Hooton, R. K. (2009). The Effect of Ground Granulated Blast Furnace Slag (Slag Cement) on the Drying Shrinkage of Concrete - A Critical Review of the Literature. *American Concrete Institute*, 79-94.

Kosmatka, S. H. (2002). *Design and Control of Concrete Mixtures.* Portland Cement Association.

McMillan, F. R. (1916). "Method of Designing Reinforced Concrete Slabs, discussion by A. C. Janni. *Transactions ASCE, 80(1738).*

Menkulasi, F. (2014). *The Development of a Composite Concrete Bridge System for Short-to-Medium-Span Bridges.* Blacksburg, VA: Virginia Polytechnic Institute and State University.

Menkulasi, T. C. (2017). *Implementation of a Precast Inverted T-Beam System in Virginia: Part I: Laboratory Investigations.* charlottesville: Virginia transportation research council.

Mindess, S. J. (1996). *Concrete, 2nd Edition.* Upper Saddle River, NJ: Pearson Education, Inc.

Mokarem, D. S. (2008). *Measurement of Early Age Shrinkage of Virginia Concrete Mixtures - VTRC 08-R9.* Charlottesville, Virginia: Virginia Transportation Research Council.

Nelson, D. A. (2013). *Investigation of Concrete Mixtures to Reduce Differential Shrinkage Cracking in Composite Bridges.* Blacksburg: Virginia Tech.

Neville, A. M. (1983). *Creep of Plain and Structural Concrete.* New York: Longman Inc.

Ozyildirim, C. G. (2005). *First Bridge Structure with Lightweight High-Performance Concrete Beams and Deck in Virginia.* Virginia Transportation Research Council: Virginia Transportation Research Council.

Ralls. (2005). *Prefabricated Bridge Elements and Systems in Japan and Europe.* U.S. DOT, FHWA.

Ribeiro, A. B. (2003). Effectiveness of Shrinkage-Reducing Admixtures on Different Concrete Mixtures. *Special Publication - 217*, 299-311.

Schmitt, T. R. (1999). Effect of Material properties on Cracking in Bridge Decks. *Journal of Bridge Engineering 4(1)*, 8-13.

Silfwerbrand, J. (1997). *Stresses and strains in composite concrete beams subjected to differential shrinkage.* ACI Structural Journal 94(4).

Stalite. (n.d.). *physical properties.* Retrieved from Stalite.com: http://www.stalite.com/uploads/PDF%20Files/Matl%20Specs%20Structural%20pg.%202%20Rev%20Nov.%202011.pdf

Thomas, M. (2007). *Optimizing the Use of Fly Ash in Concrete.* Washington DC: Portland cement association .

Wollmann, A. R.-W. (2003). CREEP AND SHRINKAGE EFFECTS IN SPLICED PRESTRESSED CONCRETE GIRDER BRIDGES. *PCI*, 92-105.

Yang, H. (2012). *Strength and Shrinkage Property of Nano Silica Powder Concrete.* Jinan, China: Department of Civil Engineering, Shandong Jiaotong University.

Ye Jiajun, H. S. (2006). Effect of Pre-wetted Lightweight Aggregate on Internal Relative Humidity and Autogenous Shrinkage of Concrete. *Journal of Wuhan University of Technology-Mater. Sci. Ed., 2006, Volume 21, Number 1*, 135.